MARTIN MARIETTA ENERGY SYSTEMS LIBRARIES
3 4456 0361301 6

CENTRAL RESEARCH LIBRARY
DOCUMENT COLLECTION

ORNL-2610
Physics and Mathematics
TID-4500 (14th ed.)

cy-6

PHYSICS DIVISION

SEMIANNUAL PROGRESS REPORT

FOR PERIOD ENDING SEPTEMBER 20, 1958

LIBRARY
REFERENCE COPY

OAK RIDGE NATIONAL LABORATORY
operated by
UNION CARBIDE CORPORATION
for the
U.S. ATOMIC ENERGY COMMISSION

CENTRAL RESEARCH LIBRARY
DOCUMENT COLLECTION
LIBRARY LOAN COPY
DO NOT TRANSFER TO ANOTHER PERSON
If you wish someone else to see this document, send in name with document and the library will arrange a loan.

Printed in USA. Price $1.75 Available from the

Office of Technical Services
U. S. Department of Commerce
Washington 25, D. C.

LEGAL NOTICE

This report was prepared as an account of Government sponsored work. Neither the United States, nor the Commission, nor any person acting on behalf of the Commission:

A. Makes any warranty or representation, express or implied, with respect to the accuracy, completeness, or usefulness of the information contained in this report, or that the use of any information, apparatus, method, or process disclosed in this report may not infringe privately owned rights; or

B. Assumes any liabilities with respect to the use of, or for damages resulting from the use of any information, apparatus, method, or process disclosed in this report.

As used in the above, "person acting on behalf of the Commission" includes any employee or contractor of the Commission to the extent that such employee or contractor prepares, handles or distributes, or provides access to, any information pursuant to his employment or contract with the Commission.

ORNL-2610
Physics and Mathematics
TID-4500 (14th ed.)

Contract No. W-7405-eng-26

PHYSICS DIVISION

SEMIANNUAL PROGRESS REPORT

for Period Ending September 20, 1958

J. L. Fowler, Director
E. O. Wollan, Associate Director

DATE ISSUED

FEB 26 1959

OAK RIDGE NATIONAL LABORATORY
Oak Ridge, Tennessee
operated by
UNION CARBIDE CORPORATION
for the
U.S. ATOMIC ENERGY COMMISSION

MARTIN MARIETTA ENERGY SYSTEMS LIBRARIES

3 4456 0361301 6

TABLE OF CONTENTS AND SUMMARY

POLARIZATION OF CONVERSION ELECTRONS FOLLOWING BETA DECAY

R. L. Becker and M. E. Rose 1

The theoretical analysis of longitudinal and transverse polarization of conversion electrons in coincidence with beta particles has been extended to include mixed multipole conversion following allowed and pure multipole conversion following first-forbidden beta transitions. Extensive numerical results have been obtained.

A UNIVERSAL WEAK BOSON-FERMION INTERACTION

T. A. Welton 4

The decay rate of the charged pion by virtual pair production of nucleons has been calculated by a new method and found to be much less than the experimental value. A new direct interaction of universal form has been postulated to account for the decay, and the decay rate of the K meson is thereby given to within 20%.

ELECTRON-ELECTRON SCATTERING WITH THE SPHERICAL MOMENTUM SPACE FORMALISM

T. A. Welton 7

The spherical momentum space formalism previously reported has been reduced to a simple computational scheme and applied to the experimentally interesting case of electron-electron collisions.

COULOMB EXCITATION OF 2^+ STATES IN SELENIUM AND TELLURIUM NUCLEI

F. K. McGowan and P. H. Stelson 11

Measurements of the Coulomb excitation of the 2^+ states in Se^{76}, Se^{78}, Se^{80}, and Te^{122} have provided information on the gamma-ray decay characteristics from these states.

DIFFERENTIAL ELASTIC NEUTRON SCATTERING FROM BERYLLIUM

H. O. Cohn and J. L. Fowler 14

The elastic scattering of neutrons from beryllium has been measured at nine energies between 0.7 and 3.0 Mev. Qualitative arguments based on the data lead to the assignment of $J = 2^+$ for the broad resonance level at 3.0 Mev.

$Al^{27}(n,\alpha)Na^{24}$ CROSS SECTION AS A FUNCTION OF NEUTRON ENERGY

H. W. Schmitt and J. Halperin 15

The cross section for the $Al^{27}(n,\alpha)Na^{24}$ reaction has been measured as a function of neutron energy in the range $6.2 \leqq E_n \leqq 8.3$ Mev and at 14.8 Mev. Measurements were made relative to the fission cross section of U^{238}, using activation techniques to determine the $Al^{27}(n,\alpha)$ events. While a number of peaks and valleys appear in the curve for cross section vs energy, there is a general increase in cross section with increasing energy, consistent with the Coulomb penetrability of the alpha particle.

$Li^6(n,\alpha)H^3$ CROSS SECTION AS A FUNCTION OF NEUTRON ENERGY FROM 1.2 TO 8 Mev

H. W. Schmitt, R. B. Murray, and J. J. Manning 17

The cross section for the reaction $Li^6(n,\alpha)H^3$ has been measured as a function of neutron energy in the range $1.2 \leqq E_n \leqq 8$ Mev. The magnitude of $\sigma_{n,\alpha}$ as measured in this experiment depends on the absolute value of $\sigma_{fission}$ (U^{238}), while the shape of the curve for cross section vs energy depends on the known energy dependence of $\sigma_{fission}$ (U^{238} or Np^{237}). Statistical and other point-to-point uncertainties range from ±5 to ±9%, while the uncertainty in absolute value of the cross section is ±7%.

PULSED VAN DE GRAAFF AND FAST TIME-OF-FLIGHT STUDIES
P. D. Miller, W. M. Good, J. H. Gibbons, R. L. Macklin, and J. H. Neiler 19

An RCL 256-channel analyzer has been added to the time-of-flight equipment. Total cross sections of a number of separated isotopes from $A = 45$ to $A = 76$ have been measured. Some preliminary work has been done on neutron capture cross sections.

PARAMETERS OF NEUTRON RESONANCES OF Pm^{147}, I^{129}, Zr^{93}, and Np^{237}
R. C. Block, J. A. Harvey, G. L. Jenkins, G. G. Slaughter, W. J. Martin, G. W. Parker, and P. Lantz 22

Total neutron cross sections of Pm^{147}, I^{129}, Zr^{93}, and Np^{237} have been measured with the fast-chopper time-of-flight spectrometer. Parameters for the resonances are given.

ABSOLUTE (p,n) CROSS SECTIONS FOR LIGHT NUCLEI
J. H. Gibbons and R. L. Macklin 25

The $H^3(p,n)He^3$ absolute cross-section measurements have been re-examined and were found larger than those previously reported by (27 ± 10) % due to protium and He^3 contamination. The $C^{14}(p,n)N^{14}$ reaction cross-section measurements have been extended to the first excited state in N^{14} and compared, by reciprocity, with $N^{14}(n,p)$ data. The agreement is reasonable.

ANTIFERROMAGNETISM IN $CrCl_3$ AND $FeCl_3$
J. W. Cable, M. K. Wilkinson, and E. O. Wollan 28

Preliminary investigations of the low-temperature antiferromagnetic ordering in $CrCl_3$ and $FeCl_3$ are reported.

NEUTRON DIFFRACTION INVESTIGATIONS OF $CoCl_2$ IN AN EXTERNAL MAGNETIC FIELD
M. K. Wilkinson, J. W. Cable, E. O. Wollan, and W. C. Koehler 30

Neutron diffraction experiments on single crystals of $CoCl_2$ in an external magnetic field have established the specific orientation of the magnetic moments in the antiferromagnetic lattice and the manner in which the moments become aligned parallel in moderate magnetic fields.

NEUTRON DIFFRACTION INVESTIGATION OF METALLIC CERIUM
H. R. Child, M. K. Wilkinson, W. C. Koehler, and E. O. Wollan 32

Preliminary observations indicate a low-temperature antiferromagnetic ordering in the hcp phase of metallic cerium and a change in the electronic configuration when the α-fcc phase is formed.

MAGNETIC NEUTRON DIFFRACTION STUDY OF 4d TRANSITION-GROUP TRIFLUORIDES
E. O. Wollan, H. R. Child, M. K. Wilkinson, and J. W. Cable 34

The antiferromagnetic structure has been determined for the compound MoF_3, in which the magnetic ion belongs to the $4d$ group of elements.

ATOMIC-BEAM DETERMINATION OF THE NUCLEAR SPINS OF I^{128} AND I^{130}
J. E. Sherwood and S. J. Ovenshine 36

The nuclear spins of 25-min I^{128} and 12.5-hr I^{130} have been determined by atomic-beam magnetic resonance. I^{128} has been found to have a spin of 1; I^{130}, however, has been found to have a spin of 5, which seems inconsistent with the observed decay of this isotope.

MICROWAVE SPECTRA AND STRUCTURE OF THE VINYL FLUORIDE MOLECULE
H. W. Morgan and J. H. Goldstein 41

Measurements of the microwave spectra of $C^{12}C^{12}H_3F$, $C^{12}C^{13}H_3F$, and $C^{13}C^{12}H_3F$ have been made. From the computed moments of inertia, precise values have been obtained for the lengths of the C=C bond (1.337 Å) and the C–F bond (1.344 Å), and for the CCF angle (121°).

PRELIMINARY CLASSIFICATION OF THE SPECTRUM OF SINGLY IONIZED ERBIUM (Er II)
J. R. McNally, Jr., and K. L. Vander Sluis 44

The first breakthrough has been made in assigning atomic energy levels to the rare-earth element erbium, $Z = 68$. The ground-state level is $4f^{12}(^3H_6)\cdot 6s(^4H_{13/2})$; levels from the configuration $4f^{12}5d$ begin about 0.6 ev above the ground state.

CLASSIFICATION OF SINGLY IONIZED PLUTONIUM (Pu II)
J. H. Wise, P. M. Griffin, and J. R. McNally, Jr. 46

Additional Zeeman measurements in the spectrum of plutonium have revealed two additional low-energy levels with possible configuration identification as $5f^6 6d$.

FURTHER EVALUATIONS OF THE DUO-PLASMATRON ION SOURCE
C. D. Moak, J. W. Johnson, R. F. King, and H. E. Banta 46

Further measurements with the Duo-Plasmatron ion source have indicated detectable and usable yields of H_1^- ions and He^{++} ions.

DELAY-LINE MEMORY PULSE SPECTROMETER
D. Maeder 47

Further work on the Hutchinson-Scarrott type of pulse spectrometer includes the development of an add-subtract circuit, a selector for splitting the memory into even and odd channels, a gate for automatic dead-time correction, a "count one" test circuit, and a linear analog display. The design of the display and the adjustment procedures required for maintaining a 3% over-all accuracy are described in detail.

AN IBM 704 PROGRAM FOR COMPUTATION OF EQUILIBRIUM ORBIT PROPERTIES IN AVF CYCLOTRONS
M. M. Gordon, T. A. Welton, T. I. Arnette, and H. C. Owens 51

A fast and flexible code for calculating the properties of equilibrium orbits in AVF cyclotrons has been completed for the IBM 704.

PHYSICS DIVISION SEMIANNUAL PROGRESS REPORT

POLARIZATION OF CONVERSION ELECTRONS FOLLOWING BETA DECAY

R. L. Becker M. E. Rose

Because of the nonconservation of parity and charge conjugation, beta decay provides a means of obtaining polarized excited nuclei.[1] A previous communication[2] has shown that conversion electrons following the beta decay should exhibit not only longitudinal but also appreciable transverse polarization in the plane of the beta and the conversion electron. It is easy to see that polarization perpendicular to the plane is impossible. It was suggested that the experimental measurement of transverse conversion polarization in coincidence with the beta might provide some advantages for investigating the beta interaction, particularly for testing the validity of the two-component theory. Also, the conversion polarization provides an additional means of determining the mixture parameter for the conversion transition. When the ordinary angular correlation is isotropic, such as after allowed beta decay, and there is no preceding gamma ray, the only alternative is a measurement of the polarization of the gamma rays or of the conversion electrons.

The present work extends the previous analysis, which was limited to pure multipole conversion following allowed beta decay, to include the cases of mixed multipole conversion following allowed beta decay and pure multipole conversion following first-forbidden beta decay. In addition, extensive numerical results have been obtained for K conversion.

Letting $\hat{e}$ be a unit vector in the direction of the beta, $\hat{e}_{\parallel}$ a unit vector along the electron momentum, and $\cos\theta = \hat{e}\cdot\hat{e}_{\parallel}$, the longitudinal and transverse polarizations are defined[2] by

$$P_{\parallel} = \left\langle \vec{\sigma}\cdot\hat{e}_{\parallel} \right\rangle \quad , \quad P_{\perp} = \left\langle -\beta\vec{\sigma}\cdot\hat{e}_{\perp} \right\rangle \quad , \tag{1}$$

where $\hat{e}_{\perp} = \hat{e}_{\parallel} \times (\hat{e} \times \hat{e}_{\parallel})/\sin\theta$. (The expectation values in Eq. 1 are calculated with Coulomb field solutions which are asymptotically a plane wave plus a converging spherical wave.) The nuclear orientation is characterized by an axially symmetric diagonal density matrix so that the magnetic substate populations have the form

$$p_m = \sum_{k=0}^{2J} \alpha_k C^{JkJ}_{m0m} \quad . \tag{2}$$

For allowed beta decay, only α_0 and α_1 are nonvanishing; for first-forbidden decay, α_2 and α_3 also contribute. Following allowed beta decay the conversion transition is most generally a magnetic L-electric

[1]This was first emphasized by S. B. Trieman, *Phys. Rev.* **110**, 448 (1958), and by H. Frauenfelder, J. D. Jackson, and H. W. Wyld, Jr., *Phys. Rev.* **110**, 451 (1958). The latter authors discuss briefly and qualitatively the longitudinal polarization of conversion electrons following a beta transition.

[2]M. E. Rose and R. L. Becker, *Phys. Rev. Letters* **1**, 116 (1958).

L' mixture, and $L' = L \pm 1$. The polarization takes the form,[2] with $q = \parallel$ or $\perp$,

$$P_q(ML,EL') = \frac{P_q^{(1)}(ML) + \bar{\delta}^2 P_q^{(1)}(EL') + 2\bar{\delta}\bar{P}_q^{(1)}(ML,EL')}{1 + \bar{\delta}^2} , \tag{3}$$

in which $\bar{\delta}^2$ is the ratio of intensities of EL' to ML. The phase of $\bar{\delta}$ is the same as that of the gamma-ray mixture parameter. The $P_q(\tau L)$, with $\tau = M$ or E, have been given previously.[2] For example,

$$\begin{aligned} P_\perp^{(1)}(ML) &= \left\{ -\frac{1}{2}[J(J+1)]^{-1/2} \frac{\alpha_1}{\alpha_0} N_0^1 \frac{2L+1}{L(L+1)} \right\} r_\perp(ML) \sin\theta , \\ P_\perp^{(1)}(EL) &= \left\{ \frac{1}{2}[J(J+1)]^{-1/2} \frac{\alpha_1}{\alpha_0} N_0^1 \frac{2L+1}{L(L+1)} \right\} r_\perp(EL) \sin\theta , \end{aligned} \tag{4}$$

where

$$N_0^1 = \frac{L(L+1) + J(J+1) - J_2(J_2+1)}{2L+1} , \tag{5}$$

J is the spin of the emitting nucleus, J_2 is that of the final nucleus, and the $r_\perp(\tau L)$ are functions of ratios of internal-conversion reduced matrix elements which we have tabulated. Figure 1 shows, as an example, $r_\perp(M1)$ vs k, the transition energy$/mc^2$, for several values of the nuclear charge Z. The $r_\perp(\tau L)$ approach zero and the $r_\parallel(\tau L)$ approach unity as $k \to \infty$, so that $P_\parallel(\tau L)$ becomes identical with the gamma-ray polarization in this limit. For most decay schemes of interest,

$$\frac{1}{24}\frac{v}{c} \leqq \left| \frac{1}{2}[J(J+1)]^{-1/2} \frac{\alpha_1}{\alpha_0} N_0^1 \frac{2L+1}{L(L+1)} \right| \leqq \frac{9}{4}\frac{v}{c}$$

and $r_\perp(\tau L)$ lies between 0.2 and 1.2. [The factors can be regrouped in such a way that each factor is less than or equal to 1 and, of course, $P_q(\tau L) \leqq 1$.] Thus transverse polarizations as large as 50% may be expected, and polarizations of $\sim$25% should not be uncommon.

The interference term may be written

$$\bar{P}_\perp^{(1)}(ML,EL \pm 1) = \frac{1}{2}[J(J+1)]^{-1/2} \frac{\alpha_1}{\alpha_0} N_{\pm 1}^1 p_\perp(ML,EL \pm 1) \sin\theta , \tag{6}$$

with

$$\begin{aligned} N_1^1 &= [(J_2 + J + L + 2)(-J_2 + J + L + 1)(J_2 - J + L + 1)(J_2 + J - L)]^{1/2} , \\ N_{-1}^1 &= [(J_2 + J + L + 1)(J_2 + J - L + 1)(J_2 + L - J)(J + L - J_2)]^{1/2} , \end{aligned} \tag{7}$$

and $p_\perp(ML,EL')$ a tabulated function of L, $L' = L \pm 1$, Z, and k. The 364-kev gamma in the decay of I^{131}, which follows an allowed GT transition, is a mixed $M1$-$E2$ transition with a not very well-known mixture parameter, $\bar{\delta}$. Figure 2 shows the transverse and longitudinal polarizations as functions of $\bar{\delta}$, assuming the

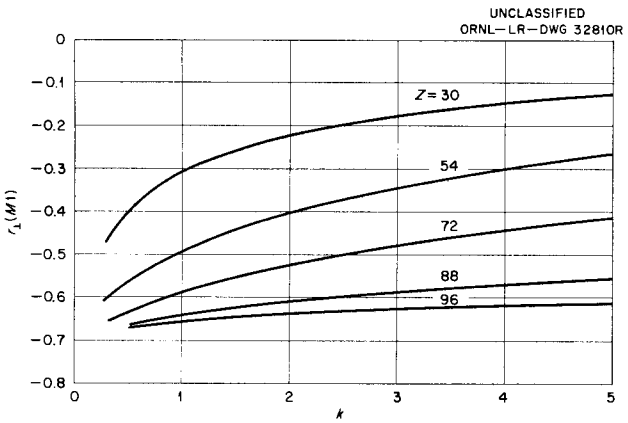

Fig. 1. Curves for $r_\perp(M1)$ vs k, the Transition Energy/mc^2.

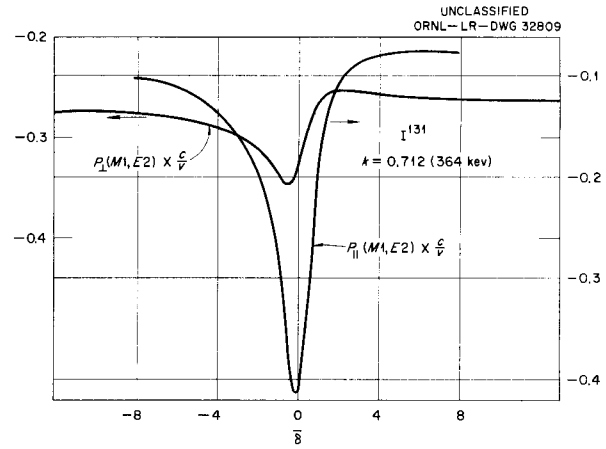

Fig. 2. Polarizations, $P_\perp(M1, E2) \times c/v$ at 90° and $P_\parallel(M1, E2) \times c/v$ at 0°, of the Conversion Electrons from the 364-kev Transition in I^{131} vs the Mixture Parameter, $\bar{\delta}$.

two-component theory. For all values of $\bar{\delta}$, a transverse polarization at $\theta = 90°$ of at least 25% can be expected.

For conversion following first-forbidden beta decay, there are additive contributions from the first- and third-rank nuclear orientations. The polarization in a pure multipole transition takes the form

$$P_q(\theta;\tau L) = \frac{P_q^{(1)}(\theta;\tau L) + P_q^{(3)}(\theta;\tau L)}{1 + (\alpha_2/\alpha_0)\,[I_2(\theta;\tau L)/I_0(\tau L)]} \quad . \tag{8}$$

The $P_q^{(1)}(\tau L)$ are the same as given previously, except that the values of the statistical tensors α_1 and α_0 are different functions of the beta-decay parameters. The contributions to $P_\perp$ from the third-rank nuclear orientations are

$$P_\perp^{(3)}(ML) = -\frac{1}{2}\frac{\alpha_3}{\alpha_0} N_0^3(L) \frac{2L+1}{L(L+1)} r_\perp(ML)\, P_3^1(\cos\theta) \quad , \tag{9}$$

$$P_\perp^{(3)}(EL) = \frac{1}{2}\frac{\alpha_3}{\alpha_0} N_0^3(L) \frac{2L+1}{L(L+1)} r_\perp(EL)\, P_3^1(\cos\theta) \quad , \tag{10}$$

where

$$N_0^3(L) = (-)^{J-J_2+L}\,(2J+1)^{1/2}\, W(JJLL;3J_2) \left[\frac{(L-1)\,L(L+1)(L+2)}{(2L-1)(2L+1)(2L+3)}\right]^{1/2} \quad . \tag{11}$$

The combinations of internal-conversion matrix elements which enter are the same as those occurring in $P_q^{(1)}$. This will be true for the contributions from all higher-rank nuclear orientations as well. The denominator in Eq. 8 gives the beta-conversion electron angular correlation, as expected.

These results for first-forbidden transitions are given in the hope of extending the list of sources with which the contemplated measurements could be carried out. It will be readily seen that the requirements

of beta and radiative lifetimes, the conversion energy, and the conversion coefficient constitute rather severe restrictions on the source, especially if one is restricted to allowed transitions. Unfortunately, all known unique ($|\Delta J| = 2$, yes) first-forbidden transitions present experimental difficulties, for example, weak branching ratios. However, the cases of Y^{88} and Pr^{144} have been calculated in detail.

A UNIVERSAL WEAK BOSON-FERMION INTERACTION

T. A. Welton

The presently known weak fermion interactions are generally assumed to be responsible for the π and K decays by means of processes involving virtual creation of a baryon pair by absorption of the boson in the vacuum, followed by annihilation of the pair associated with lepton-pair production through the weak fermion interaction. All such calculations by the standard procedures of quantum field theory unfortunately diverge in the same way as for the charge renormalization. It then remains only an assumption that a correct formalism would yield the correct decay rates and branching ratios for the boson decays. A previously reported formalism which seems to be free of the closed-loop divergences of the conventional theory can be used to calculate the above quantities for the boson decays.

Let the pion-nucleon interaction be replaced by the phenomenological pseudovector coupling, with the renormalized coupling constant. This seems likely not to falsify qualitative estimates when relatively low momenta and only a single pion-nucleon interaction are involved. If we assume the Feynman-Gell-Mann theory (V-A) for the weak interaction, the pion decay rate will be given by

$$\frac{1}{\tau} = \frac{16 f^2 (M^2 G)^2}{\mu^5 M^2} p^2 \frac{\sqrt{p^2 + m^2} - p}{\sqrt{p^2 + m^2} + p} |k_4 T_4|^2 , \tag{1}$$

where

$f^2 \cong 0.08$,

$M^2 G \cong 10^{-5}$,

μ = pion mass,

M = nucleon mass,

p = muon or electron momentum,

m = muon or electron mass,

with

$\hbar = c = 1$.

It has been assumed that G is the interaction constant for the pseudovector part of the weak interaction, and universality has been assumed, with neglect of renormalization effects. The quantity $1/\tau$ is the partial rate for emission of a lepton of mass m plus a neutrino. As is standard, the assumption of the pseudovector

interaction yields a factor which suppresses the electron mode by about 10^{-4} with respect to the muon mode. The quantity $k_4 T_4$ contains the effect of the closed loop, and conventionally diverges. The quantity k_4 is the fourth component of the momentum-energy four-vector for the pion, with the pion taken at rest for convenience.

In the work to be described, this previously divergent quantity is evaluated as follows:

(2)
$$T = k_4 T_4 = k_\mu T_\mu$$
$$= \frac{1}{16\pi^4 i\epsilon} \int dP \frac{S[(\gamma P + \gamma k + \epsilon M)\, \gamma_5 (\gamma P + \epsilon M)\, \gamma_5 \gamma_k]}{[P^2 - \epsilon^2 M^2][(P+k)^2 - \epsilon^2 M^2]} ,$$

with ϵ set equal to i. If this value is simply inserted in Eq. 2, the conventional divergent integral immediately results. Instead, T is evaluated just above the real axis of $\epsilon(T_+)$ and just below (T_-). The difference is finite:

(3)
$$T_+ - T_- = \frac{Mk^2}{2\pi} \frac{|\epsilon|}{\epsilon} \left[1 - 1 \left(1 - \frac{4\epsilon^2 M^2}{k^2} \right) \sqrt{1 - \frac{4\epsilon^2 M^2}{k^2}} \right] .$$

From this information on the discontinuity possessed by T along the real axis of ϵ, the complete function can be deduced by standard methods of complex-variable theory. For the second term in brackets, Cauchy's theorem suffices if it is assumed that the function possesses no singularities other than the line of discontinuity. For the first term, however, Cauchy's theorem gives a meaningless result because of the singularity at infinity, and, in fact, use of Cauchy's theorem in the obvious way will yield just the logarithmically divergent integral ordinarily encountered. Because of the simple form of the first term in Eq. 3, it can be handled by inspection. The function

(4)
$$f(\epsilon) = \lim_{a \to 0} \frac{i}{2\pi} \log (a^2 - \epsilon^2)$$

clearly has the property

(5)
$$f_+ - f_- = \frac{|\epsilon|}{\epsilon} .$$

This assumes that the logarithm is made analytic by cuts along the real axis from a to ∞ and from $-a$ to $-\infty$. It follows that

(6)
$$f(i) = \lim_{a \to 0} \frac{i}{2\pi} \log (1 + a^2) = 0 ,$$

so that the first term of Eq. 3 does not contribute for $\epsilon \to i$.

The second term is simply evaluated by Cauchy's theorem:

$$T(i) = -\frac{Mk^2}{2\pi}\frac{1}{2\pi i}\int_{-k/2M}^{+k/2M}\frac{d\epsilon}{\epsilon - i}\frac{|\epsilon|}{\epsilon}\sqrt{1-\frac{4\epsilon^2 M^2}{k^2}} \tag{7}$$

$$= -\frac{Mk^2}{4\pi^2 i}\int_0^{k/2M}\frac{2\epsilon\, d\epsilon}{\epsilon^2+1}\sqrt{1-\frac{4\epsilon^2 M^2}{k^2}}$$

$$= \frac{ik^4}{16\pi^2 M}\int_0^1\frac{d\xi}{1+\xi(k^2/4M^2)}\sqrt{1-\xi}\ .$$

The integral is most conveniently approximated by remembering that $k^2 = \mu^2$ and expanding in powers of $(\mu/M)^2$. This yields

$$T(i) = \frac{i\mu^4}{24\pi^2 M}\left[1 + 0\left(\frac{\mu^2}{M^2}\right)\right]\ , \tag{8}$$

where the leading term will suffice.

If now the muon mode is taken for Eq. 1,

$$\frac{1}{\tau} = 0.6\times 10^4\ \text{sec}^{-1}\ . \tag{9}$$

This rate is very much smaller than the experimental value (0.4×10^8 sec^{-1}), and it therefore seems quite possible that a new interaction is needed. In support of this point it should be stated that the formalism used to deduce Eq. 9 yields the observable results of the closed-loop processes in quantum electrodynamics. Again, divergence is avoided, although a finite charge renormalization remains. If indeed the new closed-loop formalism should be valid, it is unfortunately possible that the treatment of the strong interaction by perturbation theory may lead to completely deceptive results, so that no really strong conclusion can be drawn.

If a new weak interaction is postulated to allow pion decay, an essentially unambiguous form can be deduced. The term in the Lagrangian must be

$$\frac{h}{\mu}\frac{\partial\pi}{\partial x_\mu}\left[\bar{\psi}_\mu\gamma_\mu(1+\gamma_5)\psi_\nu\right] + \text{C.C.}\ , \tag{10}$$

where h is dimensionless, and the pion mass is assumed because of the gradient coupling. The correct decay rate for the pion will result if

$$h^2 = 0.9\times 10^{-15}\ . \tag{11}$$

A similar coupling to the electron-neutrino fields is esthetically desirable, but not necessary. It becomes necessary if the suppression ratio for the electron mode should turn out to be about 10^{-4}.

Similar arguments will apparently also hold in the case of the K-particle decay. The closed-loop mechanism for generation of muons will again be inadequate. Economy suggests that an interaction similar

to expression 10 be assumed, with the same dimensionless coupling constant. The term is

$$\frac{h}{m_K}\frac{\partial K}{\partial x_\mu}\left[\bar{\psi}_\mu \gamma_\mu (1+\gamma_5)\,\psi_\nu\right] + \text{C.C.} \tag{12}$$

A corresponding electron interaction can be introduced without conflict and is, in fact, apparently required by the equal strengths of the $\pi\mu\nu$ and $\pi e\nu$ decay modes.

The ratio of decay rates for $\pi_\pm \to \mu_\pm + \nu$ and $K_\pm \to \mu_\pm + \nu$ can be calculated simply, assuming h^2 to be universal. The value is

$$\frac{\tau_\pi}{\tau_K} = 1.43 \tag{13}$$

The experimental value is approximately 1.22, which is perhaps not bad agreement.

Extensions of these ideas to the other strange-particle decays are in progress, the idea of a universal weak boson-fermion interaction which does not conserve strangeness being a possible way of unifying the mass of material now available on lifetimes and branching ratios. If universality is to be assumed, it becomes important to find out whether the new route for conventional nuclear beta decay thus opened up will spoil the present excellent agreement with the universal weak interaction between pairs of fermions. A simple calculation has shown that the contribution to the neutron decay rate from the virtual pion emission followed by decay of the pion is several orders of magnitude below the observed rate, so that there seems to be no overlap between the phenomena which are essentially determined by the usual beta interaction and those which are determined by the new boson-fermion interaction.

ELECTRON-ELECTRON SCATTERING WITH THE SPHERICAL MOMENTUM SPACE FORMALISM

T. A. Welton

As previously reported, a formalism has been devised which allows computation of quantum electrodynamic phenomena with an elegant and apparently consistent introduction of a fundamental length.[1,2] Some difficulty in interpretation was noted which was coupled with the possibility of momentum nonconservation. This ambiguity has been resolved and the formalism applied to calculation of the electron-electron scattering at energies sufficiently high to show up effects from the fundamental length.

With the notation given previously,[2] a five-dimensional Cartesian space was introduced with rectangular coordinates z_1, z_2, z_3, z_4, z_5 $(=z_\mu, z_5)$. The unit sphere

$$z_\mu z_\mu + z_5^2 = 1 \tag{1}$$

---

[1] H. S. Snyder, *Phys. Rev.* 71, 38 (1947); 72, 68 (1947).

[2] T. A. Welton, *Phys. Semiann. Prog. Rep. March 10, 1958*, ORNL-2501, p 1–11.

forms the momentum space of the theory. The quantity κ is a fundamental momentum unit, and its reciprocal is the fundamental length. The usual operators for the coordinate components are replaced by

(2) $$x_\mu = \frac{i}{\kappa}\left(z_5 \frac{\partial}{\partial x_\mu} - z_\mu \frac{\partial}{\partial z_5}\right) ,$$

which satisfy commutation relations that limit the possible accuracy of position measurement. The author previously[2] chose a particular identification of the momentum operators:

(3) $$p_\mu = \kappa z_\mu .$$

This was shown to lead to nonconservation of momentum in the further development of the theory and hence to gross contradictions with observation. A reinterpretation was therefore made at a superficial level, without altering Eq. 3, to repair this difficulty. It now appears that it is best to change Eq. 3. Snyder[1] originally observed that it could be changed to

(4) $$p_\mu = \kappa f(z_5)\, z_\mu$$

without disturbing the elementary properties of the formalism. He preferred $f(z_5) = z_5^{-1}$ rather than $f(z_5) = 1$. This choice is in fact exactly what is needed to guarantee momentum conservation, and it will be adopted without further question.

Previously,[2] forces were introduced as superpositions of possible displacements in the momentum space. Since this space is spherical, these displacements are rotations rather than translations, and all computational work becomes, accordingly, excessively complicated. With the choice $f(z_5) = z_5^{-1}$, however, a new representation of an interaction potential can be used which takes advantage of the fact that in a two-particle collision,

(5) $$p_{1\mu} + p_{2\mu} = p'_{1\mu} + p'_{2\mu} ,$$

where 1 and 2 refer to the two particles and unprimed and primed letters to the initial and final states. It follows that a momentum transfer k_μ can be defined such that

(6) $$p'_{1\mu} = p_{1\mu} + k_\mu ,$$
$$p'_{2\mu} = p_{2\mu} - k_\mu .$$

The components of this momentum transfer can be related to the angles specifying the equivalent rotation, and, finally, the integral over these angles which represents the potential can be replaced by an integral over the four-dimensional quasi-Cartesian space of k_μ. In so doing, the momentum sphere theory is transformed into an equivalent Cartesian theory. This Cartesian theory differs in detail from the usual theory, but all calculations can be carried out by completely conventional means.

In the previous report[2] the four-vector potential is represented by

(7) $$A_\mu(x) = (4\pi^3)^{-1/2} \int dk\, |k|^{-1}\, \mathcal{A}_\mu(k)\, e^{ikx}$$

if $\kappa \to \infty$. For finite κ,

(8) $$A_\mu(x) = (4\pi^3)^{-1/2}\,\kappa^3 \int d\omega\,(\sin\alpha)^{-1}\,\mathcal{A}_\mu(k)\,e^{ikx} \quad ,$$

where e^{ikx} is now a rotation operator, and ω refers to the four angles which specify this rotation:

$$\omega = (\alpha, \beta, \gamma, \delta) \quad ,$$

with

(9) $$d\omega = \sin^3\alpha,\ \sin^2\beta,\ \sin\gamma,\ d\alpha,\ d\beta,\ d\gamma,\ d\delta \quad .$$

The replacement of $|k|^{-1}$ by $\kappa^{-1}(\sin\alpha)^{-1}$, which is clearly correct in the limit of large κ, is intuitively justified on the basis that the function should be well behaved over the sphere, with only the simple pole at $|k| = 0$ (or $\alpha = 0$), which yields ordinary light propagation. It has not yet been possible to completely motivate this choice.

The correct equivalence between k_μ and ω is easily seen to be

(10) $$\begin{aligned} k_1 &= 2\kappa\tan\frac{\alpha}{2}\sin\beta\,\sin\gamma\,\cos\delta \quad , \\ k_2 &= 2\kappa\tan\frac{\alpha}{2}\sin\beta\,\sin\gamma\,\sin\delta \quad , \\ k_3 &= 2\kappa\tan\frac{\alpha}{2}\sin\beta\,\cos\gamma \quad , \\ k_4 &= 2\kappa\tan\frac{\alpha}{2}\cos\beta \quad . \end{aligned}$$

These yield

(11) $$\frac{1}{\kappa\,\sin\alpha} = \frac{1 + k^2/4\kappa^2}{k}$$

and

(12) $$dk_1\,dk_2\,dk_4 = 8\kappa^4\frac{\sin^3\alpha/2}{\cos^5\alpha/2}\sin^2\beta\,\sin\gamma\,d\alpha\,d\beta\,d\gamma\,d\delta \quad .$$

These immediately lead to

(13) $$\frac{\kappa^4\,d\omega}{\kappa^2\,\sin^2\alpha} = \frac{dk}{k^2(1 + k^2/4\kappa^2)^2} \quad .$$

The domain of k integration is the complete, infinite, Cartesian space. It is therefore apparent that the spherical momentum space formalism will yield results identical with those of the ordinary formalism, except for a simple modification of the "photon propagator":

(14) $$\frac{1}{k^2} \to \frac{1}{k^2(1 + k^2/4\kappa^2)^2} \quad .$$

It is of interest to reduce this to a static interaction function by calculating the integral over x_4 of the Fourier inverse of Eq. 14. Thus

$$V(\vec{x}) = \frac{e^2}{4\pi^3} \int_{-\infty}^{\infty} dx_4 \int dk_4 e^{ik_4 x_4} \int d\vec{k} \frac{e^{i\vec{k}\cdot\vec{x}}}{k^2(1 + k^2/4\kappa^2)^2} \tag{15}$$

$$= \frac{e^2}{2\pi^2} \int d\vec{k} \frac{e^{i\vec{k}\cdot\vec{x}}}{|\vec{k}|^2(1 + |\vec{k}|^2/4\kappa^2)^2}$$

$$= \frac{e^2}{r}[1 - e^{-2\kappa r}(1 + \kappa r)] \ .$$

For $\kappa r >> 1$, Eq. 15 becomes just the Coulomb potential, while for $r = 0$ it approaches the finite value $e^2\kappa$, with zero slope.

It is now a trivial job to calculate the electron-electron scattering. The expression is quite complicated at moderately relativistic energies but is of course negligibly different from the conventional Moller scattering until momentum transfers comparable with κ are possible.

On the very reasonable assumption that $\kappa >> m$ and that the electrons are incident on each other with equal and opposite momenta p, the cross section becomes

$$\frac{d\sigma}{d\Omega} = \frac{e^4}{2E^2}\left[\frac{1}{(1 + p^2/\kappa^2 \sin^2\theta/2)^4} + \frac{1}{(1 + p^2/\kappa^2 \cos^2\theta/2)^4} + \right. \tag{16}$$

$$\left. + \frac{1}{\sin^2\theta/2 \cos^2\theta/2\,(1 + p^2/\kappa^2 \sin^2\theta/2)^2\,(1 + p^2/\kappa^2 \cos^2\theta/2)^2}\right]$$

As a possible experiment, consider two electron beams, each of energy 500 Mev. The scattered intensities at $\theta = 45°$ and $\theta = 90°$ are measured, and their ratio R is obtained. The parameter $x = (p/\kappa)^2$ is crucial for determining the expected deviation of R from its value if κ were infinite. It is then convenient to calculate $R(x)/R(0)$ as an indication of the experimental accuracy required to test for the existence of a κ of given size. It seems unlikely that κ is smaller than a nucleon mass M, so that x is conveniently rewritten as $x = (p/M)^2(M/\kappa)^2$, which is approximately $1/4(M/\kappa)^2$. A useful experiment would therefore need to show an effect if $x \leq 1/4$, for the 500-Mev beams. If two 1-bev beams could be produced, the interesting range of x would be $x \leq 1$. The calculated ratios of R values are given below:

x	0.0	0.1	0.2	0.3	0.4	0.6	0.8
$\frac{R(x)}{R(0)}$	1.0000	0.9953	0.9828	0.9648	0.9430	0.8927	0.8389

The proposed Princeton-Stanford experiment corresponds, then, to an effect of less than 3% at best, which is disappointingly small.

COULOMB EXCITATION OF 2^+ STATES IN SELENIUM AND TELLURIUM NUCLEI

F. K. McGowan P. H. Stelson

INTRODUCTION

The previously reported[1] measurements of the weak Coulomb excitation of the second 2^+ state in ten medium-weight even-even nuclei provided information on the $B(E2)$ for decay of the second 2^+ state. The upper cascade $B(E2)$ of Cd^{114} was, within an experimental error of ±25%, twice as large as the $B(E2)$ for the lower cascade transition. The existence of the close-lying triplet of states of 0^+, 2^+, and 4^+, corresponding to the two-phonon quadrupole excitation, seems to be established in Cd^{114}. In addition, the 0^+ and 2^+ members and the 2^+ and 4^+ members of the possible triplet state have been observed in Pd^{106} and Cd^{110}. This information is a confirmation of the prediction of the vibrational model.[2]

The heavy nuclei near platinum also exhibit levels which suggest vibrational motion. However, the previously reported[3] measurements of the Coulomb excitation of the second 2^+ state in Pt^{194}, Os^{192}, and Os^{190} showed that the upper cascade $B(E2)$ for these nuclei was one-third that predicted by the vibrational model. These departures of the upper $B(E2)$'s from the predicted value and the study of the systematics of the known levels in this region suggest that the concept of rather close-lying vibrational triplets may not be appropriate for nuclei in this region.

It is important to have more information on nuclei in the medium-weight region in order to determine the extent and degree of the applicability of the vibrational model. A knowledge of the branching ratio of cascade to crossover from the second 2^+ state and of the $E2/M1$ ratio for the upper cascade transition would be very desirable for the medium-weight nuclei in which the second 2^+ state has been observed in Coulomb excitation. We wish to report some additional measurements of the weak Coulomb excitation of the second 2^+ state in several medium-weight nuclei.

EXPERIMENTAL RESULTS

The detection of the excitation of the second 2^+ state can be accomplished only by coincidence measurements on the cascade gamma rays. In general, the direct observation of the gamma rays in the singles spectrum is limited by the chemical purity of the targets because there are gamma rays from nuclear reactions produced by bombardment of minute amounts of the light-element target impurities. The experimental arrangement of the detectors has been described previously.[1] The A-1D linear amplifiers have been replaced by A-8 linear amplifiers designed by Kelley.[4] With these amplifiers we have been able to use a resolving time 2τ of 0.05 μsec in the fast-slow coincidence system which gated the MC5 analyzer (120 channels).[5]

Se^{76}, Se^{78}, Se^{80}, and Se^{82}. – The first and second 2^+ states in Se^{76}, Se^{78}, and Se^{80} were studied by 8.024-Mev alpha-particle bombardment of targets enriched in these isotopes. A typical coincidence spectrum from Se^{76} is shown in Fig. 1. The peak at 560 kev is the random coincidence peak from the large yield of 560-kev gamma rays resulting from direct excitation of the first 2^+ state. The peak at 660 kev represents the upper cascade gamma ray in coincidence with the 560-kev gamma ray. At this bombarding energy there are about 300 excitations of the first 2^+ state for 1 excitation of the second 2^+ state.

A summary of the results from these measurements is given in Table 1. In the case of Se^{82}, only the first 2^+ state has been studied with a target containing 51.6% Se^{82}. Temmer and Heydenburg[6] have also reported energies and $B(E2)_{exc}$ for the first 2^+ states in Se^{76}, Se^{78}, Se^{80}, and Se^{82}, and our results agree, to within the assigned errors, with

[1] P. H. Stelson and F. K. McGowan, *Phys. Semiann. Prog. Rep. Sept. 10, 1957*, ORNL-2430, p 19; P. H. Stelson and F. K. McGowan, *Bull. Am. Phys. Soc.* **2**, 267 (1957).

[2] G. Scharff-Goldhaber and J. Weneser, *Phys. Rev.* 98, 212 (1955); L. Wilets and M. Jeans, *Phys. Rev.* 102, 788 (1956).

[3] F. K. McGowan and P. H. Stelson, *Phys. Rev.* 106, 522 (1957); F. K. McGowan and P. H. Stelson, *Bull. Am. Phys. Soc.* 3, 228 (1958).

[4] G. G. Kelley, *Phys. Semiann. Prog. Rep. Sept. 10, 1956*, ORNL-2204, p 55.

[5] G. G. Kelley, P. R. Bell, and C. C. Harris, *Phys. Semiann. Prog. Rep. Sept. 10, 1955*, ORNL-1975, p 99.

[6] G. T. Temmer and N. P. Heydenburg, *Phys. Rev.* 104, 967 (1956).

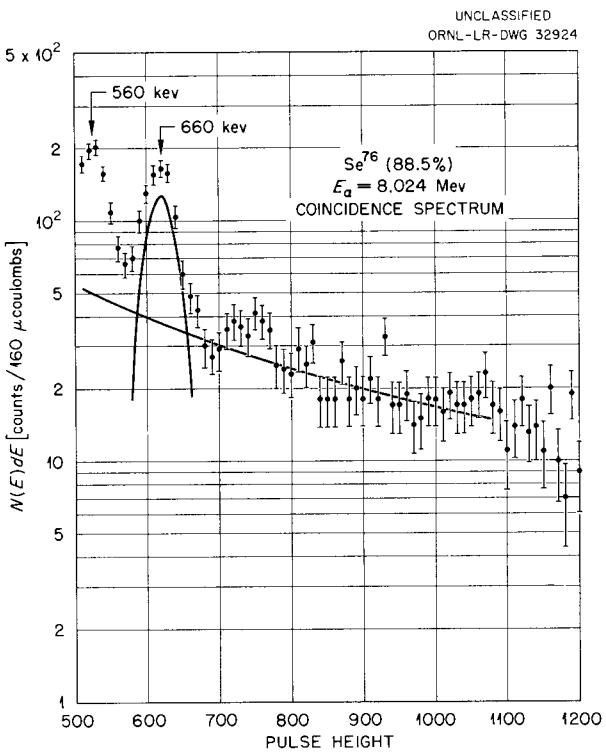

Fig. 1. Coincidence Spectrum from Coulomb Excitation of Se^{76}.

theirs for Se^{76}, Se^{78}, and Se^{80}. In Se^{82} they reported the first 2^+ state to be at 880 kev with a $B(E2)_{exc} = 5.6 \times 10^{-50}$ cm^4, which is 4 to 8 times smaller than the $B(E2)_{exc}$ for the other isotopes of selenium. We believe that they overlooked the 670-kev gamma ray which is obscured to some extent by the superposition of the gamma rays of the other isotopes ($Se^{76,78,80}$) on that of Se^{82}.

Some information[7,8] on the levels in Se^{76} and Se^{78} is available from radioactive decay measurements. The ratio of cascades to crossovers is taken from the radioactive decay work. Since this ratio is not known for the decay of the second 2^+ state in Se^{80}, we have assumed a value of 1.0, which is in accord with the known values for Se^{76} and Se^{78}. A value for $E2/M1$ for the upper cascade transition of Se^{76} is known from gamma-gamma correlation measurements.[9] With this value of 49,

[7] J. D. Kurbatov, B. B. Murray, and M. Sakai, *Phys. Rev.* 98, 674 (1955).

[8] Schram, Polak, Schoo, Girgis, and Van Lieshout, unpublished data (1957), cited by D. Strominger, J. M. Hollander, and G. T. Seaborg, *Revs. Modern Phys.* 30, 585 (1958).

[9] T. Lindqvist and I. Marklund, *Nuclear Phys.* 4, 189 (1957).

Table 1. Summary of Information Obtained from Coulomb Excitation

Nucleus	E_γ (kev)	$B(E2)_{exc}$ (cm^4)	Transition	$B(E2)_d$ (cm^4)	Cascades / Crossovers	$B(E2)_d / B(E2)_{sp}$	$B(E2,2' \to 2) / B(E2,2 \to 0)$
Se^{76}	560 ± 5	$(4.54 \pm 0.41) \times 10^{-49}$	$2 \to 0$	9.08×10^{-50}		47.5	
	660 ± 6		$2' \to 0$	6.28×10^{-50}		32.9	0.69
	1220 ± 8	$(1.48 \pm 0.30) \times 10^{-50}$	$2' \to 0$	2.97×10^{-51}	1.0	1.6	
Se^{78}	612 ± 6	$(3.55 \pm 0.32) \times 10^{-49}$	$2 \to 0$	7.10×10^{-50}		35.9	
	695 ± 7		$2' \to 2$	5.79×10^{-50}		29.2	0.81
	1307 ± 9	$(9.80 \pm 2.0) \times 10^{-51}$	$2' \to 0$	1.96×10^{-51}	1.27	1.0	
Se^{80}	665 ± 7	$(2.58 \pm 0.23) \times 10^{-49}$	$2 \to 0$	5.16×10^{-50}		25.2	
	790 ± 8		$2' \to 2$				
	1455 ± 15	$(1.93 \pm 0.40) \times 10^{-50}$	$2' \to 0$	3.87×10^{-51}	(1.0)	1.9	
Se^{82}	670 ± 10	$(1.99 \pm 0.25) \times 10^{-49}$	$2 \to 0$	3.98×10^{-50}		18.8	
Te^{122}	564 ± 5	$(6.52 \pm 0.52) \times 10^{-49}$	$2 \to 0$	1.30×10^{-49}		36	
	692 ± 7		$2' \to 2$	3.67×10^{-49}		102	2.8 ± 0.7
	1256 ± 9	$(2.14 \pm 0.43) \times 10^{-50}$	$2' \to 0$	4.28×10^{-51}	4.8	1.2	

the exceedingly small value of 3.9×10^{-4} is obtained for $B(M1)_d$. The results from Coulomb excitation and radioactive decay measurements for Se^{76} are also summarized in Fig. 2. For quadrupole vibrations of spherical nuclei, the predicted ratio of $B(E2,2' \rightarrow 2)/B(E2,2 \rightarrow 0)$ is 2.0, and the observed values for Se^{76} and Se^{78} are appreciably smaller. In addition, the crossover transition from the second 2^+ state to the ground state, which is forbidden by the model, competes favorably with the upper cascade transition. Probably these deviations should not be taken as indicating that the model failed but rather that the harmonic oscillator approximation is too much of a simplification to provide an adequate description of the low-lying states in the even-even nuclei.

Te^{122}. – The first and second 2^+ states in Te^{122} were studied by 9- to 10-Mev alpha-particle bombardment of a target containing 81.7% Te^{122}. The branching ratio of cascades to crossovers and the $E2/M1$ for the upper cascade transition are known from radioactive decay measurements.[9–11] Using these branching ratios we are able to determine the $B(E2)_d$ for the upper cascade transition. The ratio $B(E2,2' \rightarrow 2)/B(E2,2 \rightarrow 0)$ is, within experimental error, in agreement with the prediction of the vibrational model. The results are summarized in Table 1. Figure 3 shows a level diagram for Te^{122} in which our results are summarized along with the results from radioactive decay measurements.

[10] M. J. Glaubman, *Phys. Rev.* **98**, 645 (1955).
[11] B. Farrelly *et al.*, *Phys. Rev.* **99**, 1440 (1955).

UNCLASSIFIED
ORNL-LR-DWG 32925R

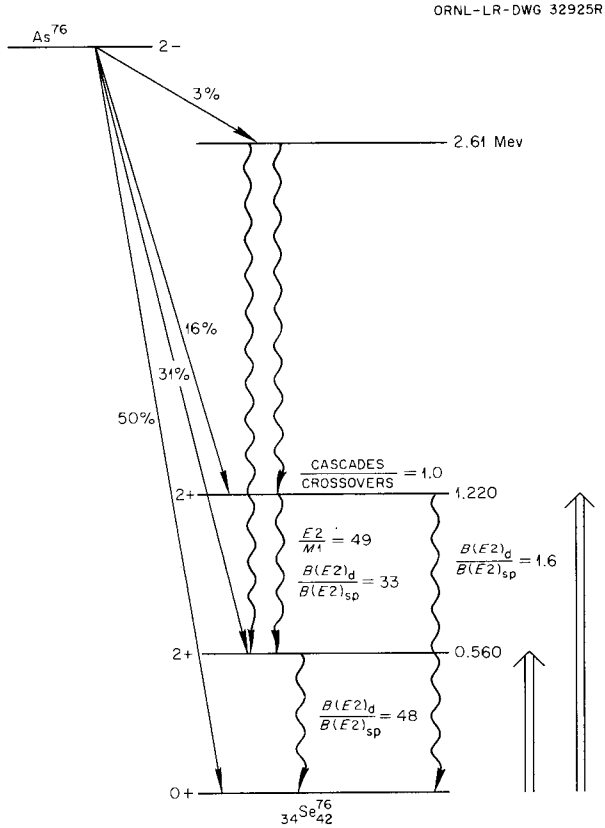

Fig. 2. Level Diagram for Se^{76}.

UNCLASSIFIED
ORNL-LR-DWG 25793R

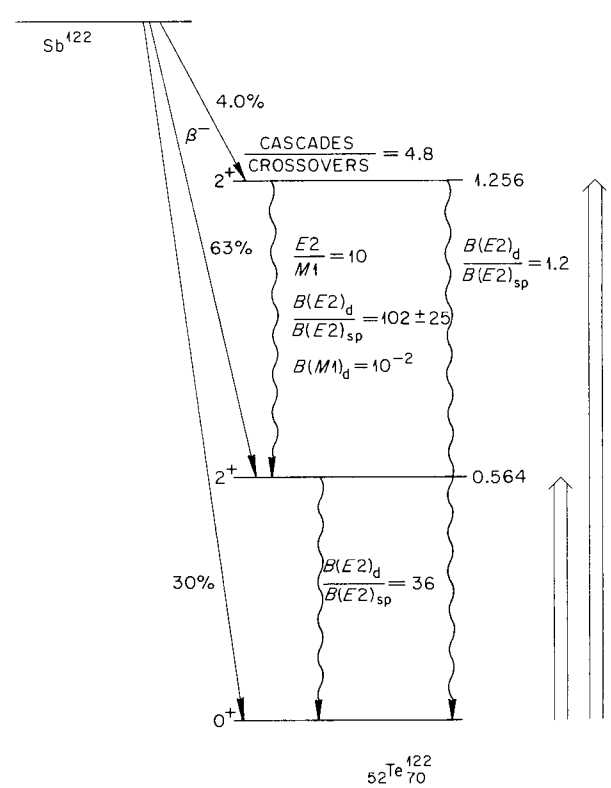

Fig. 3. Level Diagram for Te^{122}.

DIFFERENTIAL ELASTIC NEUTRON SCATTERING FROM BERYLLIUM

H. O. Cohn J. L. Fowler

In the course of an experiment[1] on elastic scattering of neutrons from oxygen, BeO samples were used so that the differential cross section of beryllium was obtained in measuring the background. For these elastic-scattering measurements, the shielded-counter technique was used in detecting the neutrons scattered from cylindrical samples.[1] Tritium gas at about ½ atm pressure was contained in the gas cell with a 0.05-mil nickel window. When bombarded with protons of suitable energy, this arrangement gives neutrons with an energy spread of about 50 kev. The samples of beryllium were cylinders 4½ in. long and 0.45 or 0.63 in. in diameter.

Figure 1 gives the differential cross section at nonresonance energies up to 2.15 Mev. On the right side the total neutron cross section from the literature is plotted against neutron energy. The arrows indicate the energy at which the differential cross sections shown on the left side of the figure were measured. Here the center-of-mass differential cross sections are plotted against cosine of center-of-mass scattering angle. This data has been corrected for multiple scattering in the sample. The large cos ϕ term present in the angular distributions below 1.75 Mev indicates large p-wave phase shifts in the potential scattering. The effects of resonances at higher energies are showing up at 2.15 Mev.

Figure 2 gives the differential cross sections when the energy is increased so as to include resonances around 3 Mev. Again, on the right side, the total cross section of beryllium is plotted against neutron energy. Also shown is the Be(n,α) cross section as

[1] J. L. Fowler and H. O. Cohn, *Phys. Rev.* **109**, 89 (1958).

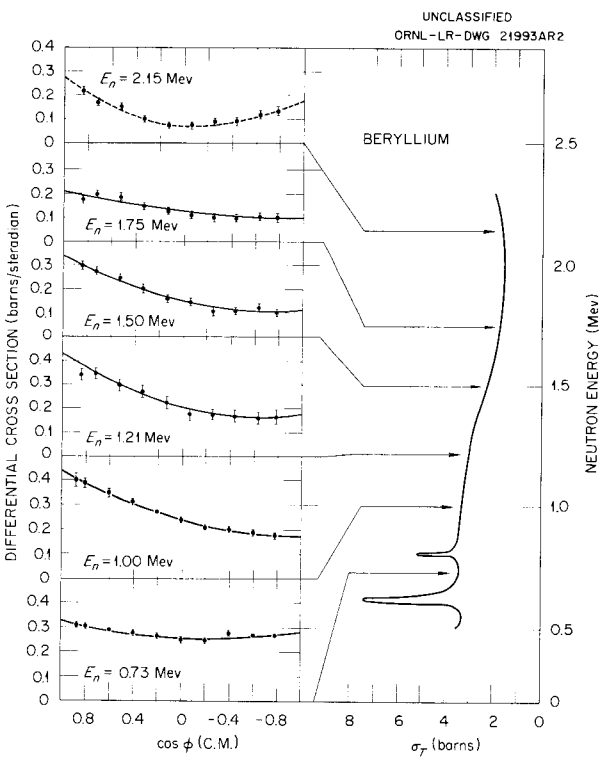

Fig. 1. Center-of-Mass Differential Cross Section of Beryllium from 0.73 to 2.15 Mev.

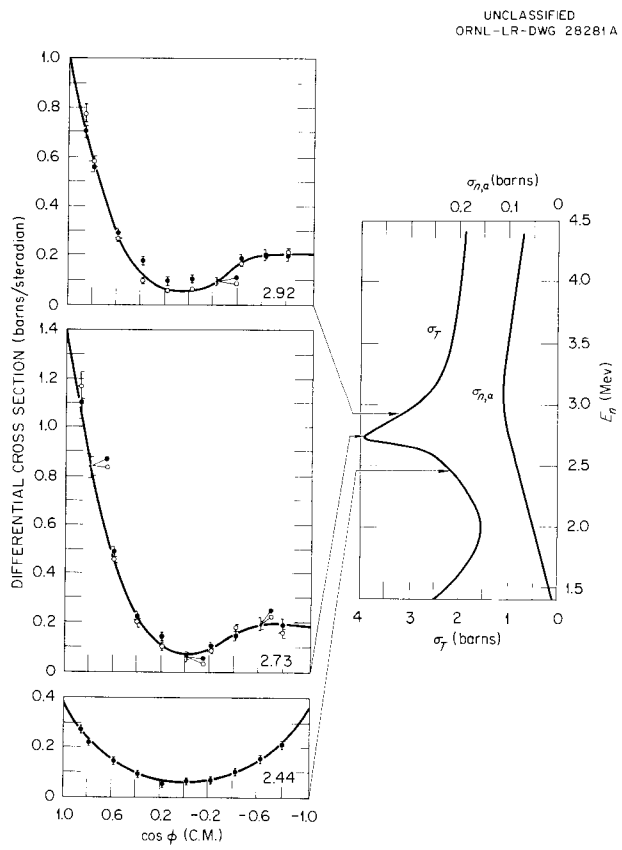

Fig. 2. Center-of-Mass Differential Cross Section of Beryllium in the Vicinity of the Levels Near 3.00 Mev. Closed symbols represent data from 0.63-in.-dia samples; open symbols represent 0.45-in.-dia samples.

measured by Stelson and Campbell.[2] The (n,α) cross section at the peak is about 0.1 barn. As before, the arrows show the energy at which the differential measurements were made. In calculating the multiple-scattering corrections for these data, consideration had to be given to the change in the differential cross section for the neutrons degraded in energy by the first scattering process. For this calculation the sample was considered to be divided into quadrants, and the attenuation of the incident and scattered neutrons was found for each quadrant.

The large asymmetry, about 90° at 2.73 Mev, is characteristic of a p-wave resonance interfering with s-wave potential scattering. At 2.44 Mev the p-wave resonance phase shifts are interfering with the potential scattering p-wave phase shifts, as was beginning to happen at 2.15 Mev, so that only the effect of an even-parity level is showing up. In the energy region covered in Fig. 2 there are two levels – one broad p-wave level and one of even orbital angular momentum, probably d wave. The broad p level at the upper energy is associated with the (n,α) cross section, as an examination of the total and (n,α) cross-section data reveals.

[2]P. H. Stelson and E. C. Campbell, *Phys. Rev.* 106, 1252 (1957).

With this information, the quantum parameters can be fixed. The reactions are

$$\begin{array}{ccccccc}
Be^9 & + & n & \longrightarrow & Be^{10*} & \longrightarrow & Be^9 + n \\
 & & & & \not{\beta}^+ & & \tfrac{3}{2}^- \quad \tfrac{1}{2}^+ \\
 & & & & 2^+ & \searrow & He^6 + \alpha \\
\tfrac{3}{2}^- & & \tfrac{1}{2}^+ & & \not{\gamma}^+ & & 0^+ \quad 0^+ \\
 & & l = 1 & & & & l = 2
\end{array}$$

Intrinsic spins and parities of each nucleus are as indicated. With neutrons where $l = 1$, the parity of the compound state is +. From the two-channel spins 2 and 1, the possible values of total angular momentum are 3, 2, and 1; $J = 0$ is not allowed because the differential cross section in that case would be isotropic. Since the Be^{10*} state decays into He^6 and an alpha particle, both of which have + parity, the parity due to their relative motion must be +, either angular momentum $l = 0$ or $l = 2$. Conservation of total angular momentum allows only the latter; hence $J = 2^+$ for the level at 3.0 Mev.

The conclusion is, therefore, that at 3.0 Mev there is a p-wave level with a full width at half maximum of ~2.5 Mev, corresponding to an even-parity state of total angular momentum $J = 2$. The alpha width is roughly two-tenths of the neutron width or ~ ½ Mev.

$Al^{27}(n,\alpha)Na^{24}$ CROSS SECTION AS A FUNCTION OF NEUTRON ENERGY

H. W. Schmitt J. Halperin[1]

The $Al^{27}(n,\alpha)Na^{24}$ cross section has been measured as a function of neutron energy in the range $6.2 \leq E_n \leq 8.3$ Mev and at 14.8 Mev. The experimental arrangement used in these measurements is shown schematically in Fig. 1. Source neutrons were obtained from the $H^2(d,n)He^3$ reaction with the ORNL 5.5-Mv Van de Graaff generator. Neutrons in a small cone about 0° with respect to the incident charged-particle beam were incident on aluminum metal samples and on a thin deposit of U^{238}. The number of target neutrons incident on the sample was determined by counting fission fragments from the thin fissile deposit in the ionization chamber.

The number of $Al^{27}(n,\alpha)Na^{24}$ reactions occurring during the irradiation was obtained from a subsequent measurement of the gamma activity in the sample due to Na^{24} (half life = 15.0 hr). A 1½ × 2 in. well-type scintillation crystal was used to count the 1.75- and 1.38-Mev gamma rays from the Na^{24} decay. Calibration was accomplished by comparison with a standard calibrated gamma-ray detector. Except for the initial activity (9.5-min half life) due to Mg^{27} formed from the $Al^{27}(n,p)Mg^{27}$ reaction, only the characteristic 15.0-hr decay of Na^{24} was observed.

[1]Chemistry Division.

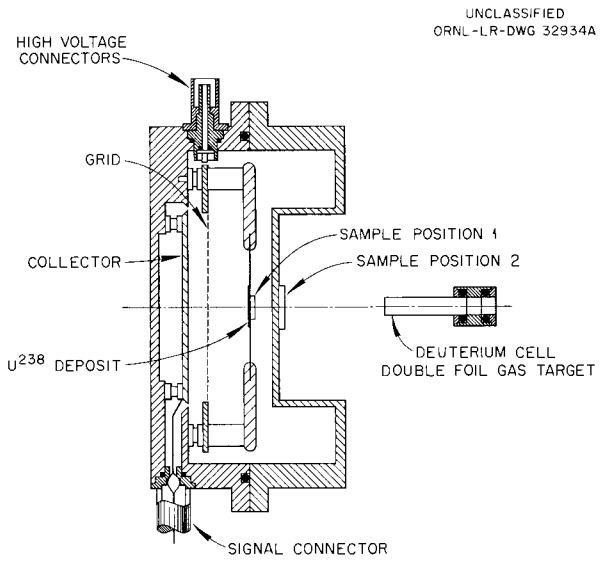

Fig. 1. Experimental Arrangement for Measurement of the $Al^{27}(n,\alpha)Na^{24}$ Cross Section. Aluminum samples were placed in position 1 for experiments 1 and 2, and in position 2 for experiment 3.

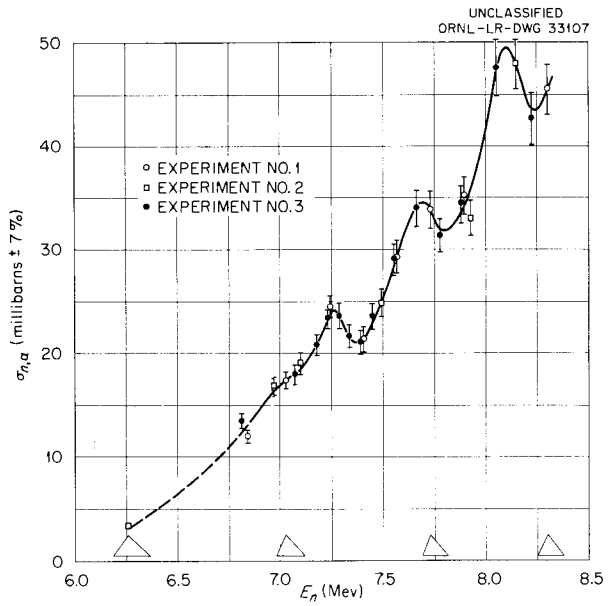

Fig. 2. The $Al^{27}(n,\alpha)Na^{24}$ Cross Section as a Function of Neutron Energy. Bases of the triangles indicate total neutron energy spread, including effects of energy degradation of deuterons in the target and of angular spread of the sample.

The (n,α) reaction cross section was obtained for each neutron energy from the following equation:

$$\sigma_{n,\alpha} = \sigma_f(E_n) \times \frac{n_\alpha}{n_f} \times \frac{\bar{\phi}(U^{238})}{\bar{\phi}(Al)} , \qquad (1)$$

where $\sigma_f(E_n)$ represents the known[2] fission cross section of U^{238}, n_α the number of (n,α) reactions per aluminum atom in the sample, n_f the number of U^{238} fission counts per atom of U^{238}, and $\bar{\phi}(U^{238}$ or Al) the average neutron flux (neutrons·cm^{-2}·sec^{-1}) incident on the U^{238} or the Al. Determination of the ratio $\bar{\phi}(U^{238})/\bar{\phi}(Al)$ in the present experiment was analogous to that of a similar ratio in another experiment and is described in detail in the following section.

The results obtained from these measurements are shown in Fig. 2. Experiments 1 and 2 yielded absolute values of the cross section. Experiment 3 was designed for convenient change of aluminum samples, so that the shape of the curve for cross section vs energy could be readily obtained in detail. Cross-section values obtained from experiment 3 are therefore normalized to the absolute value obtained in experiments 1 and 2.

The peaks observed in the curve for cross section vs energy probably do not represent isolated levels in the compound nucleus, but groups of levels. Similar behavior has been observed previously[3] in a measurement of the $S^{32}(n,\alpha)Si^{29}$ cross section. The general increase in cross section with increasing energy is expected, of course, from penetration of the Coulomb barrier by the alpha particle.

A measurement of the $Al^{27}(n,\alpha)Na^{24}$ cross section at a neutron energy of 14.76 Mev yielded a cross section of 117 ± 7 mb. This value is the weighted mean of four experiments in which various U^{238} monitor foils and various aluminum samples were employed in the apparatus of Fig. 1. This value is in excellent agreement with that obtained by Kern and Kreger[4] at this energy and is consistent with the values obtained by Grundl *et al.*[5] and

[2] R. L. Henkel, *Summary of Neutron-Induced Fission Cross Sections*, LA-2114 (Feb. 25, 1957).

[3] H. W. Schmitt, *Phys. Semiann. Prog. Rep. March 10, 1958*, ORNL-2501, p 22.

[4] Communicated by B. D. Kern, 1958.

[5] J. A. Grundl, R. L. Henkel, and B. L. Perkins, *Phys. Rev.* 109, 425 (1958).

Yasumi[6] at 14.1 Mev. The present result appears to be inconsistent with measurements in this energy region by Forbes[7] and by Paul and Clarke.[8]

[6]S. Yasumi, *J. Phys. Soc. Japan*, 12, 443 (1957).

[7]S. G. Forbes, *Phys. Rev.* 88, 1309 (1952).

[8]E. B. Paul and R. L. Clarke, *Can. J. Phys.* 31, 267 (1953).

The curve of Fig. 2 is generally consistent with recent values obtained by Grundl *et al.*[5] for three neutron energies up to 8.1 Mev. The present results are inconsistent, however, with earlier Los Alamos data (cited in ref 6) giving the shape of the curve for cross section vs neutron energy for energies below about 7.5 Mev.

$Li^6(n,\alpha)H^3$ CROSS SECTION AS A FUNCTION OF NEUTRON ENERGY FROM 1.2 TO 8 Mev

H. W. Schmitt R. B. Murray[1] J. J. Manning[1]

INTRODUCTION

The $Li^6(n,\alpha)H^3$ reaction is convenient for use in neutron spectrometry in the Mev energy range, since both products of the reaction are energetic charged particles (Q = 4.78 Mev) and hence easily detected. The detection efficiency of a neutron spectrometer which makes use of the $Li^6(n,\alpha)H^3$ reaction depends, of course, directly on the cross section of the reaction; hence it is of interest to measure the $Li^6(n,\alpha)H^3$ cross section in detail in the energy range above 1 Mev. Also, there have been fairly extensive theoretical attempts,[2] by means of resonance analysis, to derive theoretical fits to the Li^6 total neutron cross section and to the $Li^6(n,\alpha)H^3$ cross section as a function of neutron energy. In view of some of the existing discrepancies, a detailed knowledge of the (n,α) cross section is of interest.

In the present experiment the $Li^6(n,\alpha)H^3$ reaction cross section was measured by use of an $Li^6I(Eu)$ scintillation crystal to detect the (n,α) events. A discussion of the response of such crystals and their possible use in neutron spectrometry has been presented elsewhere.[3] The principal feature in the present experiment is that, by carrying out pulse-height analysis of pulses from the crystal, distinction can readily be made between those (n,α) events induced by the primary target neutrons and those induced by slow or degraded (e.g., room-scattered) neutrons. The importance of this feature is emphasized by the large thermal cross section (945 barns) for this reaction and, of course, by the general rise in cross section with decreasing energy to thermal energies.

[1]Neutron Physics Division.

[2]For example, J. J. Devaney, *An Analysis of Li^6 Neutron Cross Sections*, LA-1960 (1955); T. I. Kopaleishvili, *Zhur. Eksptl. i Teoret. Fiz.* 33, 788 (1957).

[3]R. B. Murray, *Nuclear Instr.* 2, 237 (1958).

METHOD

The apparatus used in this measurement is shown schematically in Fig. 1. Source neutrons were obtained from the $H^3(p,n)He^3$ and $H^2(d,n)He^3$ reactions with the ORNL 5.5-Mv Van de Graaff generator.

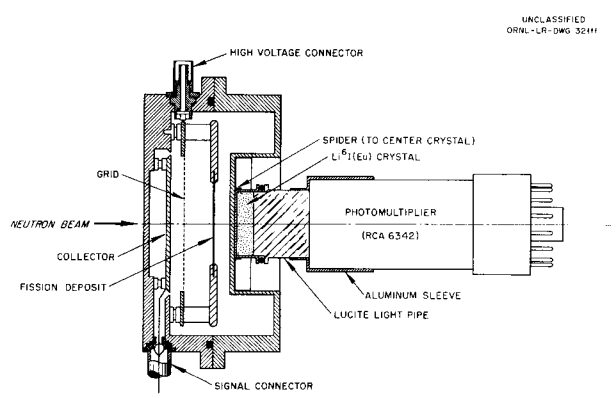

Fig. 1. Schematic Diagram of Experimental Arrangement for Measurement of the $Li^6(n,\alpha)H^3$ Cross Section.

Neutrons emitted in a small cone about 0° with respect to the incident charged-particle beam were used in an essentially back-to-back measurement. Thus a thin cylindrical $Li^6I(Eu)$ scintillation crystal was placed adjacent to and concentric with a thin-walled ionization chamber containing a deposit of fissile material (U^{238} or Np^{237}). Pulse-height analysis of the counts from the crystal permitted a determination of those (n,α) events arising from primary target neutrons. The fast-neutron flux

was determined by counting fission fragments from the thin fissile deposit in the ionization chamber.

The experiment was carried out under a wide variety of conditions. In various runs different geometries were used, also different crystals and fission detectors. A general description has been given in another report;[4] a detailed description of these and other features of the measurement is being prepared for publication.

DATA AND RESULTS

When a U^{238} deposit was used as the fission monitor, the cross section was calculated from the following equation:

$$(1)\quad \sigma_{n,\alpha}(E_n) = \sigma_{\text{fission}}(E_n) \times \frac{(n,\alpha)\ \text{counts}}{\text{fission counts}} \times \frac{\text{mass } U^{238}}{\text{mass } Li^6} \times \frac{\text{at. wt } Li^6}{\text{at. wt } U^{238}} \times \frac{\bar{\phi}(U^{238})}{\bar{\phi}(Li^6)} .$$

In this equation $\bar{\phi}(U^{238})$ represents the average neutron flux (neutrons·cm^{-2}·sec^{-1}) incident on the U^{238} deposit, and, similarly, $\bar{\phi}(Li^6)$ represents the average neutron flux incident on the $Li^6I(Eu)$ crystal. The ratio $\bar{\phi}(U^{238})/\bar{\phi}(Li^6)$ was calculated from the geometry of the experiment and from the published angular distributions[5] of neutrons from the source reactions. Confirmation of the validity of this calculated ratio was obtained from an auxiliary experiment in which the counting rate in the detector was measured as a function of the source-to-detector distance. The calculated and measured counting rates were in excellent agreement.

When an Np^{237} foil was used, an equation similar to Eq. 1 applied. In this case, however, to obtain the absolute value of $\sigma_{n,\alpha}(E_n)$, the absolute value of the neptunium fission cross section was not used. In an auxiliary experiment the fission counting rate from the Np^{237} deposit was determined relative to that of the U^{238} foil by simultaneous counting of fission events in a back-to-back geometry. It can be easily seen that this comparison permits analysis of the data in terms of the known energy dependence of the fission cross sections of U^{238} (ref 6) and Np^{237} (ref 7) and the absolute value of the fission cross section of U^{238} (ref 6) only.

The results obtained from these measurements, shown in Fig. 2, are in very good agreement with the previous work of Ribe[8] and are consistent with recent measurements[9] at Rice Institute extending to 4 Mev. One feature noted in Fig. 2 which has not been explicitly observed previously is the broad hump (or plateau) at 2 Mev. A possible explanation for this effect may be sought in the process of neutron capture to form the Li^7 compound nucleus in a state previously observed[10] at about 9.6 Mev.

---

[4] R. B. Murray, H. W. Schmitt, and J. J. Manning, *Neutron Phys. Ann. Prog. Rep. Sept. 1, 1958*, ORNL-2609, p 145.

[5] J. L. Fowler and J. E. Brolley, Jr., *Revs. Modern Phys.* **28**, 103 (1956).

[6] R. L. Henkel, *Summary of Neutron-Induced Fission Cross Sections*, LA-2114 (Feb. 25, 1957).

[7] D. J. Hughes and R. B. Schwartz, *Neutron Cross Sections*, BNL-325, 2d ed. (July 1, 1958).

[8] F. L. Ribe, *Phys. Rev.* **103**, 741 (1956).

[9] T. W. Bonner, private communication, 1958.

[10] F. Ajzenberg and T. Lauritsen, *Revs. Modern Phys.* **27**, 77 (1955).

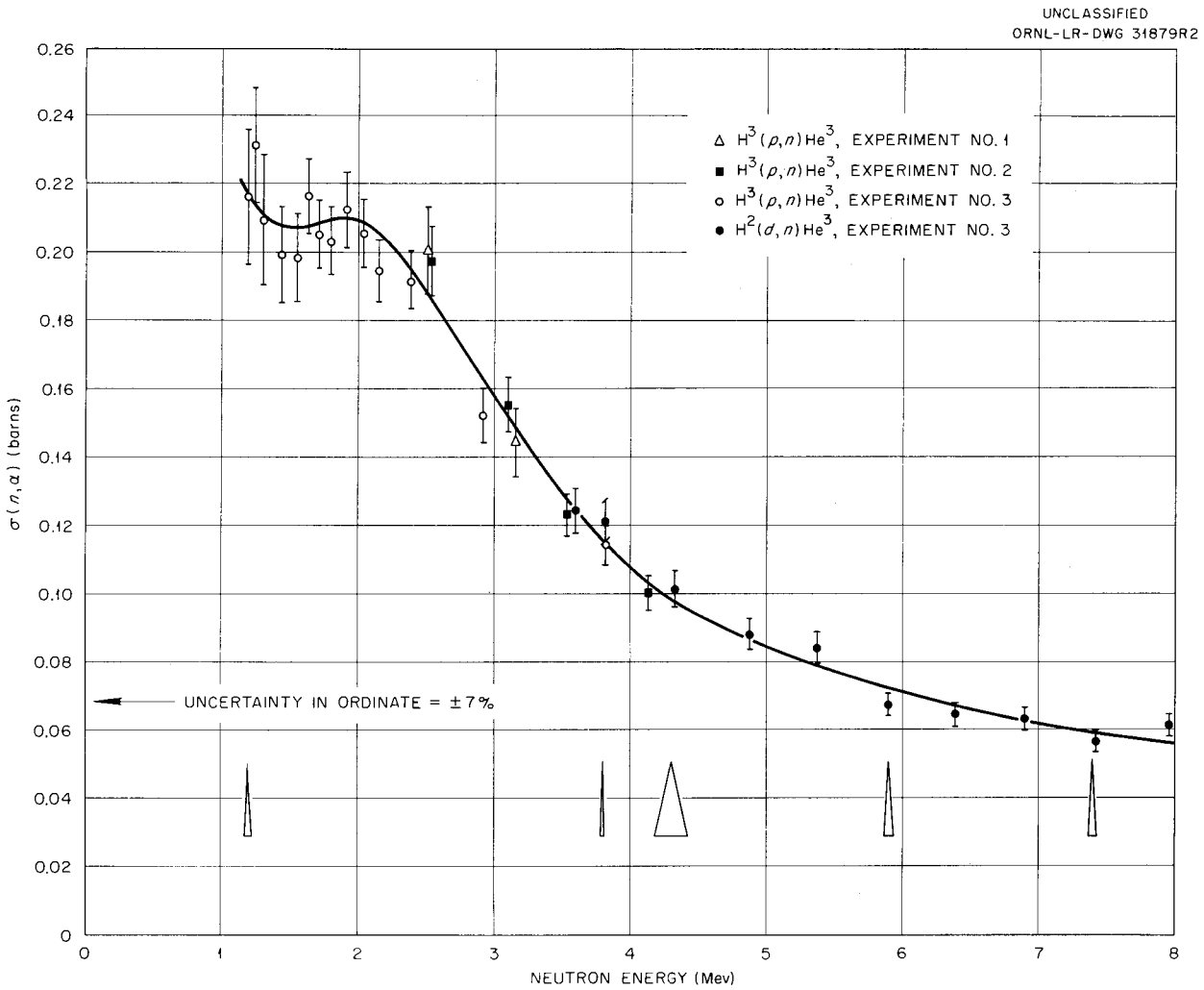

Fig. 2. The $Li^6(n,\alpha)H^3$ Cross Section as a Function of Neutron Energy. Wings on the datum points indicate point-to-point uncertainties (standard deviation); the uncertainty in absolute value of the cross section is ±7%. The bases of the triangles just above the energy axis indicate typical neutron energy spreads.

PULSED VAN DE GRAAFF AND FAST TIME-OF-FLIGHT STUDIES

P. D. Miller
W. M. Good
J. H. Gibbons
R. L. Macklin
J. H. Neiler

The performance of the 3-Mv pulsed Van de Graaff accelerator has continued to improve. The pulser has been modified to accept more of the beam, which has resulted in a better focus at the entrance to the 90° analyzing magnet. This has increased the available beam current by about 25%. With the larger beam currents, flight paths of 3 m have been used for total-cross-section measurements. The present ion source has run for about 300 hr and has shown no signs of deterioration.

An RCL 256-channel analyzer has been installed and has greatly facilitated data-taking. The following features are particularly noteworthy:

1. Provision is made for cathode-ray tube display of the memory contents, so that time spectra may be inspected while they are accumulating.
2. The dead-time correction is made automatically.

3. The contents of the memory are printed out decimally in about 1 min.

4. For qualitative inspections, the contents of the memory may be recorded on a Brown recorder.

The high-voltage supply to the circuits associated with the memory of the analyzer has been stabilized to improve the reliability of the memory. Independent inputs for the four groups of 64 channels have been installed, so that it is now possible to use the analyzer as four 64-channel analyzers for correlation studies, etc.

A paper-punch output unit for the RCL analyzer has been ordered. The punched paper tapes will be in binary form so that they may be used as primary input data for the Oracle.

During the most recent total-cross-section run, Sc^{45}, V^{51}, Fe^{57}, Co^{59}, Cu^{63}, Zn^{66}, Zn^{68}, Ge^{70}, Ge^{72}, Ge^{74}, and Ge^{76} were studied. A number of new resonances were observed, isotopic assignments were made, and previously unresolved levels were split. Energies of the peak cross sections of some of the most prominent of these resonances are given below:

Sc^{45}	3.23, 4.19, 6.55, 7.9, 9.2, 12, 22, 24, 30, 32
V^{51}	6.5
Fe^{57}	3.9, 6.1
Co^{59}	4.9, 8.0, 10.4, 17, 22, 25, 26, 30
Cu^{63}	5.2, 7.6, 10.2, 12.2, 20, 21, 23
Zn^{66}	10.1, 13.5, 18.3
Zn^{68}	18
Ge^{70}	3.3, 5.6, 6.2, 6.6, 8.5, 10.0, 12.7
Ge^{72}	4.9, 9.0, 11.6
Ge^{74}	4.9, 20
Ge^{76}	4.9, 22, 25, 29

The Fe^{57} measurement was a repeat of a previous measurement with a thinner sample. The new peak cross sections compared with those previously reported[1] are given in Table 1. The new measurements indicate that the 3.9-kev level is most likely $J = 0$, in which case its width from an area analysis of the thick-sample data is 0.22 kev. The 6.1-kev level is most likely $J = 1$, indicating a width of 0.42 kev from the thick-sample area analysis. The difficulty encountered in the previous measurement was a result of a poor determination of the background. The 6.1-kev resonance appeared to have a transmission of 4%, whereas when the background was corrected the sample was black. The transmission on the peak of the resonances for the thin sample was about 40%.

Progress is being made on an Oracle program for processing the data. Transmissions and cross sections will be obtained, and the time scale will be converted into an energy scale. The remainder of the data obtained during the July and August run will be processed by the Oracle. Future runs will be facilitated by the acquisition of the punch.

Some preliminary work has been done on measuring neutron capture cross sections by use of a large liquid scintillator. With this equipment two types of operation, illustrated in Figs. 1 and 2, have shown initial success. With the mode of operation illustrated in Fig. 1, higher sensitivity is achieved with less equipment, but only a few neutron energies are available. A typical time spectrum, taken with the equipment set up as in Fig. 1, is shown in Fig. 3. The scintillator tank was biased to accept events corresponding to total gamma-ray energies from 3 to 10 Mev. Figure 4 illustrates a typical time spectrum, taken of a silver sample, obtained with the external collimator. This spectrum was taken before a 4-in. lead shield was added to the tank. The lead shield has reduced the background to the point that σ vs E measurement should be possible with several materials.

[1] W. M. Good, J. H. Neiler, and J. H. Gibbons, *Phys. Semiann. Prog. Rep. March 10, 1958*, ORNL-2501, p 24–26.

Table 1. Parameters of Fe^{57} Resonances

E_0 (kev)	σ_0 Calculated (barns)		σ_0 Observed (barns)	
	$J = 0$	$J = 1$	$n = 2.05 \times 10^{22}$ atoms/cm^2	$n = 0.26 \times 10^{22}$ atoms/cm^2
3.90 ± 0.05	180	540	160	180
6.10 ± 0.05	113	339	115	240

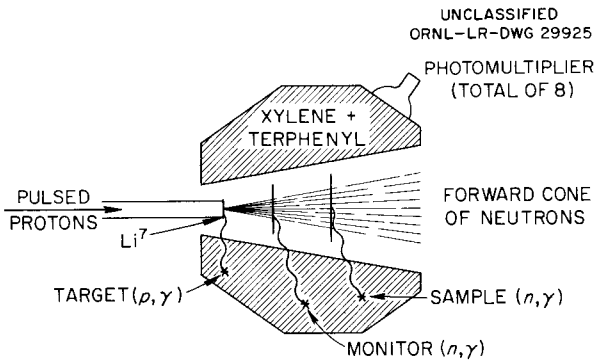

Fig. 1. Threshold Neutron Capture Experiment. The scintillator tank is being used at threshold, utilizing the kinematic collimation of the neutrons.

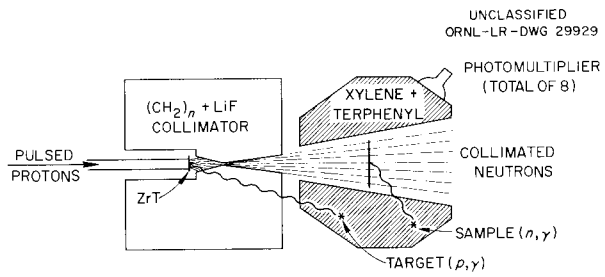

Fig. 2. Externally Collimated Neutron Capture Experiment. The scintillator tank is being used above threshold with a lithium-loaded paraffin collimator.

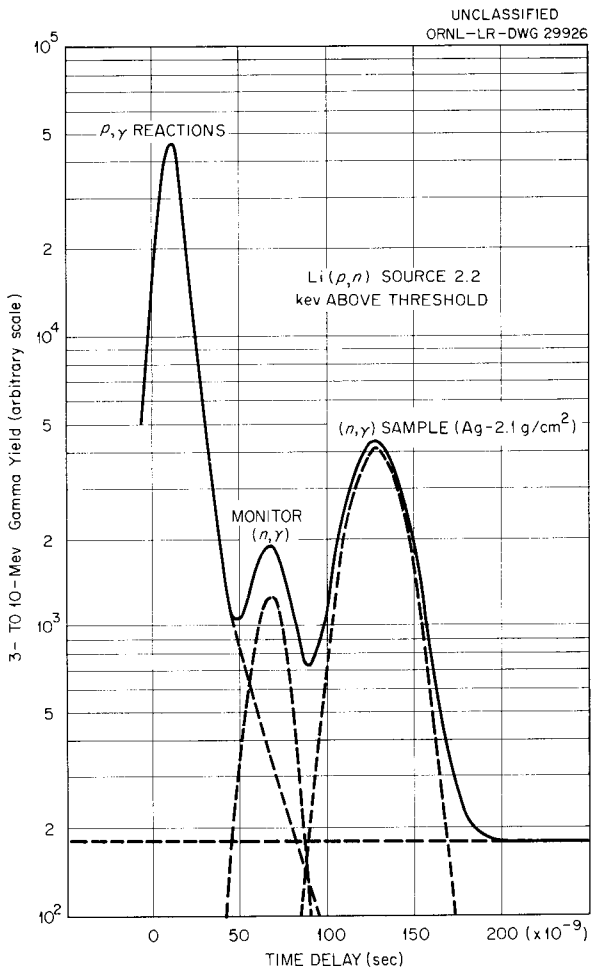

Fig. 3. Time Delay Spectrum for Neutron Capture Experiment. Equipment set up as in Fig. 1. The standard monitor is silver.

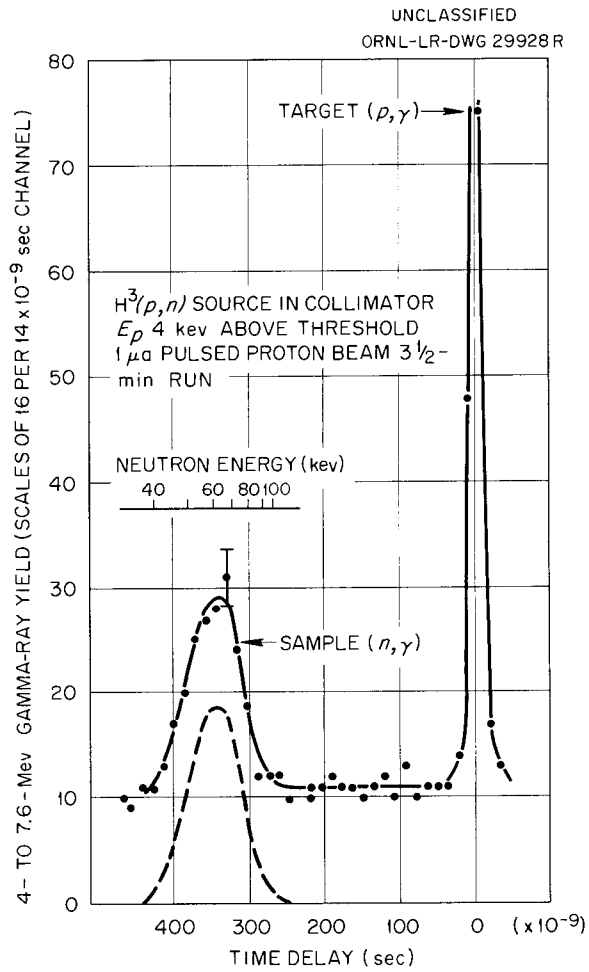

Fig. 4. Time Delay Spectrum from Silver (2.1 g/cm^2) at 116 cm, with the External Collimator as in Fig. 2.

PARAMETERS OF NEUTRON RESONANCES OF Pm^{147}, I^{129}, Zr^{93}, AND Np^{237}

R. C. Block
J. A. Harvey
G. L. Jenkins[1]
G. G. Slaughter
W. J. Martin[2]
G. W. Parker[2]
P. Lantz[2]

The high-intensity, fast-chopper, time-of-flight neutron spectrometer described in the last semiannual report[3] has been used to measure the total neutron cross section of samples of Pm^{147}, I^{129}, Zr^{93}, and Np^{237}. The transmission curves have been analyzed, with the area method of analysis used to obtain the parameters of the resonances.

The samples were all prepared from highly irradiated fuel elements. The promethium was separated from other rare-earth fission products with a resin column. A thin promethium sample (containing ~10 mg of Pm^{147}) was prepared by dissolving $Pm(NO_3)_3$ in D_2O. The total cross section of Pm^{147} obtained from this liquid sample is shown in Fig. 1. Since Pm^{147} decays to Sm^{147} with a 2.52-year half life, resonances were also observed in Sm^{147} as indicated in Fig. 1. The amount of Sm^{147} in the sample was computed from the known parameters of the Sm^{147} resonances. With the date of the last chemical separation from samarium known, the promethium content could be computed and was found to be 47 mg/cm^2. The parameters of the promethium resonances based on a radiation width of 0.070 ev are given in Table 1. The values in the table were determined principally from the data obtained with the liquid sample; however, the data obtained previously[4] with thicker oxide samples have also been considered. These parameters give an average level spacing per spin state of 8 ± 2 ev and a strength function ($\overline{\Gamma}_n^0/D$) of $(4.2 \pm 1.2) \times 10^{-4}$.

The fission product iodine was obtained from the off-gas from plutonium production. The transmission of two fission product iodine samples has been measured, and several resonances have been assigned to I^{129}. Figure 2 shows the transmission in the energy range 171 to 41.4 ev of a sample containing 3.03 g/cm^2 of iodine which contained 71% I^{129} and 29% I^{127}. The parameters derived for these resonances are in good agreement with previously reported[3] measurements on natural iodine. A thinner sample containing 0.97 g/cm^2 of fission product iodine was also measured, and most of the resonances seen with the thick sample were observed. The energy region from 2 to 42 ev was measured with the thick sample, but only the three resonances in I^{127} were observed. The parameters of the resonances in I^{129} derived from area analysis of the two transmission curves are given in Table 1. The average level spacing per spin state and the $\overline{\Gamma}_n^0/D$ ratio computed from these parameters up to 170 ev

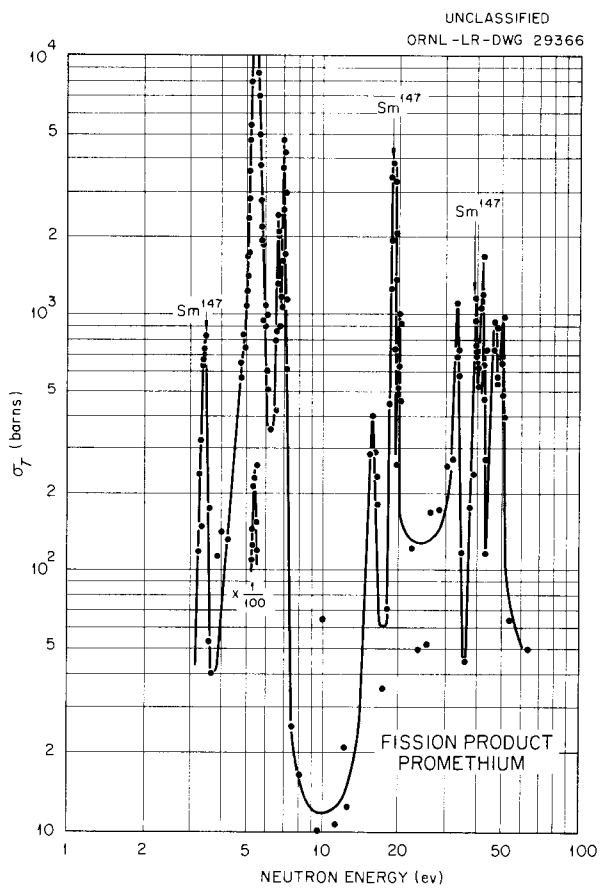

Fig. 1. Total Cross Section of Fission Product Promethium.

[1]Research participant, Stetson University.

[2]Chemistry Division.

[3]G. G. Slaughter, R. C. Block, and J. A. Harvey, *Phys. Semiann. Prog. Rep. March 10, 1958*, ORNL-2501, p 26–28.

[4]J. A. Harvey, R. C. Block, and G. G. Slaughter, *Phys. Semiann. Prog. Rep. Sept. 10, 1957*, ORNL-2430, p 32.

Table 1. Neutron Resonance Parameters of Pm^{147*} and I^{129**}

Pm^{147} [a]			I^{129} [a]		
E_0 (ev)	$2g\Gamma_n$ (10^{-3} ev)	$2g\Gamma_n^0$ (10^{-3} ev)	E^0 (ev)	$2g\Gamma_n$ (10^{-3} ev)	$2g\Gamma_n^0$ (10^{-3} ev)
1.04	0.0055	0.0054	66.2	0.9 ± 0.5	0.11
5.43	33 ± 3	14.2	72.4	16 ± 2	1.9
6.64	1.5 ± 0.2	0.58	95.6	1.2 ± 0.6	0.12
7.00	4.4 ± 0.4	1.7	129	3.0 ± 1.0	0.26
15.6	2.0 ± 0.6	0.5	149	90 ± 20	7.4
20.0	3.7 ± 0.7	0.8	154	25 ± 5	2.0
33.4	9 ± 2	1.6			
41.4	60 ± 20	9.5			
43.2	8 ± 4	1.2			
46.6, 47.8	50 ± 15	7.3			
50.3	40 ± 15	5.6			

[a] Based on $\Gamma_\gamma = 0.070$ ev.
[b] Based on $\Gamma_\gamma = 0.10$ ev.

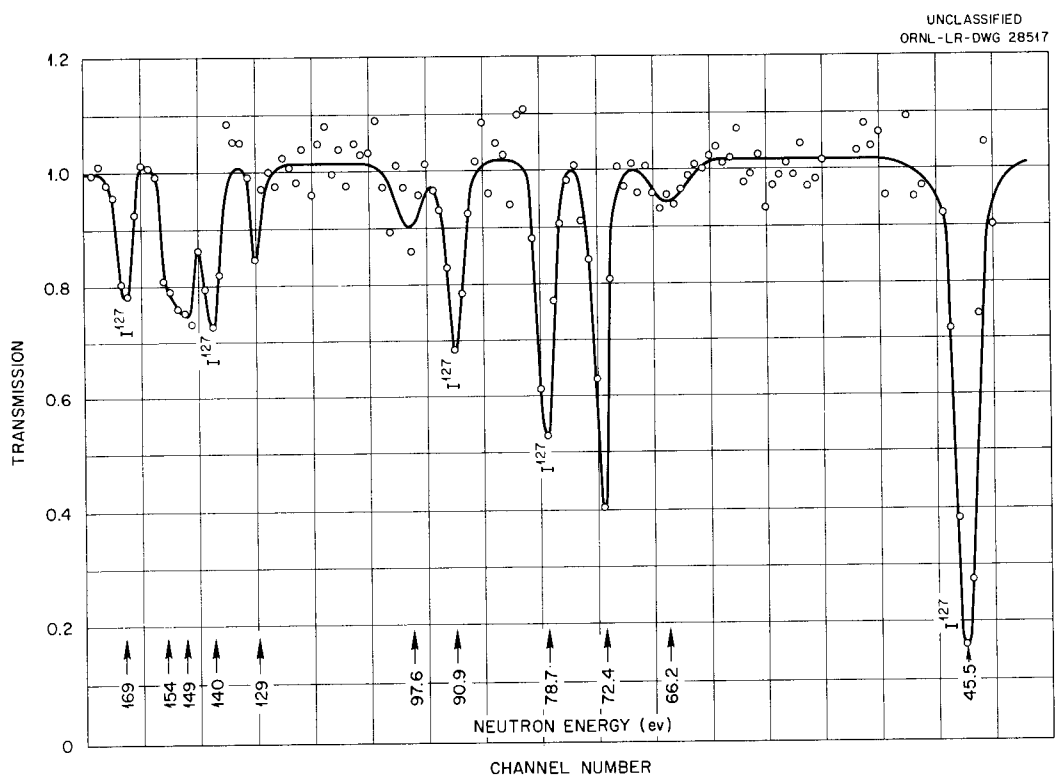

Fig. 2. Transmission of I^{129}.

are 55 ± 20 ev and (0.4 ± 0.2) × 10^{-4}, respectively. This strength function is about a factor of 3 smaller than that of I^{127}.

Fission product zirconium and Np^{237} were obtained from Hanford-irradiated slugs. The fission product zirconium was chemically separated from other fission products, and approximately 260 mg of ZrO_2 containing 38.8 mg of Zr^{93} and 35.9 mg of Zr^{91} was obtained for cross-section measurements. The transmission of fission product zirconium was investigated up to 1000 ev with a sample of zirconium having a thickness of 0.74 g/cm^2. Only two resonances were observed; a resonance at 298 ev with a Γ_n of 1.1 ev is assigned to Zr^{91}, and the resonance at 110 ev with a Γ_n of 0.27 ev is assigned to Zr^{93}.

The Np^{237} was recovered from the fission products by solvent extraction. Two samples of NpO_2 were used, one of which contained 4.84 g/cm^2 and the other 0.860 g/cm^2 of neptunium. With these samples, 32 resonances were found in the energy range 0.2 to 36 ev. A liquid sample of $Np(NO_3)_5$ in D_2O containing 0.0880 g/cm^2 of neptunium was also prepared for measuring the strong resonances. Parameters for the resonances are given in Table 2, based on a Γ_γ of 0.032 ev. The level spacing per spin state is 1.5 ± 0.3 ev, considering the resonances up to 12 ev. The strength function is (1.1 ± 0.2) × 10^{-4}, based on the resonances up to 24 ev.

Table 2. Neutron Resonance Parameters of Np^{237}

(Based on Γ_γ = 0.032 ev)

E_0 (ev)	$2g\Gamma_n$ (10^{-3} ev)	E_0 (ev)	$2g\Gamma_n$ (10^{-3} ev)
0.489	0.032 ± 0.002	12.68	0.73 ± 0.09
1.328	0.029 ± 0.012	16.14	1.14 ± 0.14
1.486	0.11 ± 0.02	16.95	0.28 ± 0.05
1.981	0.018 ± 0.003	17.65	0.23 ± 0.05
3.885	0.28 ± 0.02	19.22	1.5 ± 0.3
4.283	0.033 ± 0.004	20.50	1.9 ± 0.4
4.895	0.040 ± 0.004	21.24	0.7 ± 0.2
5.816	0.65 ± 0.07	22.09	1.9 ± 0.4
6.41	0.11 ± 0.02	23.00	0.4 ± 0.2
6.764	0.0009 ± 0.0006	23.82	3.1 ± 0.8
7.46	0.17 ± 0.02	25.13	5.5 ± 1.1
8.356	0.103 ± 0.014	26.64	4.8 ± 0.9
9.036	0.07 ± 0.04	28.83	0.4 ± 0.3
9.372	0.54 ± 0.09	30.80	6.1 ± 1.5
10.97	5.3 ± 0.8	33.90	1.7 ± 0.7
12.25	0.05 ± 0.02	35.12	0.9 ± 0.5

ABSOLUTE (p,n) CROSS SECTIONS FOR LIGHT NUCLEI

J. H. Gibbons R. L. Macklin

The efficiency of the graphite-sphere neutron detector[1] is independent of neutron energy for 1 kev $< E_n < 2$ Mev; also, for neutrons produced near the center of the sphere, the efficiency is independent of neutron emission angle. These two properties have made the sphere useful in measuring (p,n) and (α,n) total cross sections. The determination of average target thickness has usually been straightforward, but in the case of T_2 has proved to be particularly troublesome. In our most recent redetermination, high-purity tritium was transferred directly to a uranium oven, and samples taken from it and from the target during the neutron yield measurements were analyzed mass spectrometrically by Savannah River and Los Alamos Laboratories for contamination. The results are given in Table 1.

The last column in the table represents the calculated tritium content at the time that the neutron yield was measured, and differs from the measured tritium percentage by the tritium decay before analysis and the indicated air in-leakage to the sample. The second sample was taken in a stainless steel container baked in vacuum and then pretreated for several hours with tritium before being used. The last three samples were taken in glass containers simply baked out under vacuum. The good reproducibility of the glass samples indicates a consistent sampling procedure and a lack of contamination (<0.5%) by the target cell. The disagreement between the second sample and the last three is consistent with hydrogen exchange somewhere in the sampling procedure. The disagreement between the first two samples is attributable either to this mechanism or to contamination by the uranium oven (or both). Because of the uncertainties in the gas purity we must assign an error of 10% to the absolute values of our $H^3(p,n)$ cross sections (Fig. 1) and the $He^3(n,p)$ cross sections (Fig. 2) derived from them by reciprocity.

The $H^3(p,n)$ data now disagree with the earlier Los Alamos values (see Fig. 2) but are in close agreement with recent integrated angular distributions.[2] The $He^3(n,p)$ values likewise disagree with the early Los Alamos values[3] but agree to about 7% with the Harwell data.[4]

The $C^{14}(p,n)N^{14}$ cross-section measurements have been extended to the first excited state of N^{14} (Fig. 3). The cross section has been normalized to previous work.[5] The $N^{14}(n,p)$ cross section derived by reciprocity is compared with direct measurements[6] in Fig. 4. Allowing for a slight difference in resolution, the agreement is satisfactory.

[1] R. L. Macklin, *Nuclear Instr.* 1, 335 (1957).

[2] J. E. Perry, private communication.

[3] J. H. Coon, *Phys. Rev.* 80, 488 (1950).

[4] R. Batchelor, R. Aves, and T. H. R. Skyrme, *Rev. Sci. Instr.* 26, 1037 (1955).

[5] R. M. Sanders, *Phys. Rev.* 104, 1434 (1956).

[6] C. H. Johnson and H. H. Barschall, *Phys. Rev.* 80, 818 (1950).

Table 1. Gas Analysis of Tritium Samples

Major Constituents	Analysis (at. %)				
	Initial*	Uranium Oven*	Target** A	Target** B	Uranium Oven**
Hydrogen	0.58	18.36	10.07	9.95	10.59
Deuterium	0.06	0.19	0.08	0.10	0.08
Tritium	99.24	80.50	88.25	88.73	87.46
Helium-3		0.62	1.57	1.21	1.21
Air	0.11	0.06	0.03		0.63
Tritium at sampling time		81.0	88.8	89.3	88.9

*Savannah River.

**Los Alamos.

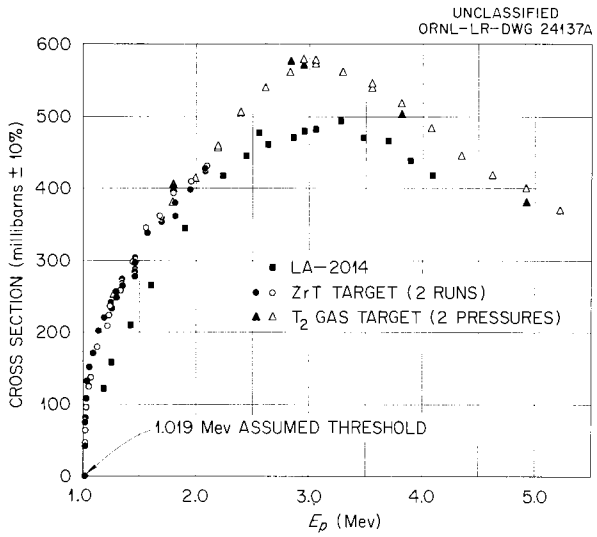

Fig. 1. The $H^3(p,n)He^3$ Cross Section as a Function of Laboratory Energy.

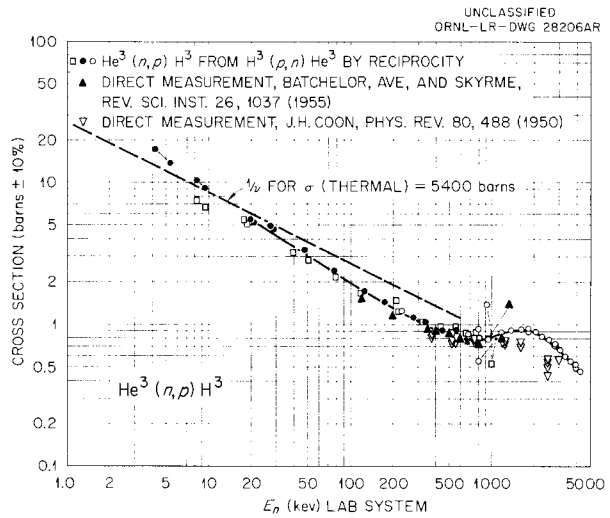

Fig. 2. The $He^3(n,p)H^3$ Cross Section as a Function of Laboratory Energy.

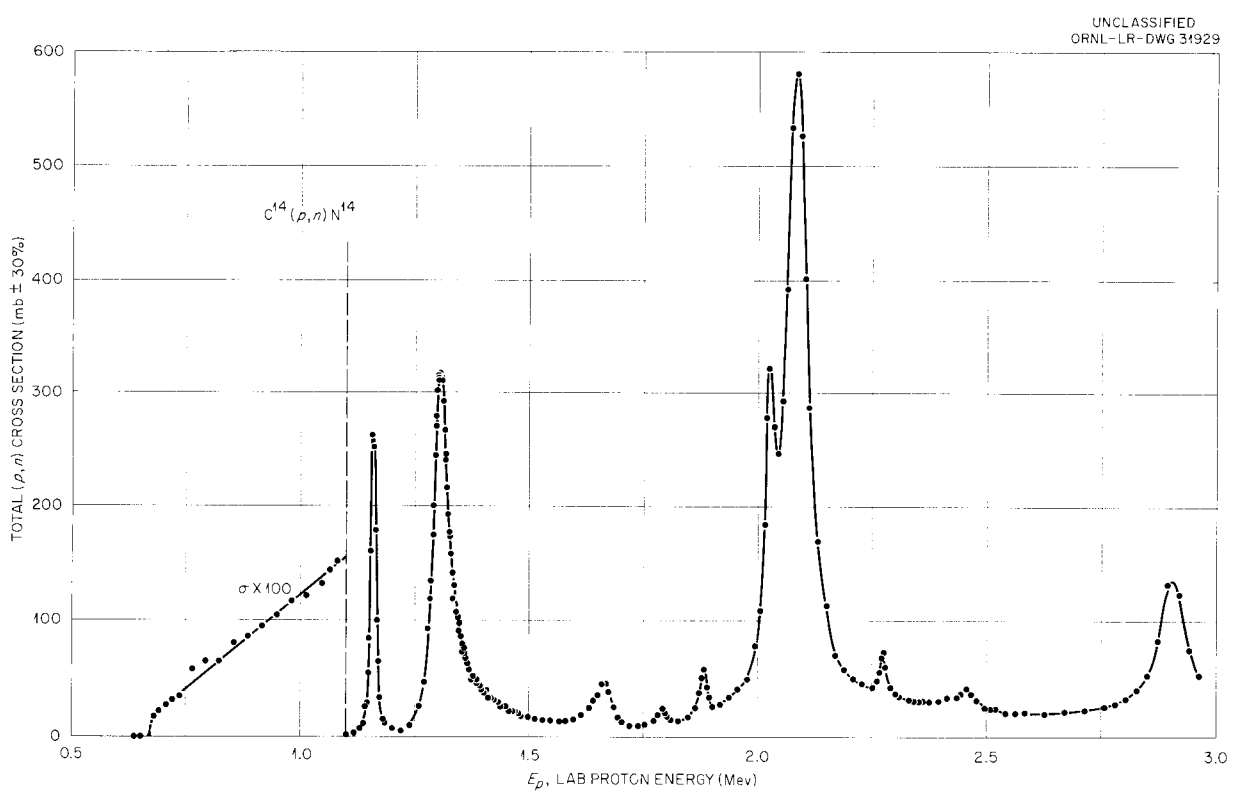

Fig. 3. The $C^{14}(p,n)N^{14}$ Cross Section as a Function of Laboratory Energy. The cross-section scale is normalized at the peak of the 1314-kev resonance.

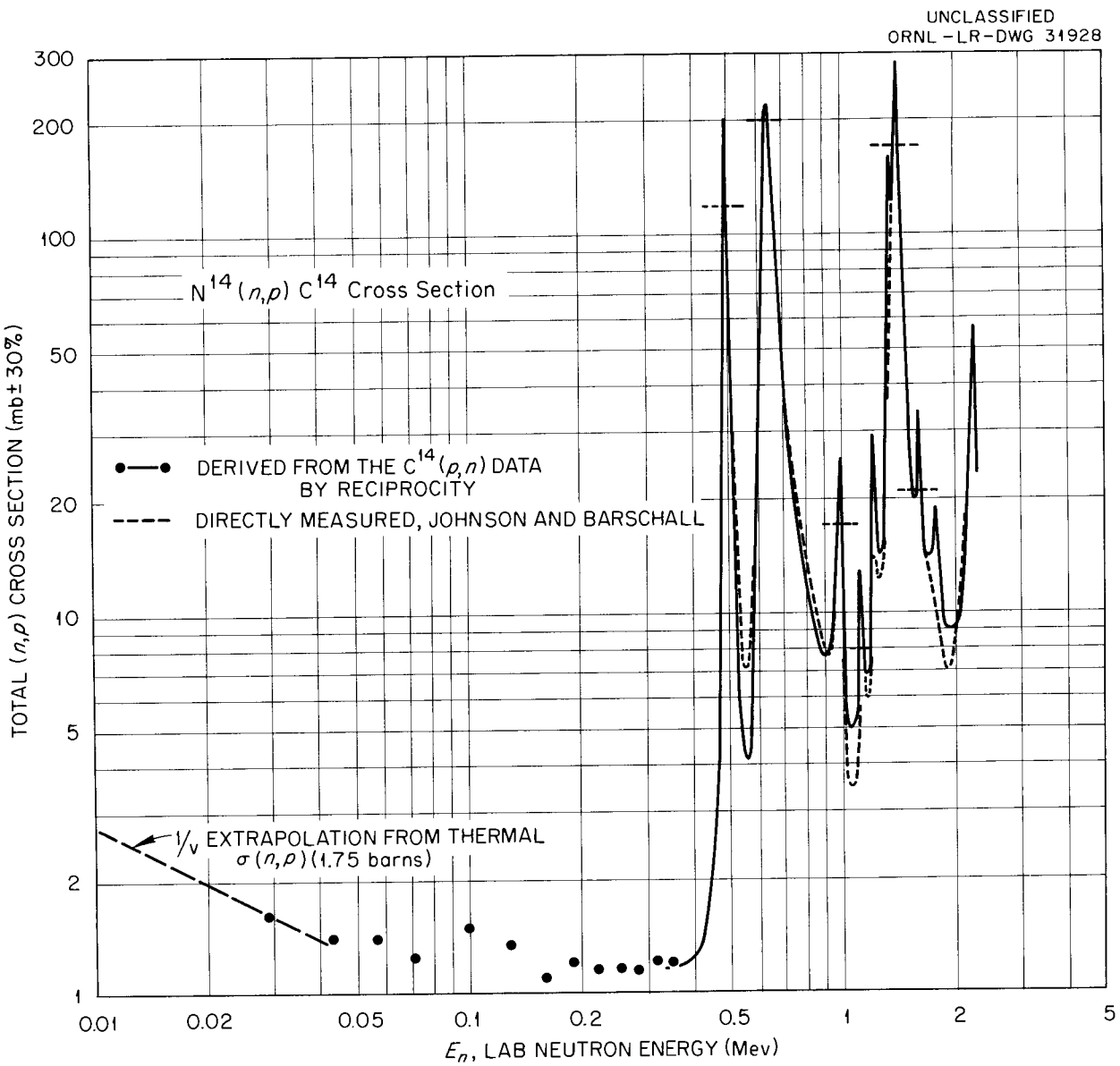

Fig. 4. The $N^{14}(n,p)C^{14}$ Cross Section as a Function of Laboratory Energy.

ANTIFERROMAGNETISM IN $CrCl_3$ AND $FeCl_3$

J. W. Cable M. K. Wilkinson E. O. Wollan

INTRODUCTION

Anhydrous $CrCl_3$ and $FeCl_3$ crystallize in slightly different modifications of a hexagonal layer type of structure in which the metal-ion layers are separated by two layers of chloride ions. In such a lattice there are two anion sites for each cation site, so that in these salts one-third of the cation lattice sites are vacant. In the $CrCl_3$ structure the anions are in a cubic close-packed arrangement, resulting in a staggering of the cation positions such that three metal layers are required for repetition along the c axis. In $FeCl_3$ the anions are hexagonally close-packed, and the cations in adjacent layers are directly above each other. However, three metal layers are again required for repetition because of the arrangement of the vacancies in the lattice sites.

Recently, Henry, Griffel, and Hansen[1] have concluded from their magnetic data that $CrCl_3$ becomes ferromagnetic at low temperatures. However, Starr, Bitter, and Kaufmann[2] found that $CrCl_3$ has the same type of anomalous magnetic properties as those exhibited by the dichlorides of iron, cobalt, and nickel: (1) the paramagnetic susceptibility follows the Curie-Weiss law, $\chi = c/(T - \theta)$, with a positive θ, (2) the susceptibility shows a large field dependence, (3) there is no spontaneous magnetization, (4) there are no hysteresis effects, and (5) there are susceptibility maxima at temperatures corresponding to lambda-type anomalies in the specific-heat curves. The first two are characteristic of ferromagnetism, while the last three are usually associated with antiferromagnetism. A neutron diffraction study[3] of $FeCl_2$ and $CoCl_2$ has shown that the magnetic structure consists of ferromagnetic alignment of the moments within the hexagonal layers and a relatively weak antiferromagnetic coupling between the layers and that the magnetic properties are consistent with such a structure. It was expected that the same ordering would be found in $CrCl_3$.

Starr, Bitter, and Kaufmann[2] also studied $FeCl_3$ and found that it exhibits a magnetic behavior somewhat similar to that of $MnCl_2$. This is not surprising since the crystal structures are similar and the magnetic ions have the same electronic configurations. The magnetic susceptibility follows the Curie-Weiss law from room temperature to 13.9°K, with a negative Weiss constant indicating a predominant antiferromagnetic interaction. It was expected that $FeCl_3$ would order antiferromagnetically at helium temperatures with a complex moment arrangement of the type found in $MnCl_2$ (ref 4) and $MnBr_2$ (ref 5).

This report is concerned with the results of a preliminary investigation of the neutron scattering from polycrystalline $CrCl_3$ and $FeCl_3$.

EXPERIMENTAL RESULTS

$CrCl_3$. – The sample was prepared by vacuum sublimation of the commercially available anhydrous material. The sublimate was passed through a 100-mesh screen, sealed in a thin-walled cylindrical aluminum cell in a helium atmosphere, and mounted in the low-temperature cryostat of the magnet spectrometer. Diffraction patterns were taken at sample temperatures of 78 and 4.2°K. The 78°K pattern contains the Bragg reflections for nuclear scattering as calculated from the known crystal structure. The magnetic scattering is incoherent and shows up as an angularly dependent diffuse background. At 4.2°K, additional coherent scattering is observed at superlattice positions and is accompanied by a decrease in the paramagnetic scattering. This is shown in Fig. 1, which is a 4.2 – 78°K difference pattern. The negative background represents the decrease in paramagnetic scattering after the moments have ordered and corresponds to a magnetic moment of 3.10 ± 0.40 Bohr magnetons per chromium ion. This is in good agreement with the spin-only

[1] W. E. Henry, M. Griffel, and W. N. Hansen, paper presented at "Conference on Magnetism and Magnetic Materials," Pittsburgh, Pennsylvania, June 1955.

[2] C. Starr, F. Bitter, and A. R. Kaufmann, *Phys. Rev.* 58, 977 (1940).

[3] M. K. Wilkinson, J. W. Cable, E. O. Wollan, and W. C. Koehler, "Neutron Diffraction Investigations of the Magnetic Ordering in $FeBr_2$, $CoBr_2$, $FeCl_2$, and $CoCl_2$," *Phys. Rev.* (in press).

[4] M. K. Wilkinson *et al.*, *Phys. Semiann. Prog. Rep. Sept. 10, 1957*, ORNL-2430, p 65.

[5] E. O. Wollan, W. C. Koehler, and M. K. Wilkinson, *Phys. Rev.* 110, 638 (1958).

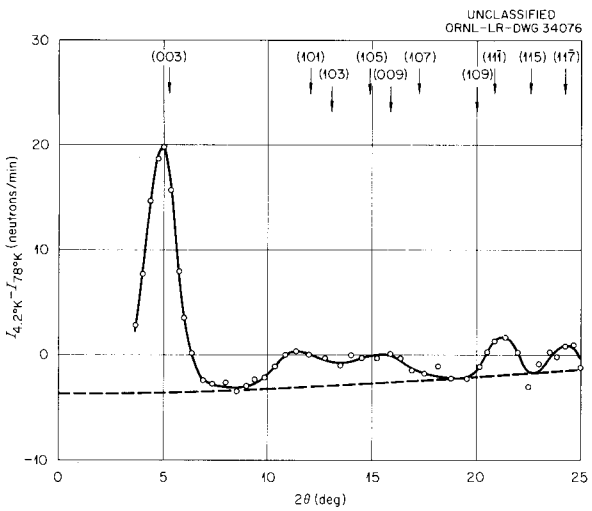

Fig. 1. Temperature Difference Pattern (4.2 – 78°K) for $CrCl_3$.

value of 3.00 reported in the previously mentioned magnetic investigation.[1] The indices are based on a hexagonal cell (with the same *a* axis but twice the *c* axis of the chemical unit cell) corresponding to ferromagnetic ordering of the moments within a layer and antiparallel alignment between layers. Qualitatively, the pattern is consistent with the model, but the resolution and intensities of the reflections are such that the model cannot be firmly established.

In order to enhance the intensities, a pressed rod of $CrCl_3$ was prepared. The powder was pressed in a cylindrical die at 5000 psi and then subjected to a hydrostatic pressure of 50,000 psi, resulting in a cylindrical rod with a packing density of 0.95. The rod was sealed in an aluminum cell and mounted with a heater coil and thermal impedance between the sample and the helium bath, and a calibrated copper-constantan thermocouple was used to measure the sample temperature. The intensity of the largest magnetic reflection exhibited the usual Brillouin type of temperature dependence with a transition temperature of 17 ± 1°K. This shows that the lambda-type anomaly at 16.8°K in the specific heat data[6] is associated with the transition to the antiferromagnetic state. Neutron patterns were also obtained for this pressed sample at temperatures of 298, 43, and 4.2°K. Here again the data are consistent with the model but are insufficient for a good determination of the magnetic structure. An attempt is now being made to grow a single crystal of $CrCl_3$ for a continuation of this study.

$FeCl_3$. – The powder sample was prepared in the same manner as the $CrCl_3$ sample. Neutron patterns were obtained at several temperatures from room temperature to 1.3°K. Coherent magnetic scattering indicative of antiferromagnetic ordering was observed at helium temperatures, and this is shown in the 4.2 – 298°K difference pattern of Fig. 2. The room-temperature paramagnetic scattering represented by the negative background corresponds to a moment of 4.75 ± 0.60 Bohr magnetons, in satisfactory agreement with the expected spin-only value of 5 for the Fe^{++} ion.

The temperature dependence of the largest magnetic reflection was taken by means of the same heater coil arrangement as in the $CrCl_3$ case. The data, corrected for the temperature variation of the paramagnetic and short-range-order background, are shown in Fig. 3, and exhibit a Brillouin-type dependence. The transition temperature of 16°K corresponds to the onset of long-range antiferromagnetic order. Above 16°K the Bragg reflection is replaced by a broad diffuse peak which persists at temperatures up to 43°K. This type of critical

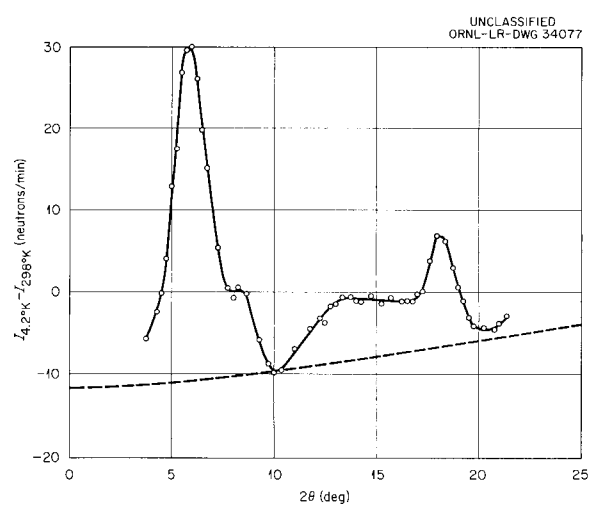

Fig. 2. Temperature Difference Pattern (4.2 – 298°K) for $FeCl_3$.

[6] W. N. Hansen and M. Griffel, *J. Chem. Phys.* **28**, 902 (1958).

scattering is characteristic of antiferromagnetic short-range order and was also observed in $MnCl_2$ and $MnBr_2$. The ferromagnetic sheet structures,[3] typified by $FeCl_2$ and $CoCl_2$, do not show this behavior but instead exhibit ferromagnetic short-range-order effects. (The lack of pronounced antiferromagnetic short-range order in $CrCl_3$ is consistent with a ferromagnetic sheet structure.) Preliminary attempts to determine the magnetic structure from the powder data have been unsuccessful, but the over-all behavior of this compound indicates that the antiferromagnetic order is similar to that of $MnCl_2$ and $MnBr_2$, which required single-crystal data for the determination of magnetic structures. A single crystal has now been grown and will soon be examined.

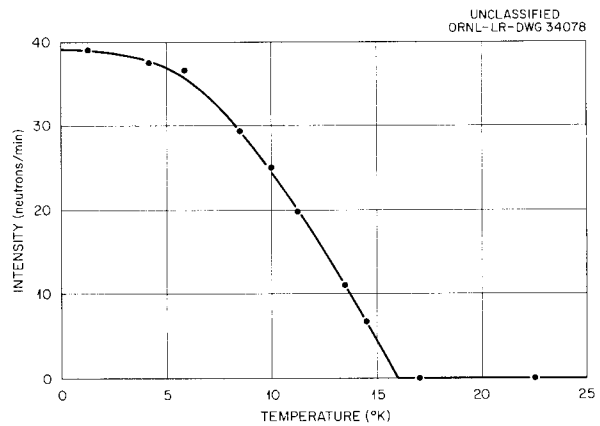

Fig. 3. Temperature Dependence of the Small-Angle Magnetic Reflection of $FeCl_3$.

NEUTRON DIFFRACTION INVESTIGATIONS OF $CoCl_2$ IN AN EXTERNAL MAGNETIC FIELD

M. K. Wilkinson J. W. Cable E. O. Wollan W. C. Koehler

Neutron diffraction measurements made on powdered samples[1] and single crystals[2] of $CoCl_2$ at temperatures down to 4.2°K have shown that this compound has an antiferromagnetic transition at about 25°K. In the antiferromagnetic structure the magnetic moments within a metal layer are coupled ferromagnetically, and adjacent layers have the moments aligned antiparallel. Although in the previous experiments it was established that the moments are oriented parallel to the layers of atoms, the specific orientation within these layers could not be determined, and the moments have been assumed to be directed along the hexagonal axes. Recent experiments have been made on single crystals of $CoCl_2$ in an external magnetic field to determine the moment orientation and to examine the manner in which the moments are rotated into parallel alignment by moderate magnetic fields.

Investigations of the intensity changes of several magnetic reflections, after the field was applied at various angles parallel to the hexagonal layer and then removed, suggested that the moments were directed along equivalent <210> directions. However, these experiments involved the repopulation of the antiferromagnetic domains when the field was removed, and the interpretation was not completely unambiguous. This moment direction appears to be confirmed by close examination of the intensity changes of the (101) and (113) magnetic reflections when small fields are applied parallel to the scattering vectors of those planes. (The magnetic reflections have been indexed on the basis of a hexagonal unit cell containing six molecules. This cell has the same *a* axis as the chemical hexagonal cell, but the *c* axis has been doubled.) The results are shown in Fig. 1, and the diagrams within the figure represent an interpretation of the intensity changes with the moments oriented along <210> directions in zero magnetic field. The variation of the (113) intensity with an external field involves merely a domain transformation. That domain with the moment orientation perpendicular to the field direction is stabilized, and the domain pattern changes until the entire crystal is transformed into one domain direction with an applied field of about 1.2 kilo-oersteds. On the other hand, when the field is applied along the scattering vector of the (101) reflection, the

[1] M. K. Wilkinson and J. W. Cable, *Phys. Semiann. Prog. Rep. March 10, 1956*, ORNL-2076, p 44.

[2] M. K. Wilkinson *et al.*, *Phys. Semiann. Prog. Rep. March 10, 1958*, ORNL-2501, p 42.

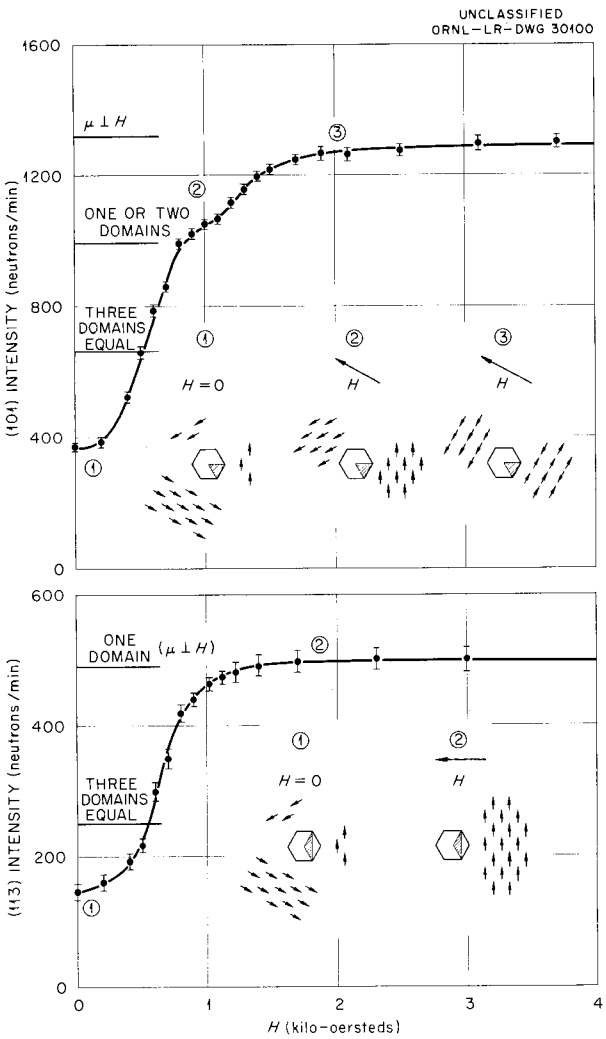

Fig. 1. Comparison of the Field Dependence of the (113) and (101) Magnetic Reflections from $CoCl_2$.

intensity variation seems to involve two processes. First, there is a domain transformation in which all the moments become oriented in the two domains which have the axes of antiferromagnetism most nearly perpendicular to the field direction. (The results do not permit a determination of the relative population of the two domains.) This transformation is completed at about the same field value that is required when the field is applied along the scattering vector of the (113) planes. [Because of the relative orientation of the field and the moment directions in the two experiments, the field required for a domain transformation should be slightly larger when applied along the scattering vector of the (101) planes.] However, as the external field is increased further, a critical field is exceeded and the moments flip perpendicular to the field from the preferred crystallographic direction. This process is completed with a field of about 2 kilo-oersteds. Since the intensities at zero field depend on previous applications of the magnetic field, these experiments were started for both reflections with a domain population which minimized the intensities of the reflections that were studied. Values for the intensities which should have been observed for these reflections if there had been equal population of the domains are shown on Fig. 1. These two values are experimental determinations of the average intensities of those reflections which are equivalent to the (113) and the (101) reflections. The experimental values representing equal domain population were then used to calculate the intensities expected for the various moment orientations that were suggested by the intensity variation with applied field. These calculated values are also shown on the figure, and the experimental measurements are in good agreement.

After all the moments are oriented perpendicular to the direction of the field, larger fields rotate these moments into the field direction, thereby producing a net magnetization at moderate fields. This effect, which had been observed in magnetic susceptibility measurements,[3,4] is shown in Fig. 2,

[3] C. Starr, F. Bitter, and A. R. Kaufmann, *Phys. Rev.* 58, 977 (1940).

[4] H. Bizette, C. Terrier, and B. Tsai, *Compt. rend.* 243, 1295 (1956).

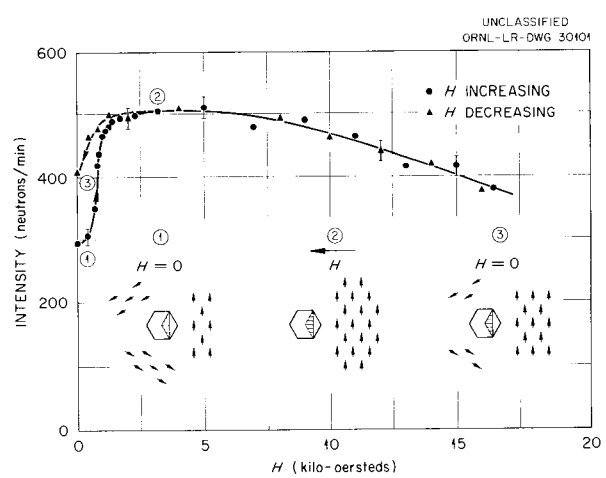

Fig. 2. Variation of the Intensity of the (113) Antiferromagnetic Reflection from $CoCl_2$ in an External Magnetic Field.

where the intensity of the (113) reflection decreases at fields larger than about 5 kilo-oersteds. Similar results were also obtained for the intensity variation of the (101) reflection. Rough calculations based on the magnetization values in the powder susceptibility measurements[3] show that this intensity should be about 5% below the maximum at 10 kilo-oersteds and about 20% below it at 16.5 kilo-oersteds. The results in Fig. 2 are in good agreement with these predictions. The relatively high intensity when the field was removed shows that much of the domain transformation remained.

According to Néel's calculations[5] based on a two-sublattice model of an antiferromagnet, parallel moment alignment in which the moments first turn perpendicular to the field direction will occur only if the ratio of the anisotropy energy to the exchange energy is small. This condition would be expected in $CoCl_2$, since the anisotropy energy which must be overcome in rotating the moments normal to the field is the small value associated with the preferred crystallographic direction within the layer of atoms. These experiments do not give any information concerning the anisotropy energy associated with the unique crystal axis in $CoCl_2$, but it is undoubtedly a much larger value.

[5]L. Neel, *Institus Solvay, Brussels*, p 251, Institut International de Physique, Brussels, 1954.

NEUTRON DIFFRACTION INVESTIGATION OF METALLIC CERIUM

H. R. Child M. K. Wilkinson W. C. Koehler E. O. Wollan

Measurements of the specific heat[1,2] and the magnetic susceptibility[3] of metallic cerium have shown anomalies which cannot be easily interpreted, since they are strongly dependent on the previous history of the sample. Recent x-ray measurements[4] have shown that such a behavior is not surprising, since there are three crystallographic forms of cerium that exist between 77 and 450°K, and the relative concentrations of the three phases are dependent both on the sample temperature and on the condition of the sample. For example, in a previously uncooled annealed sample, a face-centered cubic phase (fcc) with $a_0 = 5.15$ Å is stable at room temperature, but as the sample is cooled, a double hexagonal close-packed structure (hcp) begins to form at about 263°K and a collapsed face-centered cubic phase (α-fcc) with $a_0 = 4.85$ Å starts to form at about 103°K. There is a very large hysteresis in the phase transformations, so that when the temperature of this same sample is raised, the α-fcc phase starts to disappear at about 170°K, while the disappearance of the hcp phase does not begin until about 363°K. Furthermore, if the original sample had been cold-worked before cooling, different phase concentrations would have been present at the various temperatures.

After these interesting x-ray results had been obtained down to 77°K, a neutron diffraction investigation was initiated in collaboration with McHargue, Yakel, and Jetter of the Metallurgy Division on samples of metallic cerium which were prepared by special methods to obtain different conditions with respect to the phase concentrations. Since the nuclear reflections in a neutron diffraction pattern furnish a method of determining the relative phase concentrations in the sample, investigations of the magnetic scattering can give information on the magnetic properties of cerium under known crystallographic conditions. There were two particular points of interest which these experiments should help to clarify. One concerned the formation of the α-fcc phase, which, according to suggestions by Pauling[5] and Zachariasen,[6] involved the promotion of a $4f$ electron to the $5d$ state. The other was the indication from Lock's susceptibility measurements[3] that an antiferromagnetic transition occurs at about 12.5°K.

Neutron diffraction experiments have been performed from room temperature to 4.2°K on three

[1]D. H. Parkinson, F. E. Simon, and F. H. Spedding, *Proc. Roy. Soc. (London)* **A207**, 137 (1951).

[2]D. H. Parkinson and L. M. Roberts, *Proc. Phys. Soc. (London)* **B70**, 471 (1957).

[3]J. M. Lock, *Proc. Phys. Soc. (London)* **B70**, 566 (1957).

[4]C. J. McHargue, H. L. Yakel, Jr., and L. K. Jetter, *Met. Ann. Prog. Rep. Oct. 10, 1957*, ORNL-2422, p 207 (classified).

[5]Cited by A. F. Schuck and J. H. Sturdivant, *J. Chem. Phys.* 18, 145 (1950).

[6]Cited by P. W. Bridgman, *Phys. Rev.* 48, 825 (1935).

specimens of polycrystalline cerium rod which were prepared by different methods. The first sample (sample I) was a previously uncooled annealed specimen, the second (sample II) was a specimen which was severely cold-worked, and the third (sample III) was the same specimen referred to as sample II after it had been thermally cycled 100 times by being dipped into liquid helium and then warmed to room temperature. This procedure was followed for sample III in an attempt to duplicate the specimen prepared by Lock which did not show large hysteresis loops in the susceptibility measurements between 40 and 200°K.

The relative concentrations that were determined from the neutron measurements for the three samples as the temperatures were decreased are shown in Fig. 1. Similar results were also obtained for increasing sample temperatures, and the concentrations in samples I and II at specific temperatures were considerably different because of the thermal hysteresis effects. The relatively small change in the concentrations in sample III as a function of temperature did not permit any significant hysteresis and indicates the reason why Lock observed no such effects on a sample which had been temperature-cycled in this manner. The points represent the actual temperatures where data were obtained, and they are merely connected by straight lines. The feet on the points represent estimated errors, and these feet are much larger on samples II and III since the lattice distortions and preferred orientation introduced by cold work and thermal cycling made accurate phase determinations very difficult. The results at room temperature and at 77°K for sample I agreed very well with x-ray results on a sample prepared similarly, although the x-ray results showed that the changes were not linear between these temperatures. Prior to the neutron results below 77°K, it had been expected that the α-fcc phase was developed only from the fcc phase. However, below 77°K, it is apparent that this collapsed cubic phase also develops at the expense of the hcp phase. There was no evidence for a collapsed hexagonal phase. The phase concentrations in sample II did not agree particularly well with those observed in a sample prepared in a similar manner and examined by x-ray techniques. Whereas the x-ray sample at room temperature was essentially 100% fcc, sample II contained about 25% of the hcp phase at that temperature. This difference merely emphasizes that the amount of cold work is very important in establishing the sample conditions.

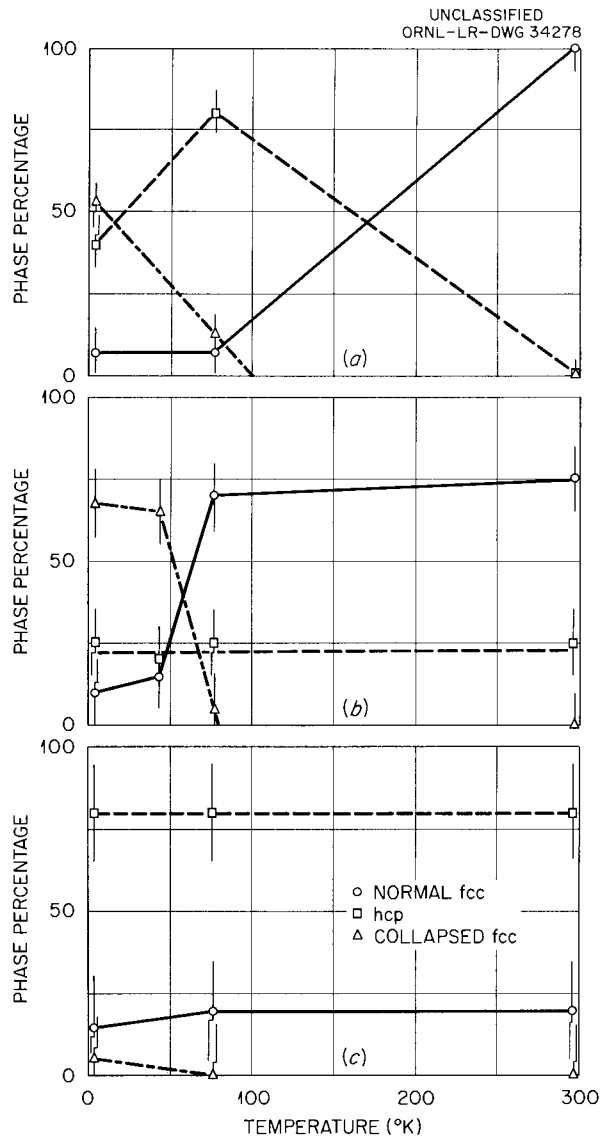

Fig. 1. Relative Concentrations of the Crystallographic Phases in Three Specially Prepared Cerium Samples as the Temperatures Were Decreased. (*a*) Sample I (annealed, previously uncooled); (*b*) sample II (cold-worked); (*c*) sample III (cold-worked, temperature-cycled).

Although this investigation has not been completed, certain facts seem to be definite on the basis of preliminary observations. In both sample I and sample II there is a very large decrease in the diffuse scattering which can be correlated with the growth of the α-fcc phase at temperatures below 77°K. In fact, the diffuse background at 4.2°K is only about 50% of its value at room temperature. In

sample III, where little or no α-fcc phase appeared, there was a relatively small change in the diffuse scattering as the sample was cooled to low temperatures. This is exactly the effect which would be expected in the paramagnetic diffuse scattering if formation of the α-fcc structure results from the promotion of $4f$ electrons to the $5d$ shell. While accurate calculations of the absolute intensity of the paramagnetic scattering from the various samples at different temperatures have not been completed, these results should give information on the specific electronic configurations in the three crystallographic phases.

In addition to the decrease in diffuse scattering which accompanied the growth of the α-fcc phase, the diffraction patterns at 4.2°K for all three samples showed the presence of some additional reflections which were very weak. The relative intensities of these reflections in the three samples when correlated with the relative concentrations of the three crystallographic phases show that they must be associated with the hcp phase. Although the intensities of these reflections were very small, the largest reflection in sample III was scanned with the sample at various temperatures above 4.2°K. These sample temperatures were obtained by placing a small heater between the cerium and the liquid-helium container, and temperatures were measured with a calibrated copper-constantan thermocouple. The results are summarized by the points in Fig. 2, which give the integrated intensity

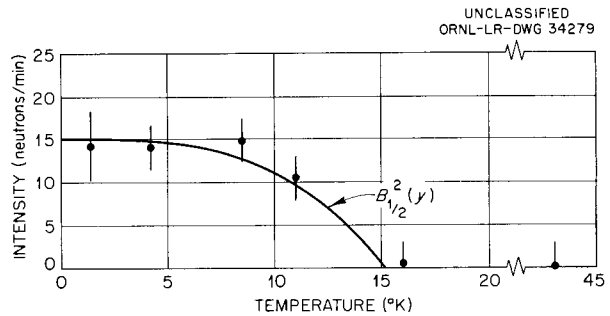

Fig. 2. Temperature Variation of the Integrated Intensity of an Antiferromagnetic Reflection from Sample III.

of this reflection as a function of temperature. The curve through the points is a Brillouin function for $S = \frac{1}{2}$, and it merely shows that the data can be represented by this type of dependence. Since the thermocouple readings in this temperature range were probably not accurate to better than 2 or 3°, the temperature corresponding to the disappearance of the reflection agrees satisfactorily with that of the susceptibility anomaly (12.5°K) which Lock observed. Hence the reflections are undoubtedly associated with antiferromagnetic ordering in the hcp crystallographic phase. Preliminary attempts have been made to determine the specific antiferromagnetic arrangement of the magnetic moments within this hexagonal structure, but these have not been successful.

MAGNETIC NEUTRON DIFFRACTION STUDY OF 4*d* TRANSITION-GROUP TRIFLUORIDES

E. O. Wollan H. R. Child M. K. Wilkinson J. W. Cable

A recent investigation[1] of the magnetic structure properties of the $3d$ transition-group trifluorides has now been extended to include trifluorides involving $4d$ transition-group elements.

The crystal structure of the trifluorides can be considered, from the point of view of their magnetic properties, as one involving minor distortions of a cubic form in which the magnetic ions occupy the corners of the cube and the fluorine ions lie nearly along the edges. In this simple structure the indirect coupling of the spins of $3d$ magnetic ions via the intervening fluorine ions was found to be interpretable on simple phenomenological grounds. For this reason it was felt that a study of the trifluorides involving $4d$ elements might prove interesting, especially since no neutron diffraction data had been obtained on $4d$ compounds.

Powder diffraction data obtained on PdF_3 and RuF_3 down to liquid-helium temperature showed no evidence of magnetic ordering. This cannot be taken as positive evidence that such ordering does not occur, however, because if these ions possessed only a single uncompensated spin the intensity in superlattice reflections would be small and might

[1] H. R. Child *et al.*, *Phys. Semiann. Prog. Rep. Sept. 10, 1957*, ORNL-2430, p 87–91.

not have been detected. This is especially true for the samples studied, for which a considerable line broadening was observed.

In the case of MoF_3, on the other hand, antiferromagnetic superlattice reflections were observed to develop at low temperatures. Figure 1 shows a difference pattern ($I_{4.2°K} - I_{298°K}$) for this compound.

The lines are indexed on the hexagonal cell and are the antiferromagnetic reflections one would expect for a *G*-type antiferromagnetic lattice where each metal atom is antiferromagnetically coupled through the intervening fluorine ion to each of its six nearest neighbors. The appearance of both the (003) and the (101) reflections indicates that the moment is in or near the basal layer of the hexagonal cell. Both these results are identical with that observed in the corresponding *3d* trifluoride, CrF_3.

Figure 2 is a warmup curve showing the behavior of the peak height of the (101) magnetic reflection as a function of temperature. The data follow a Brillouin-type curve with a Néel temperature of 185°K. This Néel temperature is considerably higher than that observed for CrF_3 (80°K), and hence the magnetic coupling in MoF_3 is stronger than in CrF_3.

The data on MoF_3 are as yet only preliminary, there being some question about the purity of the sample. This investigation will be continued on a better sample, from which it is hoped that measurements can be made of a *4d* form factor for which no experimental data have yet been obtained. The moment value obtained from the present measurements is consistent with a spin-only value of $3\mu_B$, but this also is a preliminary result.

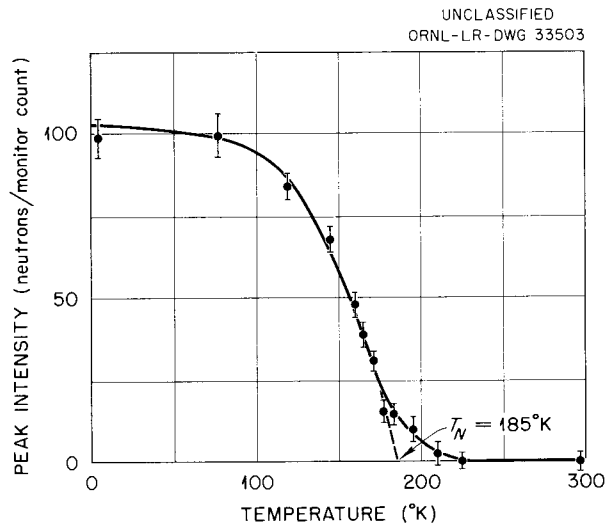

Fig. 2. Temperature Dependence of (101) Superlattice Reflection.

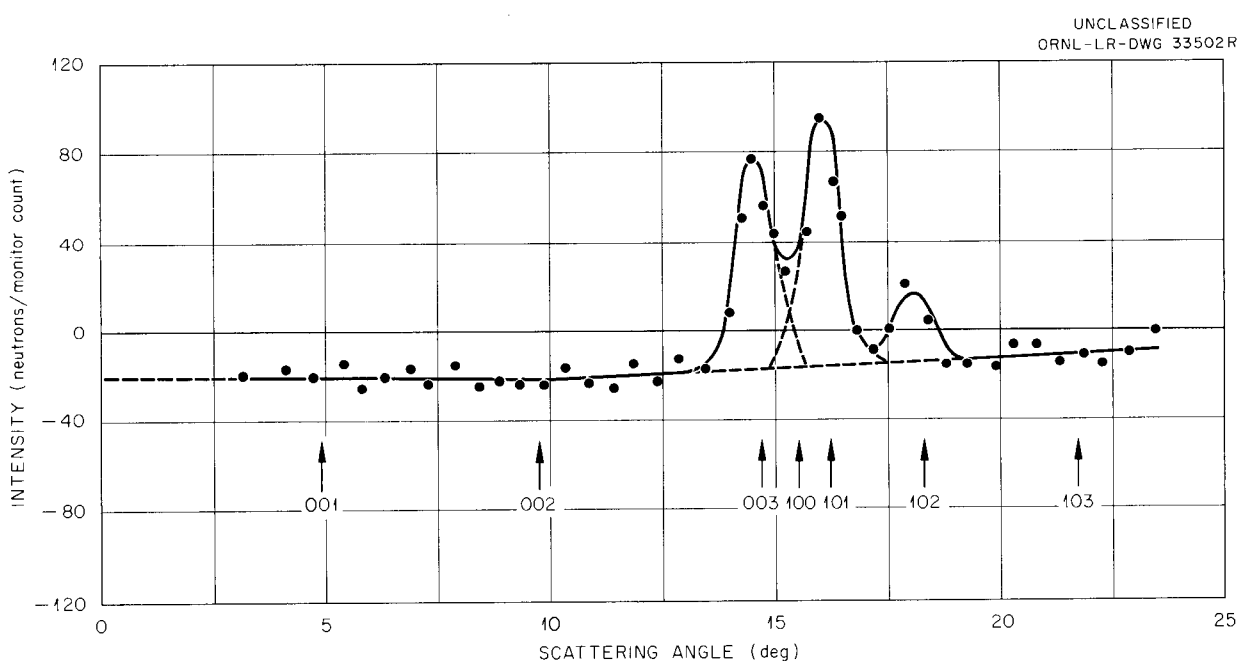

Fig. 1. Difference Pattern ($I_{4.2°K} - I_{298°K}$) for MoF_3.

ATOMIC-BEAM DETERMINATION OF THE NUCLEAR SPINS OF I^{128} AND I^{130}

J. E. Sherwood S. J. Ovenshine

GENERAL DESCRIPTION

An atomic-beam apparatus of the Rabi type has been used to measure the nuclear spins of I^{128} and I^{130}. This apparatus is conventional in principle and is intended for use with radioactive materials. Therefore extensive shielding has been incorporated, particularly around the source chamber. Detection is accomplished by allowing the beam to impinge on a cooled copper tape for a known time. The activity thus deposited is measured by moving the tape so that the hot spot is transferred to a scintillation counter and counted during the next deposition. Photographs of the whole apparatus and of the detector chamber are shown in Figs. 1 and 2.

Elemental iodine has a vapor pressure of about 0.3 mm Hg at ambient temperatures. Thus the iodine may be contained in a vial outside the vacuum system. The vapor from the sample is led into the system through a glass tube. Although the vapor of iodine is largely diatomic at ambient conditions, we obtain substantially 100% dissociation by superheating the vapor to above 650°C. This is done by allowing the vapor to pass through an oven which is heated by radiation from a tungsten filament of about 3-kw dissipation. The oven, the attached slit-forming jaws, and the tube leading to it are made of solid gold, as no other material tested seems able to withstand the corrosive action of iodine under these conditions. Figure 3 shows these features and also a cooled baffle in front of the oven to condense the iodine not directed along the axis of the machine.

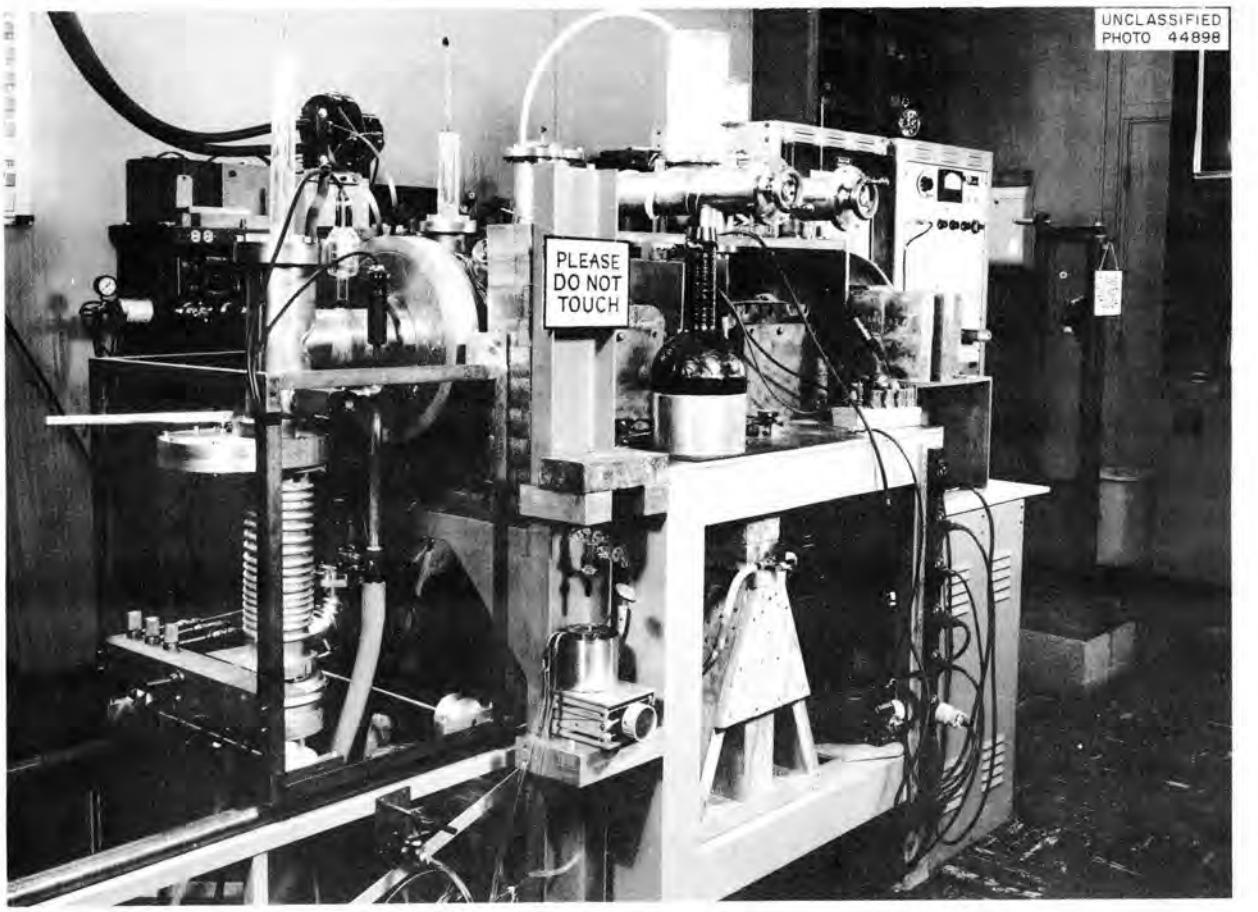

Fig. 1. Atomic-Beam Apparatus Viewed from Source End.

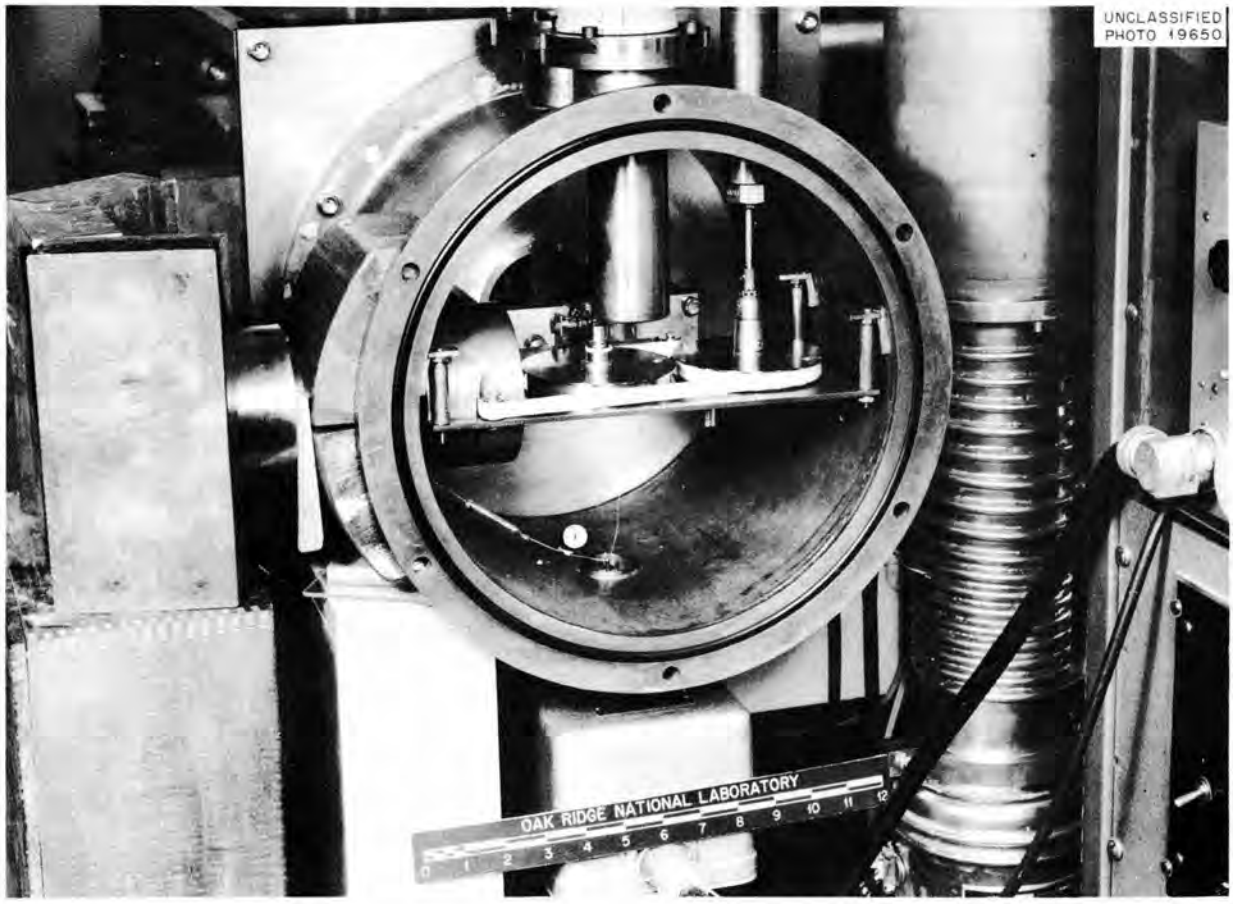

Fig. 2. Detector Chamber.

Assuming a nuclear spin of 1, for example, and making use of the known electronic ground state of iodine ($^2P_{3/2}$), the atomic energy level scheme shown in Fig. 4 may be derived. Since our machine is set up for "flop-in" experiments, only such transitions as those causing a reversal of the strong-field atomic moment can be seen – in this case, only those indicated by the double arrows. The frequency at which such transitions occur is given by

$$\nu_k = g_f \mu_0 \frac{H}{h} ,$$

where μ_0 is the Bohr magneton, H is the magnetic field intensity, h is Planck's constant, and

$$g_f = g_i \frac{f(f+1) + j(j+1) - i(i+1)}{2f(f+1)} .$$

Here $f = i + j,\ i + j - 1, \ldots, |i - j|$, and i and j are the nuclear and electronic angular momentum quantum numbers. The magnetic field H was derived from the stray field of the deflecting magnets and was calibrated by observing resonance in a beam of normal potassium atoms. Thus the two frequencies corresponding to spin 1 were found by calculation to have the values 2.99 and 3.65 Mc/sec.

SPIN OF I^{128}

The source was prepared by irradiating 100-mg quantities of ordinary elemental iodine (I^{127}) for ½ hr in the LITR in capsules made of Natural Ultra-ethylux,[1] a plastic similar to polyethylene but more machineable. Because of the short (25-min) half life, great speed was necessary in the preliminary steps of the experiment. For example, the first deposition was usually begun 9 min after the sample was removed from the reactor.

[1] Made by Westlake Plastics Co., Lenni Mills, Pa.

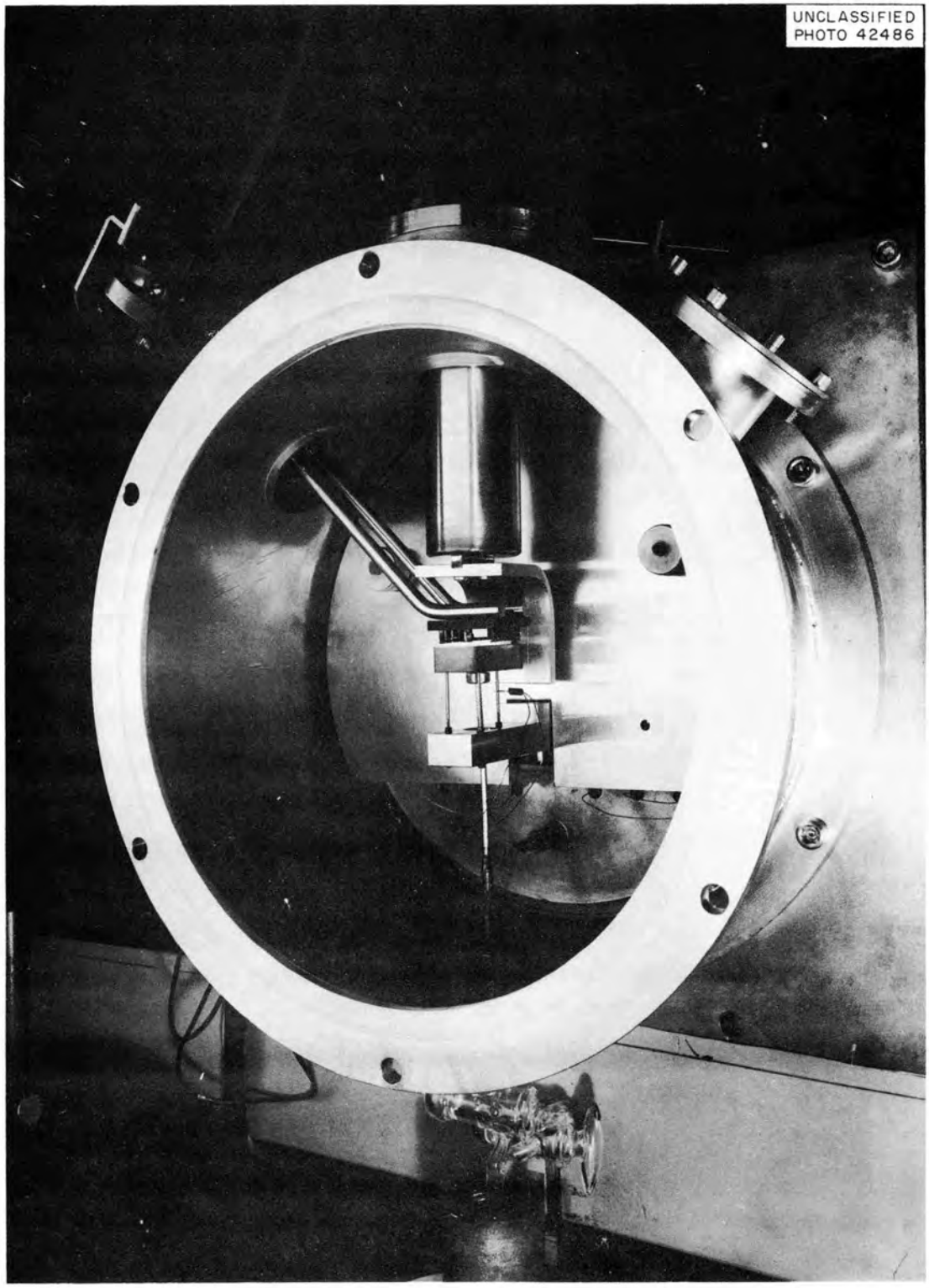

Fig. 3. Source Chamber for Use with Iodine.

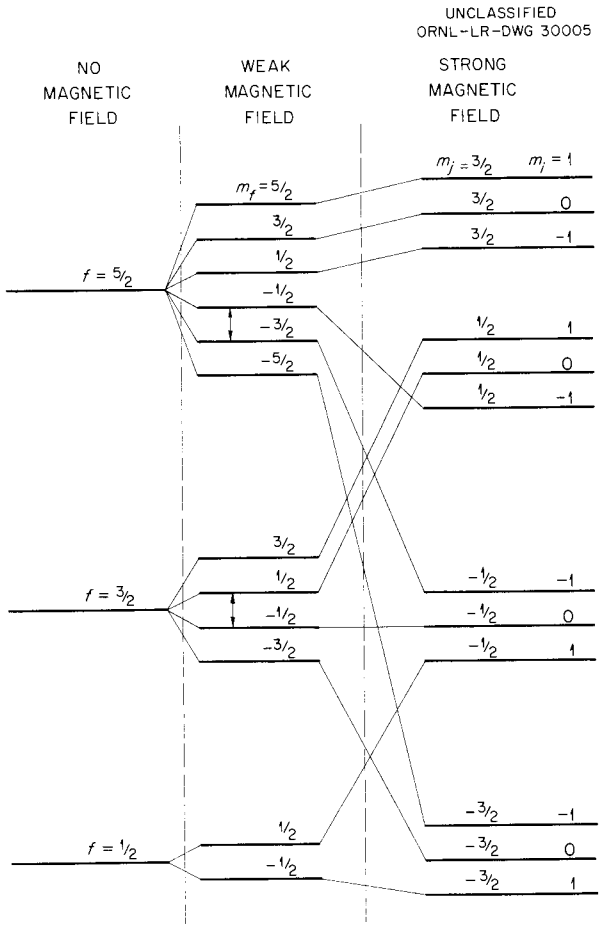

Fig. 4. Atomic Energy Levels for $j = 3/2$, $i = 1$, $\mu_i > 0$.

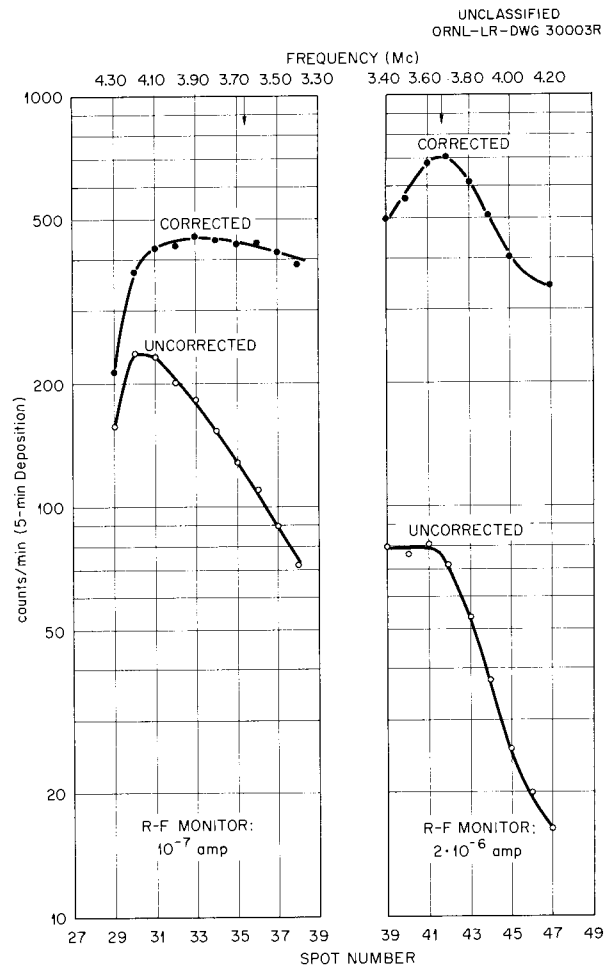

Fig. 5. Frequency Sweep for I^{128}.

Figure 5 shows the resonance obtained at 3.65 Mc. The curve at the lower left resulted from a frequency scan with very little r-f power. When the power level was raised to an optimum value determined from previous experiments, the lower right curve was obtained. Correcting these curves for 25-min decay yielded the results at the top of the figure.

Lines have been seen repeatedly at both frequencies corresponding to spin 1, but not at those corresponding to other spin values. This result is in agreement with the decay studies of Benczer *et al.*[2]

SPIN OF I^{130}

In this case the source was prepared by irradiating 80-mg quantities of a 50% I^{129}, 50% I^{127} mixture in the LITR for 6 hr. The mixture had been obtained as a fission product and reduced to the elemental form by the Radioisotopes Department. I^{128} was, of course, formed during the irradiation, but was allowed to decay before the experiment.

The results of a frequency sweep are shown in Fig. 6, in which it is seen that two lines appear at frequencies in good agreement with those calculated for spin 5. The transition field was then raised by passing a current of 3.00 ma through the *C*-field coils and was recalibrated by means of a beam of I^{128}. The high-frequency line was then observed, as shown in Fig. 7, in excellent agreement with the new spin-5 frequency. (Unfortunately, an apparatus failure prevented observation of the low-frequency line during this run.) On the basis of data of which these results are examples, we conclude that the spin of I^{130} is 5.

[2]N. Benczer *et al.*, *Phys. Rev.* 101, 1027 (1956).

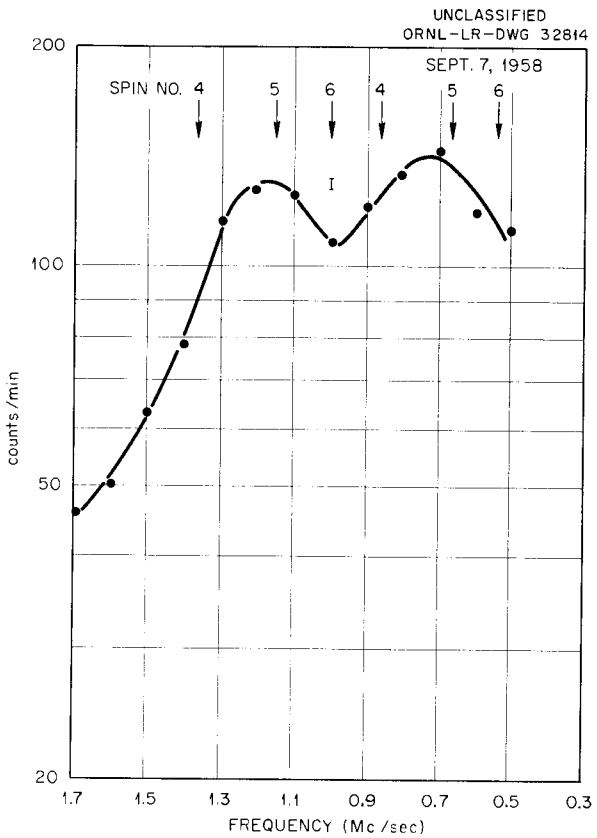

Fig. 6. Frequency Sweep for I^{130} ($I_c = 0$).

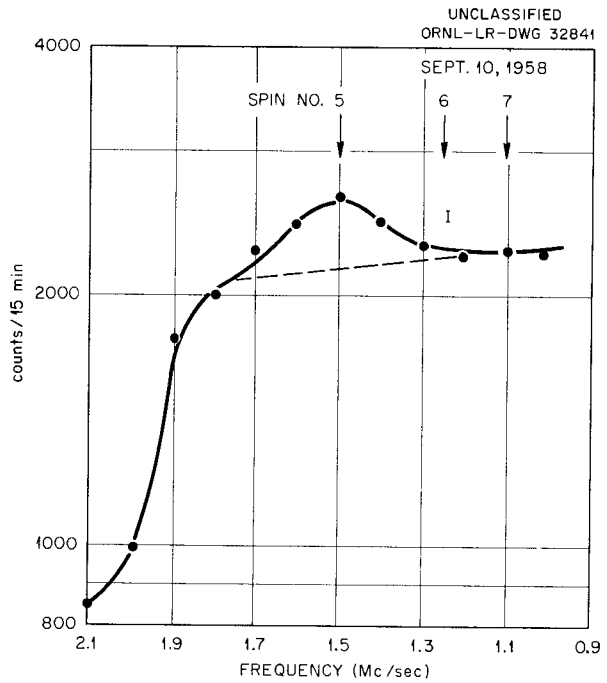

Fig. 7. Frequency Sweep for I^{130} ($I_c = 3.00$ ma).

The decay of I^{130} has been studied by several groups and a spin assignment of 6^- for the ground state has been made by Caird and Mitchell.[3] Smith, Stelson, and McGowan[4] at ORNL recently re-examined this isotope. Their observations of the decay agree with those of the previous workers. It appears very likely that the second excited state of the Xe^{130} daughter is a 4^+ level. If this is so, the I^{130} parent should beta-decay to this level. However, no such beta ray has been detected.

The authors wish to express their indebtedness to H. T. Russell of the Radioisotopes Department for his assistance in the preparation of the I^{129} samples.

---

[3] R. S. Caird and A. C. G. Mitchell, *Phys. Rev.* **94**, 412 (1954).

[4] Private communication.

MICROWAVE SPECTRA AND STRUCTURE OF THE VINYL FLUORIDE MOLECULE

H. W. Morgan J. H. Goldstein[1]

INTRODUCTION

Despite numerous investigations of the physical properties of the vinyl halides, no precise data are available on the structure of vinyl fluoride. Considerable interest attaches to such information since it reflects the nature of the bonds and the electron distribution in this molecule.

Preliminary calculations using typical structural values indicated that the $J = 0 \rightarrow 1$ microwave transition should be observed at about 20,000 Mc and the $J = 1 \rightarrow 2$ transitions at about 40,000 Mc. Since only two independent rotational constants are derivable for a planar molecule, whereas a total of nine structural parameters are required in this case, it was necessary to use two C^{13}-isotopic species and to introduce some assumed structural data. The set of structural parameters to be determined was finally reduced to three: r (C=C), r (C–F), and ∠CFF. A serious complication arose from the fact that the interior C atom lies very near the center of mass, making it difficult to determine the two distances separately. Despite this, a structure has been derived which is quite consistent with the experimental data, subject to the assumptions stated below.

EXPERIMENTAL

The microwave spectrum was observed with a Stark-effect spectrograph using square wave modulation at 100 kc. A visual presentation was used for the detection and measurement of transition frequencies. Measurements were made in the conventional manner by comparison with the harmonics of a 10-Mc crystal, calibrated and continuously monitored against WWV. Each reported frequency is the average of up to ten measurements made over a period of several months, and is estimated to be accurate to ±0.05 Mc.

The sample of normal vinyl fluoride was obtained through the courtesy of E. I. du Pont de Nemours & Co., Inc., and was used without further purification. Small quantities of vinyl fluoride enriched in C^{13} were synthesized, using $KC^{13}N$ of 61% enrichment supplied by Eastman Kodak Company. For this preparation, KCN was oxidized to $C^{13}O_2$ and collected as $BaC^{13}O_3$. Dried, finely powered $BaC^{13}O_3$ was then intimately mixed with Mg powder, pressed into pellets, and converted to BaC_2 by heating to 400°C. The reaction of H_2O with the residue generated $C_2^{13}H_2$. Combination of HF and $C_2^{13}H_2$ to form vinyl fluoride was accomplished at 250°C in contact with a zinc-mercury chromite catalyst.[2] Excess HF was removed by reaction of the product with CaO before the gas was admitted to the wave guide. No reliable estimate could be made of the yield of vinyl fluoride.

OBSERVED SPECTRA AND ANALYSIS

The spectra of the three isotopic species of vinyl fluoride are shown in Table 1. The mean deviation of all the measurements for each transition shown is ≦0.05 Mc, and the average of all mean deviations is 0.03 Mc. The last set of transitions shown, labeled $v_{12} = 1$, arises from the first excited state of the lowest vibrational mode, presumably an out-of-plane bend.

The calculated frequencies in the last column were derived from the rotational constants shown in Table 2. These were obtained by setting $b + c$ equal to $\nu(0 \rightarrow 1)$ and $2(b - c)$ equal to $\nu(1_1 \rightarrow 2_0) - \nu(1_0 \rightarrow 2_{-1})$ and then calculating the asymmetry parameter, δ, from the remaining transition. By this means it was hoped to minimize the uncertainty arising from centrifugal distortion, although this was apparently quite small. Other methods of fitting the spectra were attempted but they did not appreciably improve the over-all agreement or change the values of b and c by more than 0.02 Mc. The estimated total uncertainty in these constants does not exceed ±0.05 Mc, and in δ it is approximately ±0.0010.

The corresponding ground-state moments of inertia for the three species are shown in Table 3. Examination of the relations which determine I_a indicates that under unfavorable circumstances the uncertainty in this moment might be as large as 0.03 amu·Å^2 in a total of approximately 8 amu·Å^2. On the other hand, if values of I_a are computed by assuming planarity and from the value of δ, the two sets of results agree to within 0.003, 0.006, and

[1] Consultant, Emory University, Atlanta, Georgia.

[2] U. S. patent No. 2,401,850; see also, *Chem. Abstr.* 40, 6091_6 (1946).

Table 1. Microwave Spectra of Vinyl Fluoride

Species	Transition	Observed Frequency (Mc)	Calculated Frequency (Mc)
$H_2C^{12}C^{12}HF$	$0_{00} \rightarrow 1_{01}$	19,755.01	19,755.01
	$1_{11} \rightarrow 2_{12}$	37,991.28	37,991.37
	$1_{01} \rightarrow 2_{02}$	39,477.97	39,477.97
	$1_{10} \rightarrow 2_{11}$	41,028.57	41,028.67
$H_2C^{12}C^{13}HF$	$0_{00} \rightarrow 1_{01}$	19,717.80	19,717.80
	$1_{11} \rightarrow 2_{12}$	37,883.28	37,883.36
	$1_{01} \rightarrow 2_{02}$	39,401.13	39,401.13
	$1_{10} \rightarrow 2_{11}$	40,987.77	40,987.84
$H_2C^{13}C^{12}HF$	$0_{00} \rightarrow 1_{01}$	19,154.31	19,154.31
	$1_{11} \rightarrow 2_{12}$	36,872.34	36,872.41
	$1_{01} \rightarrow 2_{02}$	38,279.95	38,279.94
	$1_{10} \rightarrow 2_{11}$	39,744.74	39,744.83
$H_2C^{12}C^{12}HF$	$0_{00} \rightarrow 1_{01}$	19,738.83	19,738.83
($v_{12} = 1$)	$1_{11} \rightarrow 2_{12}$	37,952.07	37,952.17
	$1_{01} \rightarrow 2_{02}$	39,445.40	39,445.40
	$1_{10} \rightarrow 2_{11}$	41,003.04	41,003.15

Table 2. Spectroscopic Parameters for Vinyl Fluoride

Species	b (Mc)	c (Mc)	δ
$H_2C^{12}C^{12}HF$	10636.83	9118.18	0.02775
$H_2C^{12}C^{13}HF$	10635.02	9082.78	0.02918
$H_2C^{13}C^{12}HF$	10295.26	8859.05	0.02628
$H_2C^{12}C^{12}HF$ ($v_{12} = 1$)	10632.16	9106.67	0.02781

0.0003 amu·Å^2, respectively, for the three species. From this it is concluded that the apparent planarity defect, Δ, is less than 0.03 amu·Å^2. In support of this rather small estimate for Δ, we note that the calculated value of the defect for the state $v_{12} = 1$, involving excitation of an out-of-plane bending mode, is only 0.03 amu·Å^2. The calculated values shown in Table 3 were obtained by the procedure described in the succeeding section.

STRUCTURE CALCULATIONS

The structural parameters may be identified by reference to Fig. 1. The angles HCH and CCH

Table 3. Observed and Calculated Moments of Inertia for Vinyl Fluoride*

Species	I_b		I_c	
	Observed	Calculated	Observed	Calculated
$H_2C^{12}C^{12}HF$	47.5263	47.5223	55.4419	55.4370
$H_2C^{12}C^{13}HF$	47.5344	47.5361	55.6580	55.6577
$H_2C^{13}C^{12}HF$	49.1031	49.1011	57.0636	57.0640

*All values in amu·Å^2. The conversion factor used was 5.05529×10^5 Mc·amu^{-1}·Å^{-2}.

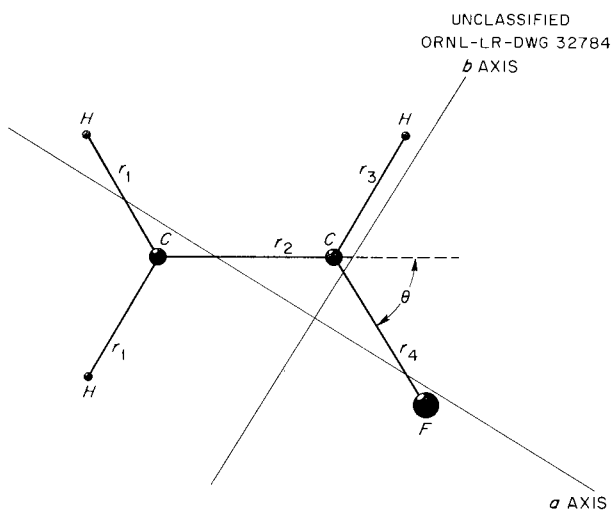

Fig. 1. Vinyl Fluoride Molecule.

were assumed to be 120°. Moments of inertia for the three isotopic molecules were then computed for 1134 structures over the following ranges (in increments of 0.005 Å) of the distance parameters:

$$r_1\ (\text{C–H}) = 1.075\text{–}1.085\ \text{Å},$$

$$r_2\ (\text{C=C}) = 1.335\text{–}1.365\ \text{Å},$$

$$r_3\ (\text{C–H}) = 1.075\text{–}1.085\ \text{Å},$$

$$r_4\ (\text{C–F}) = 1.320\text{–}1.345\ \text{Å},$$

with $\theta = 58.5$, 58.9, and 59.5°.

From a comparison of the observed and computed moments, it was determined that r_2 and r_4 had values close to 1.34 Å and that θ was approximately 59.0°. Based on the computed moments for a series of structures close to the above distances and angle, values were obtained for the derivatives of the six moments with respect to the five parameters. A least-squares fitting of all parameters was then attempted but this led to unreasonable values of the C–H distances. Consequently these were restricted to the values 1.075, 1.080, 1.085 Å while another least-squares determination of the remaining three parameters was performed. Comparison of these calculated moments with the experimental values indicated that the structure shown below gave the best fit, consistent with the assumptions described above.

r_1 (C–H)	1.075 ± 0.005 Å
r_2 (C=C)	1.337 ± 0.002 Å
r_3 (C–H)	1.080 ± 0.005 Å
r_4 (C–F)	1.344 ± 0.002 Å
∠CCF	121 ± 0.2°

A second least-squares fit, with derivatives evaluated very near the final structure, gave identical results.

The calculated moments in Table 3 were obtained with this structure and agree with experiment within 1 to 10 parts in 10^5. This is considered quite satisfactory, as, with an experimental uncertainty of 0.10 Mc in each frequency, the moments should be accurate to within 2 parts in 10^5. The mean agreement in Table 3 is of the same order of magnitude as the mean apparent planarity defect.

Although it is difficult to estimate the absolute uncertainty in the structure tabulated above, it can be shown to be rather precisely determined under the assumptions stated. Thus a variation of 0.01 Å

in r_3 is approximately equivalent in effect to variations of 0.0016 Å, 0.0007 Å, and 0.16°, respectively, in r_2, r_4, and θ. A change of 0.005 Å in r_1 changes I_b by 0.04 and I_c by 0.06 amu·Å^2. Inasmuch as recent structural studies[3] of ethylene indicated ∠HCH near 117°, we determined the sensitivity of the structure to changes in the angular positions of the carbon-hydrogen bonds. Decreasing ∠HCH by 4° is equivalent to a change of 0.005 Å in r_2 or r_4, or a change of 0.39° in θ. A variation of 2° in the angle between r_2 and r_3 is found to change the values of r_2 and r_4 by less than 0.001 Å, and θ by less than 0.05°. In all these cases, however, the compensating variations are interdependent, and the over-all structure, even for such gross variations, is not greatly affected. We have concluded from such considerations as these that the three structural parameters have been determined to within ±0.002 Å for r_2 and r_4, and ±0.2° for θ.

DISCUSSION

The precise values of the structural parameters of vinyl fluoride are of interest in connection with the general problem of heteroconjugation in unsaturated structures. The earlier diffraction data for the vinyl halides and similar compounds appear now to be open to some question. Recent structural determinations based on microwave and high-resolution vibrational spectra indicate that c–c single bond lengths in unsaturated compounds are determined largely by the state of hybridization of the atoms involved. Only a few bond lengths have been reported for unsaturated fluorocarbons and these do not often agree very well. Thus the C–F bond length in fluorobenzene has been reported to be 1.348 Å (ref 4) and 1.29 Å (ref 5). A value of 1.321 Å has been obtained for CH_2CF_2 (ref 6), but multiple fluorine substitution is known to decrease the C–F bond length in saturated compounds.[7] Recently, Allen and Plyler[3] have reported the following structural values for ethylene as determined by analysis of high-resolution infrared spectra: r(C=C) = 1.337 Å, r(C–H) = 1.086 Å, and ∠HCH = 117° 22′. Another recent structure for ethylene, as determined by electron diffraction, gives r(C=C) = 1.334 Å, r(C–H) = 1.085 Å, and ∠HCH = 116° (ref 8). Our result for r(C=C) is, therefore, very close to that for unsubstituted ethylene. On the other hand, the C–F distance in ethyl fluoride is 1.375 Å, as determined by microwave spectroscopy.[9] The fact that r(C–F) in vinyl fluoride is ~0.03 Å less may be attributed to the smaller effective radius of the sp^2 hybridization of the carbon atom.

[3] H. C. Allen, Jr., and E. K. Plyler, *J. Am. Chem. Soc.* 80, 2673 (1958).

[4] G. Erlandsson, *Arkiv. Fysik* 6, 477 (1953).

[5] K. E. McCulloh and G. F. Pollnow, *J. Chem. Phys.* 22, 1144 (1954).

[6] W. F. Edgell, P. A. Kinsey, and J. W. Amy, *J. Am. Chem. Soc.* 79, 2691 (1957).

[7] D. R. Lide, Jr., *J. Am. Chem. Soc.* 74, 3548 (1952).

[8] L. S. Bartell and R. A. Bonham, *J. Chem. Phys.* 27, 1414 (1957).

[9] J. Kraitchman and B. P. Dailey, *J. Chem. Phys.* 23, 184 (1955).

PRELIMINARY CLASSIFICATION OF THE SPECTRUM OF SINGLY IONIZED ERBIUM (Er II)

J. R. McNally, Jr. K. L. Vander Sluis

Recently, Lindner and Davis[1] published Zeeman-effect data for the spectra of erbium. Their attempts at classification of the spectra using the MIT digital computer proved unsuccessful.

Using their Zeeman data and the wavelength data of Gatterer and Junkes,[2] we have succeeded in establishing six low levels and numerous high levels. The 6 low levels and the 43 best high levels are given in Table 1. Transitions between these levels of Er II account for 147 lines of the 198 allowed transitions ($\Delta J = 0, \pm 1$). The low electron configuration is $4f^{12}6s(^{4,2}H)$, for which four levels are believed to be identified (0, 440, 7149, 7195 cm^{-1}). Two levels, probably from the configuration $4f^{12}5d$, have been located about 0.6 ev above the lowest level. Splitting by the $6s$ electron in the $4f^{12}6s$

[1] J. W. Lindner and S. P. Davis, *J. Opt. Soc. Am.* 48, 542 (1958).

[2] A. Gatterer and J. Junkes, *Spektren der Seltenen Erden*, Città del Vaticano, 1945.

configuration is small and comparable to that for thulium (ref 3) (238 and 188 cm^{-1} for $4f^{13}6s$). This small s doubling of the $f^n s$ configurations is a characteristic of the singly ionized spectra of the rare earths.[4] The level splitting in the $4f^{12}(^3H_6 - {}^3H_5)$ parent is of the order of 7000 cm^{-1}, which may be compared to the $4f^{13}6s^2(^2F)$ splitting of 10,150 cm^{-1} in Yb I (ref 5). Except for the inversion of the $f^{12}(^3H)$ parent term, it is expected that level schemes in Er II will be quite analogous to levels built on the f^2 parent term in Ce II.

[3]W. F. Meggers, *J. Opt. Soc. Am.* 31, 157 (1941).

[4]See, for example (Ce), G. R. Harrison, W. E. Albertson, and N. F. Hosford, *J. Opt. Soc. Am.* 31, 439 (1941); (Pr), N. Rosen, G. R. Harrison, and J. R. McNally, Jr., *Phys. Rev.* 60, 722 (1941); (Nd), W. E. Albertson, G. R. Harrison, and J. R. McNally, Jr., *Phys. Rev.* 61, 167 (1942).

[5]W. F. Meggers, *J. Opt. Soc. Am.* 37, 988 (1947).

Table 1. Energy Levels for Er II

Level	J	g	Level	J	g
Low Levels			**High Levels**		
0.0	13/2	1.225	31844.2	9/2	1.177
440.4	11/2	1.092	32073.5	11/2	1.178
5132.7	9/2	1.234	32267.3	9/2	1.15
5403.9	7/2	1.038	32502.9	9/2	1.223
7149.7	11/2	1.110	32528.4	13/2	1.156
7195.4	9/2	0.942	32790.3	7/2	1.147
			32896.6	9/2	1.192 ?
High Levels			33105.6	11/2	1.063
25382.4	11/2	1.158	33307.9	11/2	1.25
26098.8	13/2	1.112	33659.4	11/2	1.180
27513.6	13/2	1.096	33721.6	11/2	1.184
27642.6	11/2	1.055	33804.6	9/2	1.174
27853.7	11/2	1.068	33988.4	11/2	1.150
27932.9	9/2	1.223	34341.7	11/2	1.122
28361.7	11/2	1.021	34397.2	9/2	1.144
29011.1	9/2	1.105	34563.3	11/2	1.141
29119.8	13/2	1.092	34972.4	11/2	1.150
29492.3	11/2	1.040	35063.9	9/2	1.166
29783.8	9/2	1.155	35618.1	11/2	1.138
29858.7	11/2	1.12	36031.5	9/2	1.161
30122.8	11/2	1.120	36147.8	11/2	1.135
30157.6	11/2	1.07	36761.3	9/2	0.998
30317.9	9/2	1.07	37110.4	9/2	1.066
30621.1	13/2	1.159	37438.7	9/2	1.057
30894.6	7/2	1.268	38693.4	9/2	1.135

CLASSIFICATION OF SINGLY IONIZED PLUTONIUM (Pu II)

J. H. Wise[1] P. M. Griffin J. R. McNally, Jr.

Investigation of the spectrum of singly ionized plutonium, Pu II, has been continued.[2] One hundred fifty-three additional Zeeman patterns were measured, on a spectroscopic plate, which completed the coverage of the spectrum region from 4370 to 6800 Å (see ref 2). The g factors for these patterns were computed, by the least-squares routine reported by Vander Sluis,[3] on the Oracle. The energy-level scheme[4] and the additional levels[2] have been reported previously.

The present status of the work on the Pu II spectrum, including the data of McNally and Griffin,[4] may be summarized as follows:

Wavelength coverage, 2900–6800 Å

Measured Zeeman patterns, approximately 600

Classified Zeeman transitions, approximately 140

Unclassified Zeeman transitions, approximately 460

An intensive search to discover further low energy levels, both in the ground-state electronic configuration $[f^6(^7F)s]$ and in the expected neighboring configuration $[f^6(^7F)d]$, has been started. Preliminary results gave the following two new levels:

12007.7 cm^{-1} $J = 1/2$ $g = 0.00$

(five resolved Zeeman patterns observed)

13726.6 cm^{-1} $J = 5/2$ $g = 0.79$

(three resolved Zeeman patterns observed)

The g values of these levels are in reasonable agreement with theoretical g values in the expected neighboring electronic configuration; however, sufficient data are not available to establish a unique electronic configuration from among several possibilities.

Although greatest attention is being placed on low energy levels, the search for additional upper energy levels has been continued. No levels of higher than B quality (using the criterion established by McNally and Griffin[4]) were found, and those that were found have not been checked thoroughly enough to be included in this report.

[1]Summer employee from Washington and Lee University.

[2]J. H. Wise, P. M. Griffin, and J. R. McNally, Jr., *Phys. Semiann. Prog. Rep. Sept. 10, 1957*, ORNL-2430, p 96.

[3]K. L. Vander Sluis, *J. Opt. Soc. Am.* 46, 605 (1956).

[4]J. R. McNally, Jr., and P. M. Griffin, *Stable Isotope Semiann. Prog. Rep. Nov. 30, 1956*, ORNL-2236, p 34.

FURTHER EVALUATIONS OF THE DUO-PLASMATRON ION SOURCE

C. D. Moak J. W. Johnson R. F. King H. E. Banta

In the previous semiannual report,[1] a new ion source, developed in Germany by M. von Ardenne, was described. It was reported that this source appears capable of delivering proton currents that are limited only by the space-charge limits for the accelerating system which follows the source. Development of a miniature version of the original 1-amp source for high-intensity Van de Graaff pulse work is still in progress. Development work on filaments having long life in this application is described elsewhere.[2]

Recent interest in beams of negative hydrogen ions for use in tandem accelerators has prompted us to examine the output of the Duo-Plasmatron for traces of these ions. For this purpose it was necessary only to reverse the polarities of the extractor-accelerator electrode, the focusing lens electrode, and the field of the magnetic mass-analyzer. A miniature Duo-Plasmatron which had been designed to deliver 1 ma of protons was used in the test.

The first observation was that the Duo-Plasmatron is an extremely bright electron source; it was found

[1]C. D. Moak *et al.*, *Phys. Semiann. Prog. Rep. March 10, 1958*, ORNL-2501, p 75.

[2]C. D. Moak, R. F. King, J. W. Johnson, and H. E. Banta, "The Duo-Plasmatron Ion Source," *Instrumentation and Controls Ann. Prog. Rep. July 1, 1958*, ORNL-2647 (to be published).

that the electron current per unit aperture area was near 100 amp/cm^2. By running the arc pressure up till the discharge was in the "H_3^+ mode," the source was made to deliver detectable quantities of H_1^- ions. It is not clear where and how the H_3^+ ions are being broken up into two protons and an H_1^- ion, since no differentially pumped gas cell was used for stripping. The beam current obtained was 11 μa of H_1^- ions; this current was delivered into a focus of <1 mm diameter at a biased Faraday cup 25 in. from the focusing assembly. The focal spot was examined for a low-energy tail which might indicate stripping in the accelerator gap; no evidence of a large energy spread was found. It appears that high-quality beams of H_1^- ions of reasonably large currents can be obtained from the Duo-Plasmatron without the use of differentially pumped stripping cells.

Operating characteristics for the small source have been measured for He^+ and He^{++}. Characteristics for He^+ were very similar to those for H_1^+. Operation at low pressure gave an He^{++} component of about 5 μa. Maximum currents of 7 μa of He^{++} were obtained at very low pressures, but the arc tended to become unstable. The Duo-Plasmatron would appear to be a good source of He^{++} ions where gas economy is of considerable importance.

DELAY-LINE MEMORY PULSE SPECTROMETER

D. Maeder

SURVEY OF RECENTLY ADDED CIRCUITS

The quartz delay-line 120-channel pulse spectrometer originally constructed and described by Emmer[1] has been equipped recently with the following features:

1. The *binary adding circuit* has been changed so that it can add or subtract pulses, depending on the position of the S/A relay (or the parallel switch) in Fig. 1. This feature is desirable for automatic background subtraction as well as for the analysis of complex spectra. The circuit shown does not require complementing the memory contents in order to change from adding to subtracting or vice versa. Rather, the adder reset signal is derived in two different ways (either from the first "one" or from the first "zero" occurring at the adder output) in order to obtain both kinds of operation.

2. The *channel pulse coincidence* circuit has been changed so that it can accept either all the channel pulses or only the even or the odd channel pulses, depending on the position of two toggle switches or relays ("even-odd" and "whole-split"). In this manner the memory can be split for accumulating two different spectra, and the oscilloscope display presents the spectra in an interlaced fashion.

3. An *additional gate* has been incorporated, with its input and output available at the front panel. Gating from the pulse lengthener circuit is arranged in such a way that negative pulses ($\geq$ 5 v) from an external monitor or from a clock generator are fed to the new input and are transmitted to the new output, only if received during the live time of the spectrometer. Use of the gated clock (or monitor) provides for automatic dead-time correction. Output pulses are 10 v negative with 1 kilohm internal impedance.

4. The *"count" switch* originally provided the following three positions: count, stop, and 1000 counts/sec internal test. A flip-flop circuit has been added to this switch arrangement in order to have the internal test start or stop always at the end of a memory cycle so that uniformity of the test over the whole spectrum is ensured. A further switch position has been introduced in which an internal "count one" test can be actuated repeatedly by pressing a push button. The possibility of manually producing any desired pattern of memory pulses proved very useful for maintenance.

5. A Shannon-type *digital-to-analog converter* has been constructed, with a switch to select between two modes of analog display and the original binary display, in order to facilitate the evaluation of data. The same principle of conversion has been used by Schultz, Pieper, and Rosler,[2] but our present circuit was further developed to ensure a $\pm$3% over-all linearity and reproducibility of analog readings.

---

[1] T. L. Emmer, *I.R.E. Convention Record* 3(10), 211 (1955).

[2] H. L. Schultz, G. F. Pieper, and L. Rosler, *Rev. Sci. Instr.* 27, 437 (1956).

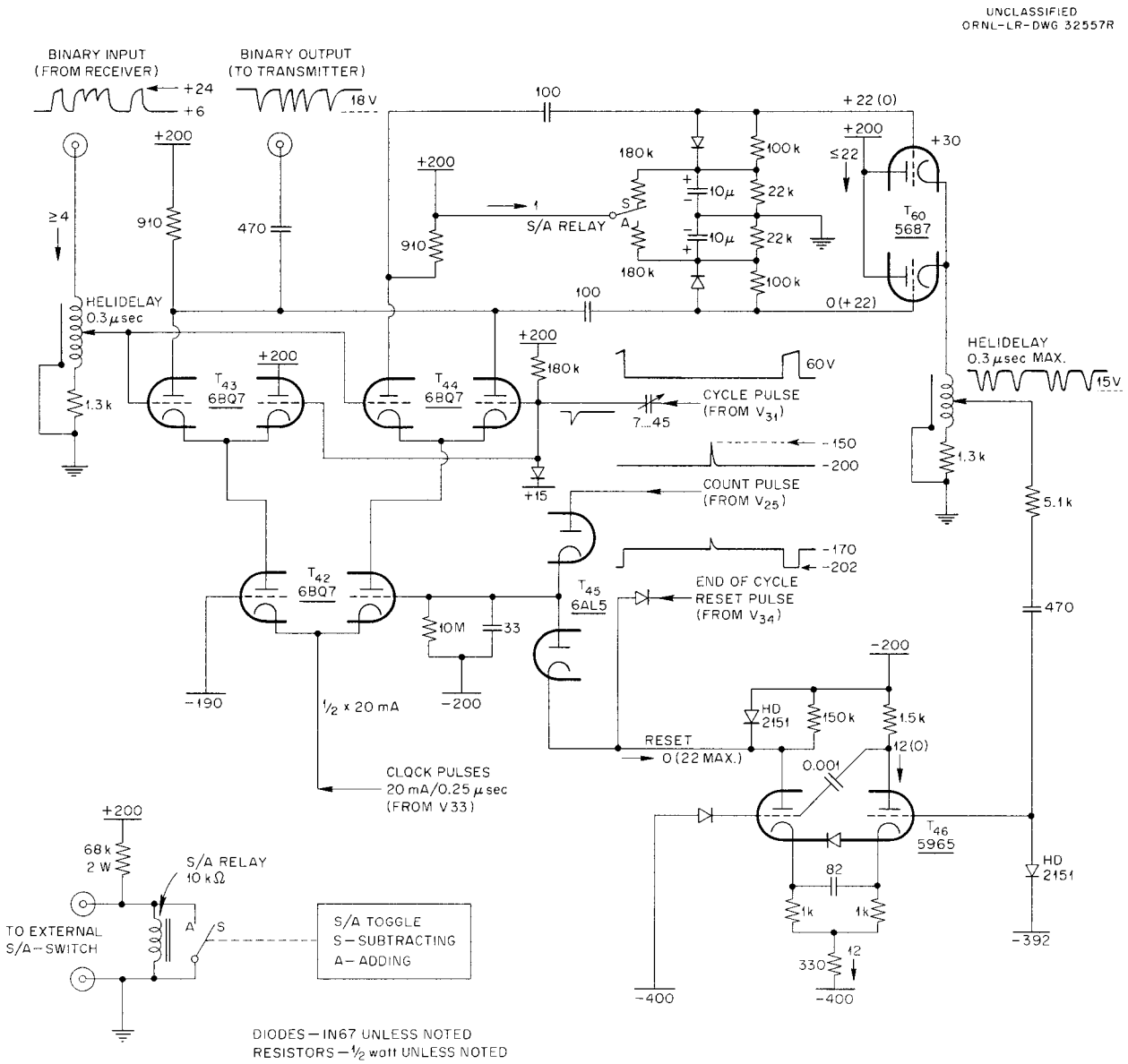

Fig. 1. Binary Add-Subtract Circuit.

OPERATION OF ANALOG DISPLAY CIRCUIT

Depending on the position of switch SW1 (see Fig. 2, "multiplier"), a certain group of bits in each channel (e.g., bits 1 to 7, 1 to 8, 1 to 9, or 2 to 10, etc.) is selected for the conversion, while time between these groups is used for the display of the converted output. Neglecting the insignificant bits permits a large display duty cycle and allows bright and well-defined spots on the oscilloscope. For an easy check of the conversion accuracy, internal calibration is provided in positions 1, 3, 5, and 7 of the "display mode" switch (SW2, see Fig. 2). In position 2 of this switch, analog signals smaller than half the maximum buildup voltage on C_2 are normally (i.e., with the P_{12} wiper in the position shown in Fig. 2) displayed between the marks "0" and "100" of the calibrated oscilloscope screen. In position 6, zero analog voltage falls outside the screen, and the calibrated range displays numbers between 100 and 200 analog units. The absolute value of these units changes with the SW1 setting as indicated in the circuit diagram. The "fine gain

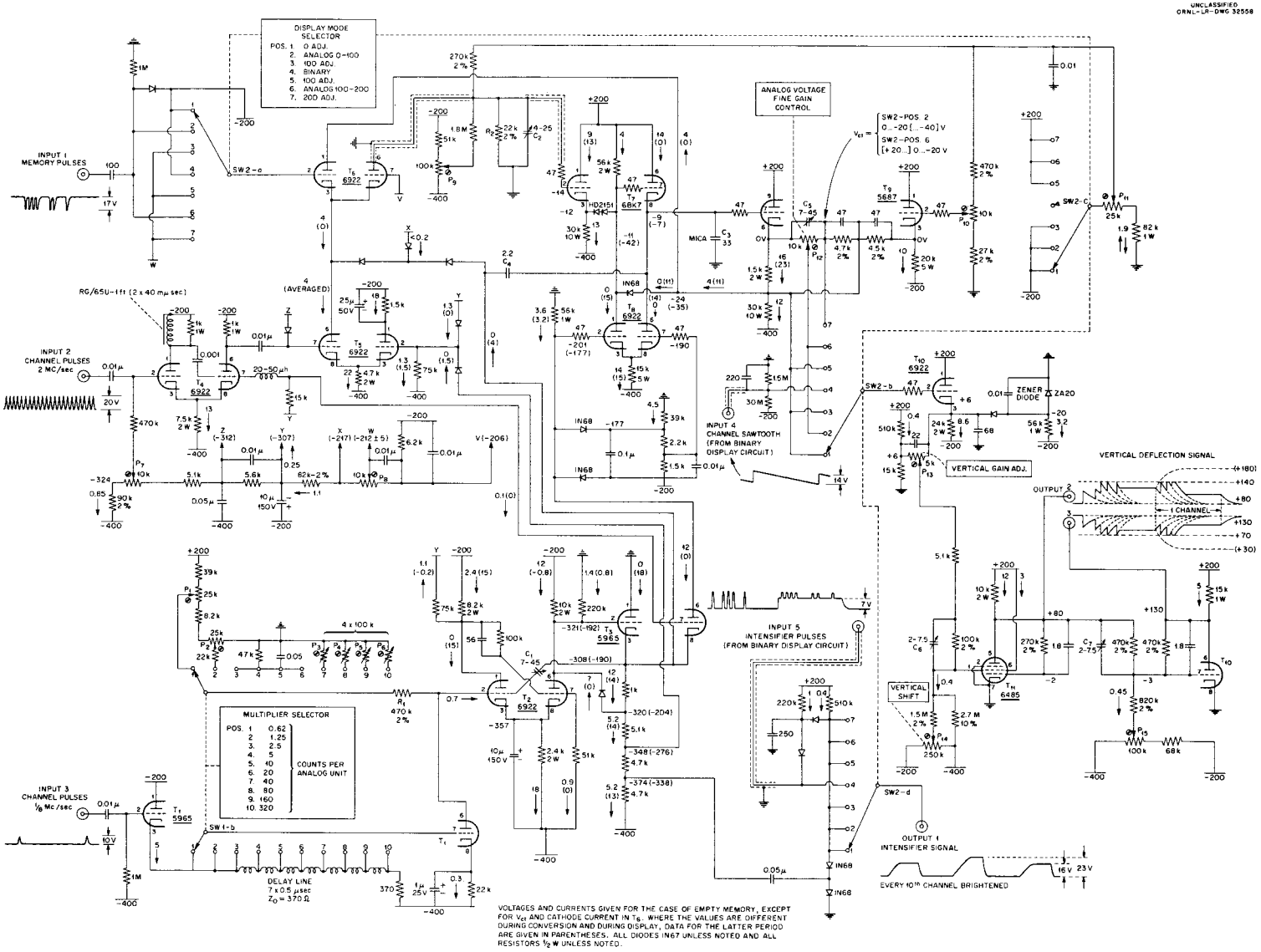

Fig. 2. Linear Analog Display Circuit.

control," P_{12}, can be used to make a point of the spectrum (e.g., a peak) coincide with the "100" mark so that another point can be read off the calibrated scale as a fraction of the intensity of the former point. In this manner a transmission factor or a peak-to-valley ratio can be read directly without reference to absolute counts. If such factors are between 0.5 and 2, the suppressed-zero presentation is useful.

It should be kept in mind that significant bits can be lost by improper setting of the "multiplier selector." In such a case, the binary remainder will be displayed in analog form.

ADJUSTMENT PROCEDURE

Accuracy of the conversion depends on the following adjustments:

Conversion Period. – The right halves of T_2 and T_3 are conducting, and short standardized pulses (20 ma, 0.11 μsec) are drawn from the common cathode of T_6. When a certain bit contains a memory pulse, the left half of T_6 is cut off to <0.5 ma for at least 0.2 μsec and the standard pulse is transferred to the R_2C_2 memory circuit. Proper positioning of the standard pulses with respect to the memory input pulses (to make charge pulses transferred to right half of T_6 independent of unavoidable input pulse shape variations) is accomplished by adjusting P_7. To make the current transfer in T_6 independent of output voltage (which is variable according to the memory pulse pattern), the output signal is fed back from T_9 to the left half of T_6, keeping the plate-cathode potential differences nearly equal in both halves of T_6.

The condition that the voltage on C_2 represents a linear analog of the binary pulse pattern (as applied to input 1) is given by

$$R^*C^* \ln 2 = \text{digit period} \quad ,$$

where

R^* = effective shunt resistance = $R_2 \parallel 270$ kilohms $\parallel$ 1.8 megohms,

C^* = effective shunt capacitance $\cong C_2 + 15\ \mu\mu f$,

and can be verified by observing the change in analog output on changing the digital input from $(2^n - 1)$ to 2^n. With proper C_2 adjustment, irregularities in these transitions ($n = 4, 5, 6, 7$) can be kept within $\pm 1.5\%$ of 100 analog units.

End of Conversion Period. – The left half of T_2 suddenly comes into conduction. The triggering is effected by T_3 (right half) at a well-defined phase of the clock oscillation (halfway between two standard pulses). The length of the conversion period is different in positions 1, 2, 3 of SW1 (adjustable by means of P_1, P_2, C_1). Although the conversion period is essentially constant for switch positions 3 ... 10, individual adjustments ($P_{3,4,5,6}$) are necessary, since the signal causing the beginning of the conversion period is increasingly distorted when taken from later sections of the 370-ohm delay line. In order to keep sampling errors <1.5%, the end of the conversion period must be reproducible within $\pm 0.015\ R^*C^*$ ($\cong 0.01\ \mu$sec), since this is the time when the analog voltage on C_2 is to be sampled into C_3 and stretched for the display. The adjustments ($P_{1...6}$) are checked by verifying the exact doubling or halving of a suitable analog pattern on the display screen when SW1 is turned.

Display Period. – The right halves of T_2 and T_3 are cut off, and the cathode current in T_8 is transferred to the left half of T_8, thereby insulating the stretching capacitor C_3. The entire range of stretched voltages on C_3 is from −11 to −99 v in SW2 position 2 (of which only the portion −11 v to −55 v is normally displayed), or from +11 to −77 v in SW2 position 6 (−33 v to −77 v displayed). The potential V_{ct} at the center tap of the divider between the two cathodes of T_9 (i.e., at the normal position of the P_{12} wiper) will now be considered. Its range for the display is always from 0 ... −20 v plus a small constant bias, and in each calibrating position of SW2 the stretched V_{ct} must coincide with one of these two marks. Prior to adjusting $P_{9,10,11}$, the common cathode resistor of T_5 should be verified as being of the proper value to give V_{ct} excursions of 40 v between empty and completely filled memory in either SW2 position 2 or 6, and P_8 must be adjusted to simulate (with respect to V_{ct}) the filled memory condition when SW2 is turned to position 3 or 7, respectively. Since the filled memory corresponds to 200 analog units, 100 analog units are derived by further voltage division (between V_{ct} and the right-hand cathode of T_9) for the calibrating positions 3 and 5. Adjustment of $P_{9,10,11}$ is made in order to meet three conditions simultaneously: (1) equal potential ($\cong 0$) on both cathodes of T_9 if memory is empty and SW2 is in position 2, (2) equal potential change (+20 v) on both cathodes of T_9 on switching SW2 from position 2 to 6, with empty memory, (3) zero change of T_{10} (left half) grid potential on switching SW2 from position 3 to 5.

Potentiometers $P_{13,14}$ permit fitting of the calibrated analog voltage range to the oscilloscope screen graticule, and can also be used for compensating slight misadjustments of $P_{9,10,11}$ which may develop during warmup; P_{15} is set to equalize the two output potentials at approximately +110 v. The output amplifier is overload-protected by a diode connected to T_{10}.

RECORDING OF SPECTRA FROM ANALOG DISPLAY

The leading edge of the intensifier signal is slowed down by a diode-RC network in order to prevent the switching transient in the analog voltage from being displayed. Additional intensification of every tenth channel is superimposed from the original binary display intensifier output (impedance, 1000 ohms) onto the analog display intensifier output via another diode. It should be kept in mind, however, that these tenth-channel intensifying pulses are not so timed as to fit the analog intensifier signals with all possible multiplier settings.

The modified spectrometer has been used with the 3-Mv Van de Graaff for measurement of neutron time-of-flight spectra. Pairs of Polaroid-Land pictures covering 60 channels each were usually taken, with the "0" and "100" analog calibration levels superimposed at a reduced exposure. Generally, several multiplier settings are used with a given spectrum, and the multiplier values (SW2, see Fig. 2) are noted, so that the photographic record contains complete information for evaluation of absolute counts.

AN IBM 704 PROGRAM FOR COMPUTATION OF EQUILIBRIUM ORBIT PROPERTIES IN AVF CYCLOTRONS

M. M. Gordon T. A. Welton T. I. Arnette H. C. Owens

Over the past four years considerable experience has been gained on a succession of Oracle codes for the computation of equilibrium orbit properties in AVF cyclotrons. The increasingly obvious limitations of these codes, combined with the acquisition of an IBM 704 computer at the K-25 plant, recently opened the possibility of a new family of codes of much greater speed and flexibility than are possible on the Oracle. The first code in this family is now complete. For input it requires the quantities B and $\partial B/r\ \partial\theta$, where B is the median plane field, stored on magnetic tape at uniform intervals of r and θ. The fields must be in units of $mc\omega/e$, and radii are in units of c/ω, where e = charge of ion, m = rest mass of ion, c = speed of light, and ω = angular frequency of accelerating voltage.

The code starts with a specified value of the independent variable, which may be p (momentum in units of mc), β, or E (total energy in units of mc^2). It calculates a guessed equilibrium orbit through one sector and at the same time calculates the derivatives of the r and p_r values with respect to the starting values. From this information, a new guess for the equilibrium orbit is found by Newton's method and the same information is found again, until the r and p_r values at the end of the sector agree with the initial values to prescribed accuracy. At this point the code integrates through one sector with all equations, including axial motion. This information at each Runge-Kutta step is stored on magnetic drums for future detailed processing, and the final values are used to obtain the following:

ν_r, ν_z = radial and axial focusing frequencies,

$r(0)$ = radius of equilibrium orbit at $\theta = 0$,

$p_r(0)$ = radial momentum of equilibrium orbit at $\theta = 0$,

$\langle r \rangle$ = mean radius of equilibrium orbit at $\theta = 0$,

$r_{max} - r_{min}$ = radial spread of equilibrium orbit at $\theta = 0$,

$\cos\sigma_r$, $\cos\sigma_z$ = $\cos 2\pi\ \nu_r/N$, $\cos 2\pi\ \nu_z/N$,

T = time for passage through one sector (units of $1/\omega$).

This information (or one of several alternate selections from the list) is printed and the independent variable is increased by a fixed increment. The complete process is then repeated until the desired table has been completed.

It has been found that the total time required is 6 sec for each value of the independent variable, as compared with 45 sec for the equivalent Oracle code. This yields a speed ratio of 7.5 as compared with an hourly cost ratio of 5.33, so that the 704 calculation is cheaper by a factor of 1.4. The cost is about 50¢ per value of the independent variable.

A detailed set of precision checks is in progress for studying the effects of radial-interval size, angular-interval size, field measurement errors, and interpolation errors in passing from a rectangular measurement grid to the polar grid required for the code. It should then be possible to design a field measurement arrangement which will give a specified accuracy for the various orbit properties with minimum effort.

Future variants of this code will adjust the radial variation of the azimuthally averaged field to yield any desired variation of orbital frequency with energy, and will print out the required correction to the input field to accomplish this.

PUBLICATIONS

Block, R. C., "Angular Distribution of Neutrons Scattered by the 2.80-kev Resonance in Sodium," *Phys. Rev.* **109**, 1217 (1958).

Block, R. C., W. Haeberli, and H. W. Newson, "Neutron Resonances in the kev Region: Differential Scattering Cross Sections," *Phys. Rev.* **109**, 1620 (1958).

Busing, W. R., and H. W. Morgan, "The Infrared Spectrum of $Ca(OH)_2$," *J. Chem. Phys.* **28**, 998 (1958).

Charles, G. W., "On the Energy Levels of the Configuration $6p^2$ in Hg I," *J. Opt. Soc. Am.* **48**, 668 (1958).

Church, E. L., M. E. Rose, and J. Weneser, "Electric-Monopole Directional-Correlation Experiments," *Phys. Rev.* **109**, 1299 (1958).

Francis, J. E., P. R. Bell, and C. C. Harris, "Scintillation Spectrometry," Chap. 4, p 32 in *External Collimation Detection of Intercranial Neoplasia with Unstable Nuclides*, Livingstone, London, 1958.

Gersch, H. A., and W. C. Koehler, "Types of Magnetically Ordered Configurations on Simple Lattices," *J. Phys. and Chem. Solids* **5**, 180–201 (1958).

Green, T. A., and M. E. Rose, "Nuclear Structure Effects in Internal Conversion," *Phys. Rev.* **110**, 105 (1958).

Harvey, J. A., and R. B. Schwartz, "Thermal and Resonance Neutron Cross Sections of Heavy Nuclei," *Progress in Nuclear Energy*, Series 1 – *Physics and Mathematics*, vol 2, p 51–90, Pergamon Press, New York, 1958.

Johnson, C. H., A. Galonsky, and J. P. Ulrich, "Proton Strength Functions from (p,n) Cross Sections," *Phys. Rev.* **109**, 1243 (1958).

Klema, E. D., "Angular Correlations of Gamma Rays in Cascade from Levels in Lu^{175} and Hf^{177}" *Phys. Rev.* **109**, 1652 (1958).

Koehler, W. C., E. O. Wollan, and M. K. Wilinson, "Paramagnetic and Nuclear Scattering Cross Sections of Holmium Sesquioxide," *Phys. Rev.* **110**, 37 (1958).

Lazar, N. H., G. D. O'Kelley, J. H. Hamilton, L. M. Langer, and W. G. Smith, "Nuclear Structure of Zr^{90}," *Phys. Rev.* **110**, 513–519 (1958).

Moak, C. D., A. Galonsky, R. L. Traughber, and C. M. Jones, "Energy Levels of Be^9, C^{12}, and C^{13}," *Phys. Rev.* **110**, 1369 (1958).

Norris, J. A., "Spectrographic Determination of Trace Elements in Metals," *Am. Soc. Testing Materials, Spec. Tech. Publ. No. 221*, p 23 (1958).

Rose, M. E., "Phenomena Affected by the Finite Size of the Nucleus," *Proceedings of the Rehovoth Conference on Nuclear Structure, Held at the Weizmann Institute of Science, Rehovoth, Sept. 8–14, 1957* (ed. by H. J. Lipkin), Interscience, New York, 1958.

Rose, M. E., and R. L. Becker, "Polarization of Conversion Electrons Following β-Decay," *Phys. Rev. Letters* **1**, 116 (1958).

Slaughter, G. G., E. M. Harth, and M. M. Block, "V-Particle Production by 1.9-Bev π^- Mesons," *Phys. Rev.* **109**, 2111 (1958).

Stelson, P. H., and F. K. McGowan, "Coulomb Excitation of Medium-Weight Even-Even Nuclei," *Phys. Rev.* **110**, 489 (1958).

Trammell, G. T., H. Zeldes, and R. Livingston, "Effect of Environmental Nuclei in Electron Spin Resonance Spectroscopy," *Phys. Rev.* **110**, 630 (1958).

Wollan, E. O., "Correlations Suggesting the *d*-Shell Configuration and a Magnetic Exchange Mechanism in Iron Group Metals," *Phys. Rev.* **110**, 1205 (1958).

Wollan, E. O., W. C. Koehler, and M. K. Wilkinson, "Neutron Diffraction Study of the Magnetic Properties of $MnBr_2$," *Phys. Rev.* **110**, 638 (1958).

PAPERS PRESENTED AT SCIENTIFIC AND TECHNICAL MEETINGS

American Physical Society, Southeastern Section Meeting, Huntsville, Alabama, April 10–12, 1958

J. H. Gibbons (invited paper), "Cross Sections of kev Neutrons."

M. M. Gordon (invited paper), "Review of Beam Deflection Theoretical Studies."

P. M. Griffin (invited paper), "Application of the Echelle Spectrograph to Zeeman Spectroscopy."

K. L. Vander Sluis (invited paper), "An Application of Digital Computers to Zeeman Spectroscopy."

J. W. T. Dabbs, L. D. Roberts, and G. W. Parker, "Low Temperature Specific Heat Measurements on $U^{235}O_2Rb(NO_3)_3$."

J. L. Fowler and H. O. Cohn, "Differential Elastic Neutron Scattering from Beryllium."

A. Galonsky, H. B. Willard, A. R. Brosi, B. H. Ketelle, H. O. Cohn, and N. H. Lazar, "Spherical Electrostatic Spin-Rotator for Electron Polarization Measurements."

J. A. Harvey, R. C. Block, and G. G. Slaughter, "A High Intensity Time-of-Flight Neutron Spectrometer."

C. H. Johnson, A. Galonsky, and C. N. Inskeep, "Cross Sections for (p,n) Reactions in Intermediate Nuclei."

F. K. McGowan and P. H. Stelson, "Coulomb Excitation of States in Pt^{195}."

J. H. Neiler, J. H. Gibbons, and W. M. Good, "Application of Pulsed Beam Techniques to Nuclear Spectroscopy."

F. J. Walter, L. D. Roberts, and J. W. T. Dabbs, "Low Temperature Characteristics of Germanium *p-n* Junction Counters."

American Chemical Society Meeting, San Francisco, California, April 13–18, 1958

P. A. Staats, "Infrared Spectra of Deuterium Substituted Phosphine Molecules."

American Physical Society Meeting, Washington, D.C., May 1–3, 1958

R. C. Block, J. A. Harvey, and G. G. Slaughter, "Neutron Resonance Parameters of Pm^{147} and Am^{241}."

J. W. Cable, M. K. Wilkinson, E. O. Wollan, and W. C. Koehler, "Neutron Diffraction Investigations of the Antiferromagnetic Ordering in MnI_2."

J. A. Harvey, G. G. Slaughter, and R. C. Block, "Spin States for Resonances in W^{183}, Ag^{107}, and Ag^{109}."

F. K. McGowan and P. H. Stelson, "Coulomb Excitation of the Second 2^+ State in Isotopes of W, Os, and Pt."

R. L. Macklin and J. H. Gibbons, "Neutron Yields from Light Element (α,n) Reactions."

J. H. Neiler, J. H. Gibbons, and W. M. Good, "Total Cross Sections for 2- to 20-kev Neutrons."

L. D. Roberts, J. W. T. Dabbs, F. J. Walter, and G. W. Parker, "Antisotropy of Fission Fragments from Oriented U^{233} Nuclei."

G. G. Slaughter, R. C. Block, and J. A. Harvey, "Parameters of Neutron Resonances in Ag, I, and Au."

F. J. Walter, J. W. T. Dabbs, and L. D. Roberts, "Fission Fragment Counting with Germanium *n-p* Junction Counters."

Association for Computing Machinery, Annual Meeting, Urbana, Illinois, June 11–13, 1958

T. I. Arnette, "An Interpolation Procedure for Closed Curves."

Symposium on Molecular Structure and Spectroscopy, Ohio State University, Columbus, Ohio, June 16–20, 1958

H. W. Morgan and J. R. Lawson, "The Infrared Spectra of HNCS and DNCS."

Gordon Research Conference on Nuclear Chemistry, Meriden, New Hampshire, June 23–27, 1958

L. D. Roberts (invited paper), "Alpha Particle Emission from Oriented Actinide Nuclei."

P. H. Stelson (invited paper), "Some Recent Experimental Coulomb Excitation Results."

International Low Temperature Conference (Kamerlingh Onnes), Leiden, The Netherlands, June 23–28, 1958

J. W. T. Dabbs (invited paper), "Alpha-Particle and Fission Anisotropies from Oriented Actinide Nuclei."

W. C. Koehler, E. O. Wollan, M. K. Wilkinson, and J. W. Cable, "Neutron Diffraction Studies of Antiferromagnetic Rare Earth Compounds."

International Conference on Magnetism, University of Grenoble, Grenoble, France, July 2–5, 1958

W. C. Koehler, M. K. Wilkinson, J. W. Cable, and E. O. Wollan (invited paper), "Single Crystal Neutron Diffraction Studies of Antiferromagnets at Low Temperatures in Applied Magnetic Fields."

International Congress on Nuclear Physics, Paris, France, July 7–12, 1958

F. K. McGowan (invited paper), "Coulomb Excitation."

7th Annual Conference on Industrial Applications of X-Ray Analysis, Denver, Colorado, August 13–15, 1958

W. F. Peed (invited paper), "Wavelength Measurements of Radioactive Materials."

American Physical Society Meeting, Vancouver, British Columbia, August 26–28, 1958

M. E. Rose, "Depolarization of Mu Mesons in Bound States."

*2nd Geneva Conference on the Peaceful Uses of Atomic Energy, Geneva, Switzerland, September 1–13, 1958**

J. A. Harvey, R. C. Block, and G. G. Slaughter, "Low Energy Neutron Cross Sections of radioactive Fission Product Nuclides."

R. L. Macklin, "Neutron Absorption at Intermediate Energies."

L. D. Roberts, J. W. T. Dabbs, and G. W. Parker, "Alpha Emission from Oriented Np^{237} and U^{233} Nuclei."

American Chemical Society Meeting, Chicago, Illinois, September 7–12, 1958

M. K. Wilkinson (invited paper), "Neutron Diffraction Investigations of Antiferromagnetism at Low Temperatures."

*Papers to be included in the Geneva Conference Proceedings.

LECTURES

Visiting Scientist Lecture Program in Physics, Sponsored by the American Institute of Physics and the American Association of Physics Teachers

R. C. Block, "Research and the Government Laboratories." (Carson-Newman College, Jefferson City, Tennessee, April 25, 1958).

J. L. Fowler, "Fundamental Particles of Physics" (Kenyon College, Gambier, Ohio, May 7–8, 1958).

J. H. Neiler, "The Work of a Nuclear Physicist" (Atlanta University Center, Atlanta, Georgia, April 23–25, 1958).

Fisk University Infrared Institute, Nashville, Tennessee, August 25–29, 1958

H. W. Morgan (invited lectures)

1. "The Use of Isotopes in Molecular Spectra Studies."
2. "Experimental Techniques in Infrared Spectra."
3. "Force Constants, Fudge Factors, and Potential Fields."

P. A. Staats, "Applications of Infrared Spectroscopy to Industrial Problems."

ANNOUNCEMENTS

Additions to the Physics Division staff during this period were as follows: P. D. Miller (High Voltage Group) and R. L. Robinson (Classification of Low-Lying Nuclear Energy Levels).

J. Walter, formerly of the Reactor Experimental Engineering Division, has transferred to the Physics Division's Low Temperature Group, where he will work toward the Ph.D. degree in physics.

T. A. Carlson of the Chemistry Division is on loan to the Charge Spectrometry Group.

The appointment of D. G. Maeder (from the Physikalisches Institut in Zurich, Switzerland) has been extended for one year; he will continue work with the Scintillation Spectrometry and Instrument Development Group.

Co-op students assigned to the High Voltage Group during this period include D. O. Patterson, M. C. Taylor, and C. E. Hughey from the University of Tennessee (Martin Branch) and A. F. Nickle from the University of Tennessee (Knoxville).

R. A. Mann (University of Alabama) and C. P. Bhalla (University of Tennessee) have been granted Oak Ridge Graduate Fellowships. They will complete work toward the Ph.D. degree with the Theoretical Physics Group.

Summer personnel during this period included the following research participants and visitors: G. L. Jenkins (Head of the Physics Department at Stetson University), Neutron Velocity Selector Program; M. S. McCay (Head of the Physics Department at the University of Chattanooga) and J. H. Wise (summer visitor, Washington and Lee University), Spectroscopy Research; W. G. Smith (Assistant Professor of Physics at Purdue University), Classification of Low-Lying Nuclear Energy Levels; H. A. Gersch (summer visitor, Georgia Institute of Technology) and A. W. Saenz (summer visitor, on loan from the Naval Research Laboratory), Neutron Diffraction Group; F. S. Levin (summer visitor, University of Maryland), High Energy Accelerator Studies; R. R. Lewis, Jr. (summer visitor, University of Michigan), Theoretical Physics; J. N. Thurston (summer visitor, Clemson College), Scintillation Spectrometry and Instrument Development Group.

W. C. Koehler (Neutron Diffraction Group) is on a year's leave of absence to do research at the University of Grenoble in Grenoble, France, under a Guggenheim Foundation Fellowship and a Fulbright Scholarship. L. D. Roberts (Low Temperature Physics Group) is on a year's leave of absence for study of low-temperature nuclear physics at the Clarendon Laboratory in Oxford, England, under a Guggenheim Foundation Fellowship and a Fulbright Scholarship.

M. M. Gordon (High Energy Accelerator Studies) returned to the University of Florida, having completed a one-year appointment with the Laboratory.

INTERNAL DISTRIBUTION

1. C. E. Center
2. Biology Library
3. Health Physics Library
4–6. Central Research Library
7. Reactor Experimental Engineering Library
8–19. Laboratory Records Department
20. Laboratory Records, ORNL R.C.
21. A. M. Weinberg
22. L. B. Emlet (K-25)
23. J. P. Murray (Y-12)
24. J. A. Swartout
25. E. H. Taylor
26. E. D. Shipley
27. J. L. Fowler
28. M. L. Nelson
29. A. H. Snell
30. A. Hollaender
31. K. Z. Morgan
32. F. L. Culler
33. M. T. Kelley
34. D. Phillips
35. E. O. Wollan
36. H. E. Seagren
37. A. S. Householder
38. L. D. Roberts
39. R. B. Briggs
40. R. N. Lyon
41. W. C. Koehler
42. E. P. Blizard
43. M. E. Rose
44. G. E. Boyd
45. W. H Sullivan
46. R. W. Stoughton
47. C. E. Winters
48. W. H. Jordan
49. E. C. Campbell
50. D. S. Billington
51. M. A. Bredig
52. R. S. Livingston
53. C. P. Keim
54. F. C. Maienschein
55. C. E. Clifford
56. R. C. Block
57. C. D. Susano
58. C. J. Borkowski
59. M. J. Skinner
60. M. K. Wilkinson
61. J. W. Cable
62. P. M. Reyling
63. G. deSaussure
64. W. M. Good
65. G. C. Williams
66. F. K. McGowan
67. R. W. Johnson
68. J. R. McNally, Jr.
69. J. L. Gabbard
70. R. A. Charpie
71. G. G. Slaughter
72. Eugene Guth
73. R. W. Peelle
74. P. R. Bell
75. G. G. Kelley
76. C. C. Harris
77. H. G. MacPherson
78. P. H. Stelson
79. J. E. Sherwood
80. W. Zobel
81. R. B. Murray
82. H. B. Willard
83. J. Schenck
84. J. H. Neiler
85. J. A. Harvey
86. C. F. Barnett
87. N. H. Lazar
88. R. R. Dickison
89. A. Simon
90. J. H. Gibbons
91. J. J. Penajian
92. S. Bernstein
93. F. Pleasonton
94. C. A. Preskitt
95. H. R. Child
96. C. G. Gardner
97. C. J. McHargue
98. J. A. Lane
99. C. S. Harrill
100. A. J. Miller
101. E. P. Wigner (consultant)
102. S. C. Lind
103. J. H. Van Vleck (consultant)
104. M. S. Livingston (consultant)
105. J. R. Richardson (consultant)

106. R. F. Christy (consultant)
107. M. Goldhaber (consultant)
108. W. A. Fowler (consultant)
109. J. A. Wheeler (consultant)
110. N. F. Ramsey (consultant)
111. H. Feshbach (consultant)
112. ORNL – Y-12 Technical Library, Document Reference Section

EXTERNAL DISTRIBUTION

113–202. Given external distribution
203–738. Given distribution as shown in TID-4500 (14th ed.) under Physics and Mathematics category (75 copies – OTS)